Spin drag and transport equations in systems with spin-polarized currents

Thomas Bagger Stibius Jensen

July 29, 2002

Contents

Chapter 1

Introduction

> Your theory is crazy, but it's not crazy enough to be true. *Niels Bohr*

The quest for developing spin electronic components (spintronics) has been increasing throughout the last decade. In traditional electronic circuits the current, J, is unpolarized, but in spintronics the current through devices may be polarized meaning that $J_\uparrow \neq J_\downarrow$. Here J_s is the current component which is carried by spin s electrons. It is hoped that in the future such novel components will give an important contribution to the commercial field of electronics, and perhaps even in quantum computing. For this reason, but of course also for academical interest, it is relevant to study aspects of spin-polarized transport.

In 2000, D'Amico and Vignale published an article [5], describing and calculating the so-called spin drag rate in a three dimensional electron gas (3DEG). Spin drag occurs when a spin-polarized current runs in a system since electron-electron interactions between spin $\uparrow$ and $\downarrow$ electrons will try to balance the spin current components. This is described as the majority component trying to drag the minority component along via some kind of frictional force, and the effect has therefore been named 'spin drag'.

A similar type of drag has been thoroughly observed and studied over the last 10-15 years in double quantum well (DQW) structures, in which adjacent two dimensional electron gas (2DEG) layers (quantum wells), typically constructed in AlGaAs/GaAs heterostructures, lie closely spaced. Experiments conducted for such systems show that a driving current in one layer induce a weak current in the other, even when electrons cannot tunnel between the two wells.

After having read the article on spin drag and some on DQW drag, it seemed appropriate to calculate the spin drag rate for both a 2DEG and a 3DEG. D'Amico and Vignale had found that the three dimensional rate was considerably higher than the calculated and observed DQW rate's, but their final expression diverged slightly from the one which could be expected glancing at the DQW expressions. Generalizing the DQW rate to spin drag, we [10] found that the three dimensional rate is of the same magnitude as the D'Amico rate, and that the two dimensional rate is even larger. This indeed is interesting, since the calculations showed that the spin drag rate is comparable to the electron-impurity and other scattering rate's determining the resistivity of the electron gas. The spin drag may therefore have practical implications for spin-polarized transport, and we chose to investigate it further.

Two questions now emerge. The first is to ask how much the resistivity of the driving component is enhanced by the drag effect. One would think that this question has already been answered for DQW drag, but, probably because the DQW rate is minute compared to the ordinary transport rate, this does not seem to be the case. For spin-polarized transport the spin drag effect is not insignificant and the question is relevant.

The second question is somewhat more complicated, and in fact has to be investigated before one can fully answer the first. In DQW drag calculations, the possibility that electrons can tunnel between the two quantum wells is completely neglected, an approximation that is very often justified. In spin drag there is a mechanism equivalent to DQW electron tunnelling, namely spin-inverting (also called spin-flip) processes.

Here an electron with spin s interacts typically with a magnetic impurity and end up with spin $-s$, i.e. "tunnel" from one component to the other. In spin-polarized transport such spin-flip processes are often not negligible and therefore has to be incorporated in some way or another. The question that remains is how to do this.

Pursuing these questions gradually directed attention toward the transport equations that traditionally are assumed to govern spin-polarized transport. These were originally proposed as empirical equations [34], but were in 1993 derived by Valet and Fert [33], using a semiclassical Boltzmann equation approach that incorporated spin-flip scattering, but neglected electron-electron interactions. In a sense, this was the opposite situation campared to D'Amico's spin drag calculation (and those of DQW drag as well), where spin-flip (tunnelling in the DQW case) was neglected, but electron-electron interactions were included.

The obvious route to take was now to combine the drag and the transport equation calculations, and find a generalized set of transport equations that include both spin flip and electron-electron scattering. Having such equations it would be easy to answer the question of the enhanced spin drag resistivity, and other effects of spin drag could also be found. The aim of this thesis therefore has been to improve Valet and Fert's equations describing spin-polarized transport by including electron-electron interactions.

The method by which this should be attempted was equally obvious. Since many DQW drag calculations use the semiclassical Boltzmann equation linearized in the electrical field, and Valet and Fert's derivation does the same, this is the way to go. The restriction of the validity to the semiclassical domain is not critical, and is by far outweighed by the advantage of avoiding more challenging quantum field theoretical calculations. Unfortunately it proved difficult to find an exact solution to the linearized Boltzmann equation when both spin-flip and electron-electron scattering terms are present, and we had to search for a plausible approximative solution instead. One candidate was right at hand. A family of functions which we have named shifted Fermi-Dirac (SFD) distributions, and which we found to be exact solutions to the Boltzmann equation for several closely related systems. The SFD distributions has another advantage as well, since they are the simplest type of distributions that describe spin-polarized transport. Since the SFD distributions solve the Boltzmann equation for the related systems, it is tempting to assume that the transport equations one find, when inserting SFD distributions into the Boltzmann equation, is a good approximation to the exact transport equations. This we call the SFD anzats, and it is the fundamental assumption on which the calculations of the generalized transport equations found in this thesis are based.

The structure of the text are as follows. Some degree of fundamental knowledge in the field of solid state physics is needed in order to appreciate and understand the systems, models and calculations that appear in the text. This basic theory is given in chapter 2. Chapter 3 briefly reviews some of the ideas and articles that has directed the path of our investigation. The kernel of the thesis is chapter 4, where the SFD distribution is introduced and examined, and where the generalized transport equations are calculated using the SFD anzatz. Using these transport equations we find some consequences of spin drag, among those the drag enhanced resistivity, followed by an analytically calculation of the two- and three dimensional drag rate. Even though the transport equations are calculated in detail only for a 2DEG, the generalization to a 3DEG is straightforward, and the result for both the two- and three dimensional electron gas[1] is given. Finally in chapter 5 we make some concluding remarks.

[1]The Boltzmann equation can not be used for the one dimensional electron gas (1DEG), and therefore the case of a 1DEG is not considered.

Chapter 2

Basic theory

> It is wrong to think that the task of physics is to find out how nature is. Physics concerns what we can say about nature. *Niels Bohr*

2.1 The electron gas

2.1.1 Non-interacting electron gas in a box

The study of N non-interacting electrons confined in a box lay the foundation on which the model of a metal or semiconductor is build, and furthermore provides an opportunity to introduce some fundamental concepts.

The Fermi sphere and density of states

We begin by considering a 3 dimensional electron gas (3DEG) in a box with volume $V = L^3$. Since the electrons are assumed not to interact, the eigenfunctions, Ψ_N, to the total N-particle Hamiltonian, $H_N = \sum_1^N H$, can be written as a simple Slater determinant

$$\Psi_N(\mathbf{q}_1, \ldots, \mathbf{q}_N) = \frac{1}{\sqrt{N!}} \begin{vmatrix} \psi_{\mathbf{k}_1 s_1}(\mathbf{q}_1) & \psi_{\mathbf{k}_2 s_2}(\mathbf{q}_1) & \cdots & \psi_{\mathbf{k}_N s_N}(\mathbf{q}_1) \\ \psi_{\mathbf{k}_1 s_1}(\mathbf{q}_2) & \psi_{\mathbf{k}_2 s_2}(\mathbf{q}_2) & \cdots & \psi_{\mathbf{k}_N s_N}(\mathbf{q}_2) \\ \vdots & \vdots & \ddots & \vdots \\ \psi_{\mathbf{k}_1 s_1}(\mathbf{q}_N) & \psi_{\mathbf{k}_2 s_2}(\mathbf{q}_N) & \cdots & \psi_{\mathbf{k}_N s_N}(\mathbf{q}_N) \end{vmatrix}. \tag{2.1}$$

Here $\mathbf{q}_i = (\mathbf{r}_i, \xi_i)$ is the spatial and spin coordinates of the "i'th" electron, and $\psi_{\mathbf{k}s}$ are solutions to the one-particle Schrődinger equation

$$H\psi_{\mathbf{k}s}(\mathbf{r}) = -\frac{\hbar^2\nabla^2}{2m}\psi_{\mathbf{k}s}(\mathbf{r}) = \varepsilon_{\mathbf{k}s}\psi_{\mathbf{k}s}(\mathbf{r}) \tag{2.2}$$

for an electron in a box. The eigenfunctions and energies for an electron in a box are well known and can, choosing periodic boundary conditions $\psi(x + \mathbb{Z}L, y + \mathbb{Z}L, z + \mathbb{Z}L) = \psi(x, y, z)$, be written as

$$\psi_{\mathbf{k}s}(\mathbf{r}) = e^{i\mathbf{k}\cdot\mathbf{r}}\chi_s, \quad \varepsilon_{\mathbf{k}s} = \frac{\hbar^2 k^2}{2m}, \tag{2.3}$$

where χ_s is a spin s spinor, and the components of $\mathbf{k}$ satisfies

$$k_x, k_y, k_z \in \mathbb{Z}\frac{2\pi}{L}. \tag{2.4}$$

The total energy, E, of the N-particle system is the sum of the one-particle energies, $E = \sum_n \varepsilon_{\mathbf{k}_n s_n}$.

At zero temperature the ground state is the Slater determinant consisting of the N one-particle eigenfunctions, $\psi_{\mathbf{k}s}$, with lowest energy. In $\mathbf{k}$-space this is described by the Fermi sphere, i.e. the sphere where states with energy less than a certain energy, ε_F, are filled and all other states are empty. The radius of the Fermi sphere, k_F, is called the Fermi wave number and the energy, ε_F, the Fermi energy.

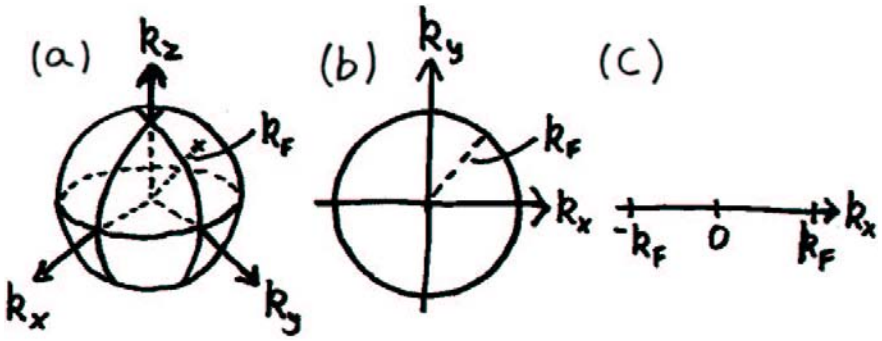

Figure 2.1: The zero temperature ground state pictured in $\mathbf{k}$-space. (a) The Fermi sphere for a 3DEG. (b) The Fermi circle for a 2DEG. (c) The Fermi line for a 1DEG.

Using (2.4) the density of states per spin, $D_{3D}(k)$, in $\mathbf{k}$-space is found to be

$$D_{3D}(k) = \frac{1}{\Delta k_x \Delta k_y \Delta k_z} = \frac{V}{(2\pi)^3}, \tag{2.5}$$

so counting the number of states in the Fermi sphere gives

$$N = 2\int_{FS} d\mathbf{k} D_{3D}(k) = 2\frac{V}{(2\pi)^3}\frac{4}{3}\pi k_F^3 = \frac{V k_F^3}{3\pi^2}, \tag{2.6}$$

where the factor of 2 accounts for the spin summation. This leads to a relation $k_F^3 = 3\pi^2 n$, where $n = N/V$ is the electron density of the 3DEG. Usually everything is calculated per volume unit, so the density of states per volume unit and spin, $d_{3D}(k) = (2\pi)^{-3}$, is from now on included in all $\mathbf{k}$ integrations, unless stated otherwise.

At nonzero temperatures, the ground state is no longer the simple zero temperature Fermi sphere. At any given time, there will be some electrons in the gas that have been thermally exited and are in states with energies higher than ε_F. Since N is large, we can use the result from statistical physics which say, that the average number of electrons occupying a state, $\psi_{\mathbf{k}s}$, is given by the Fermi-Dirac distribution

$$f_s^0(\mathbf{k}) \equiv f^0(\varepsilon_{\mathbf{k}s}) \equiv f_{FD}(\varepsilon_{\mathbf{k}s} - \mu) = \frac{1}{e^{\beta(\varepsilon_{\mathbf{k}s}-\mu)} + 1}, \tag{2.7}$$

where $\beta = (k_B T)^{-1}$ and μ is called the chemical potential. All three notations in (2.7) will be used throughout this thesis.

The chemical potential is determined by the electron density, n, in the gas, according to

$$n = \sum_s \int \frac{d\mathbf{k}}{(2\pi)^3} f_{FD}(\varepsilon_{\mathbf{k}s} - \mu). \tag{2.8}$$

It is straightforward that

$$\frac{\partial \varepsilon}{\partial k} = \frac{\hbar^2 k}{m} = \hbar v, \quad \frac{\partial k}{\partial \varepsilon} = \sqrt{\frac{m}{2\hbar^2 \varepsilon}}, \tag{2.9}$$

and we can find the energy dependent state density per volume unit and spin, $d_{3D}(\varepsilon)$, using

	3D	2D	1D
$d(k)$	$\frac{1}{(2\pi)^3}$	$\frac{1}{(2\pi)^2}$	$\frac{1}{2\pi}$
$d(\varepsilon)$	$\frac{m}{2\pi^2\hbar^2}\sqrt{\frac{2m\varepsilon}{\hbar^2}}$	$\frac{m}{2\pi\hbar^2}$	$\frac{m}{2\pi\hbar^2}\sqrt{\frac{\hbar^2}{2m\varepsilon}} = \sqrt{\frac{m}{8\pi^2\hbar^2\varepsilon}}$
n	$\frac{k_F^3}{3\pi^2} = \frac{1}{3\pi^2}\left(\frac{2m\varepsilon_F}{\hbar^2}\right)^{3/2}$	$\frac{k_F^2}{2\pi} = \frac{m\varepsilon_F}{\pi\hbar^2}$	$\frac{2k_F}{\pi} = \frac{\sqrt{8m\varepsilon_F}}{\pi\hbar}$

Table 2.1: State densities per volume unit and spin for 3D, 2D and 1D electron gasses and the relation between the electron density, n, and k_F, ε.

$$\int d\varepsilon d_{3D}(\varepsilon) = \int d\mathbf{k} d_{3D}(k) = \int \frac{d\mathbf{k}}{(2\pi)^3} = \frac{4\pi}{(2\pi)^3}\int dk k^2 = \frac{4\pi}{(2\pi)^3}\int d\varepsilon \frac{\partial k}{\partial \varepsilon}\frac{2m\varepsilon}{\hbar^2} = \int d\varepsilon \frac{m}{2\pi^2\hbar^2}\sqrt{\frac{2m\varepsilon}{\hbar^2}}. \quad (2.10)$$

Comparing the first and last expression in (2.10) we see that

$$d_{3D}(\varepsilon) = \frac{m}{2\pi^2\hbar^2}\sqrt{\frac{2m\varepsilon}{\hbar^2}}, \quad (2.11)$$

revealing that the density of states in a 3DEG is proportional to the square root of the energy.

These considerations for the 3DEG can easily be generalized to both a 2DEG and a 1DEG. Here the zero temperature ground state is described by a Fermi circle and a Fermi line (figure 2.1) in $\mathbf{k}$-space. The densities of states are found in a manner similar to the one for a 3DEG, and the results are summarized in table 2.1 with $d(\varepsilon)$ sketched in figure 2.2.

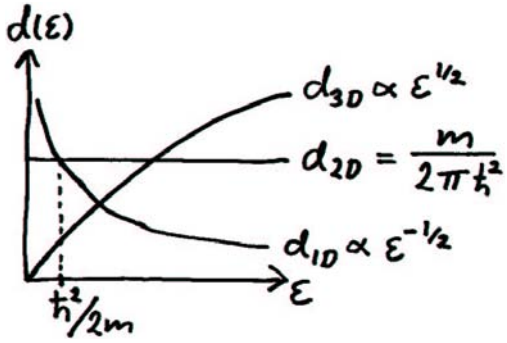

Figure 2.2: The energy dependent density of states per volume and spin for a 3, 2 and 1 dimensional electron gas.

The Fermi-Dirac distribution and the chemical potential

In figure 2.3a, $f^0(\varepsilon)$ is sketched at different temperatures. Since for the chemical potential, μ, we have that $f^0(\mu) = 1/2$, it is clear that μ is temperature dependent. On the figure it is seen that at zero temperature μ is equal to the Fermi energy, and as the temperature is increased, the chemical potential decrease and eventually becomes negative.

It is in general not possible to find an analytical expression for $\mu(T)$. The involved integrals are unsolvable and one has to resolve to approximated expressions. For a 2DEG, however, the integrals are simplified because the density of state, d_{2D}, is energy independent (see table 2.1), and can be solved exactly.

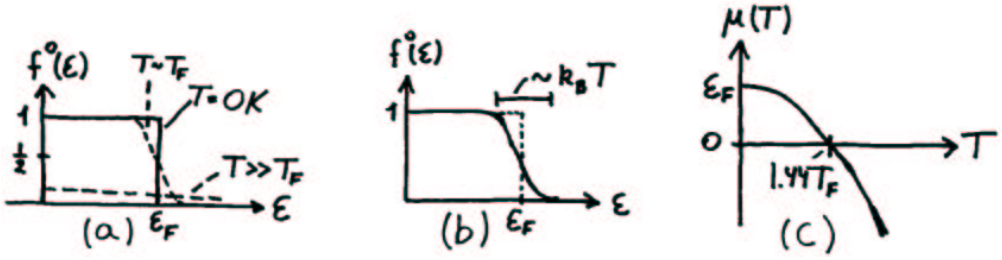

Figure 2.3: (a) The Fermi-Dirac distribution at different temperatures. (b) The width of the region where the nonzero temperature distribution differs from the zero temperature distribution is of the order k_BT (in fact several k_BT). (c) Sketch of the calculated chemical potential in a 2DEG.

PROPOSITION 2.1.1 *The chemical potential, $\mu(T)$, for a 2DEG is*

$$\mu(T) = k_BT \ln(e^{T_F/T} - 1), \tag{2.12}$$

where $T_F = \varepsilon_F/k_B$ is called the Fermi temperature.

PROOF. The density, n, of a 2DEG can be written

$$n = 2\int_0^\infty d\varepsilon d_{2D}(\varepsilon) f^0(\varepsilon) = \frac{m}{\pi\hbar^2}\int_0^\infty d\varepsilon \frac{1}{e^{\beta(\varepsilon-\mu)}+1}. \tag{2.13}$$

Using that $n = m\varepsilon_F/\pi\hbar^2$ (table 2.1), and introducing $x = \varepsilon - \mu$, we find that (2.13) is equivalent to

$$\begin{aligned} \varepsilon_F &= \int_{-\mu}^\infty dx \frac{1}{e^{\beta x}+1} = \Big[x - \frac{1}{\beta}\ln(1+e^{\beta x})\Big]_{-\mu}^\infty = \mu + \frac{1}{\beta}\ln(1+e^{-\beta\mu}) \Rightarrow \\ e^{\beta\varepsilon_F} &= e^{\beta\mu}\big(1+e^{-\beta\mu}\big) = e^{\beta\mu}+1 \Rightarrow \mu = k_BT\ln(e^{T_F/T}-1), \end{aligned} \tag{2.14}$$

using $\beta = (k_BT)^{-1}$ and defining $T_F = \varepsilon_F/k_B$.

We see that the Fermi temperature naturally appears in (2.12). The chemical potential becomes zero at $T = T_F/\ln 2 \approx 1.44T_F$, and gets increasingly negative for higher temperatures (figure 2.3c). It is customary to consider two limiting temperature intervals, namely $T \ll T_F$ and $T \gg T_F$.

The electron gas is called degenerate when $T \ll T_F$. We see from (2.12), that at these temperatures

$$\mu(T) \approx k_BT \ln e^{T_F/T} = k_BT_F = \varepsilon_F, \tag{2.15}$$

for a 2DEG. The Fermi-Dirac distribution for a degenerate electron gas is distorted only slightly from the zero temperature step function, and it is a very useful approximation to put

$$\frac{\partial f^0(\varepsilon)}{\partial\varepsilon} \approx \frac{\partial\theta(\varepsilon_F-\varepsilon)}{\partial\varepsilon} = -\delta(\varepsilon-\varepsilon_F) \tag{2.16}$$

in calculations.

Figure 2.3a shows that when $T \gg T_F$ the step-function like appearance has completely vanished. Since $T_F/T \ll 1$, we find that for a 2DEG

$$\mu(T) \approx k_BT\ln(1+T_F/T-1) = -k_BT\ln\frac{T}{T_F} < 0. \tag{2.17}$$

This means that the Fermi-Dirac distribution can be written as the classical Maxwell-Boltzmann distribution

$$f^0(\varepsilon) = e^{-\beta(\varepsilon-\mu)}, \tag{2.18}$$

and using (2.17), that

$$f^0(\varepsilon) = \frac{T_F}{T} e^{-\beta\varepsilon}, \tag{2.19}$$

for a 2DEG.

We can not find an exact analytical expression for $\mu(T)$ in 3 or 1 dimensional electron gasses, but the Fermi-Dirac distributions behavior is similar to the one in a 2DEG. The Fermi temperature plays the same role and all the considerations hold in both 3 and 1 dimensions. This especially means that $\mu(T) \approx \varepsilon_F$ as well as (2.16) can be used in the degenerate limit, and that (2.18) hold when $T \gg T_F$.

2.1.2 Crystals

In the beginning of the last century, X-ray experiments showed that in most solids the atomic nuclei are not distributed randomly, but form periodic structures known as crystals. A crystal is formally described by a mathematical space point lattice called a Bravais lattice and a basis of atomic nuclei connected to each lattice point. Bravais lattices has the property that the crystal looks identical from any lattice point and it can be shown that there only exist 14 fundamentally different such lattices. Figure 2.4 shows three of these, called the simple cubic (sc), the body centered cubic (bcc) and the face centered cubic (fcc).

Figure 2.4: Three different cubic Bravais lattices. The bcc can also be described as a sc lattice with lattice constant a and a two atom basis where the atoms are placed in (0,0,0), $\frac{1}{2}(a,a,a)$, and the fcc as a sc with a four atom basis in (0,0,0), $\frac{1}{2}(a,a,0)$, $\frac{1}{2}(a,0,a)$, $\frac{1}{2}(0,a,a)$.

A vector connecting two lattice points is called a lattice vector and three linear independent lattice vectors, $\mathbf{a}_1$, $\mathbf{a}_2$, $\mathbf{a_3}$, are called primitive, if every lattice vector, $\mathbf{a}$, can be written $\mathbf{a} = n_1\mathbf{a}_1 + n_2\mathbf{a}_2 + n_3\mathbf{a}_3$, where $n_1, n_2, n_3 \in \mathbb{Z}$. If $\mathbf{a}_1$, $\mathbf{a}_2$ and $\mathbf{a}_3$ are primitive vectors, they are said to generate the Bravais lattice and the parallelipiped spanned by the three vectors is called a primitive cell for the lattice.

It is convenient to introduce a lattice, called the reciprocal lattice, in Fourier space also known as **k**- or reciprocal space. The reciprocal lattice is generated by three reciprocal primitive lattice vectors, $\mathbf{b}_1$, $\mathbf{b}_2$, $\mathbf{b}_3$, defined by the real space primitive vectors, $\mathbf{a}_1$, $\mathbf{a}_2$, $\mathbf{a}_3$, as

$$\mathbf{b_1} = 2\pi\frac{\mathbf{a}_2 \times \mathbf{a}_3}{\mathbf{a}_1 \cdot \mathbf{a}_2 \times \mathbf{a}_3}, \quad \mathbf{b_2} = 2\pi\frac{\mathbf{a}_3 \times \mathbf{a}_1}{\mathbf{a}_1 \cdot \mathbf{a}_2 \times \mathbf{a}_3}, \quad \mathbf{b_3} = 2\pi\frac{\mathbf{a}_1 \times \mathbf{a}_2}{\mathbf{a}_1 \cdot \mathbf{a}_2 \times \mathbf{a}_3}. \tag{2.20}$$

It is readily seen that $\mathbf{a}_i \cdot \mathbf{b}_j = 2\pi\delta_{ij}$.

Being seemingly a very mathematically and abstract construction, it is instructive to note that the reciprocal lattice is directly observable in electron microscope diffraction patterns. It can be proved [17] that these depict two dimensional cuts through the reciprocal lattice, an example is given in figure 2.5.

Another important construction in reciprocal space is the first Brillouin zone, defined as the wave vectors lying closer to $\mathbf{0}$ than to any other reciprocal lattice vector $\mathbf{G} \neq \mathbf{0}$. It is easy to see that for every $\mathbf{q}$ in reciprocal space there exist a $\mathbf{k}$ in the first Brillouin zone and a reciprocal lattice vector $\mathbf{G}$, so that $\mathbf{q} = \mathbf{k} + \mathbf{G}$. In systems with a periodic potential, all information using wave vectors can be given with vectors from the first Brillouin zone.

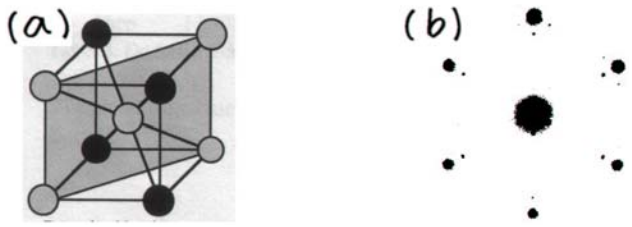

Figure 2.5: (a) A cut through the reciprocal lattice, which is a bcc lattice, of a fcc crystal. (b) The corresponding electron microscope diffraction pattern.

2.1.3 Bloch theory

In order to construct a convincing model describing metals and semiconductors, the origin of the conduction electrons must be explained and the periodic nature of the crystal potential must be taken into account.

The chemical bonds that bind atoms together in a crystal originate primarily from the way electrons are "shared" between the atoms. Ionic bindings form when the electrons are distributed so the atoms in the solid are different charged ions that bind via the Coulomb attraction.

Another binding, called covalent, proves to be extremely important. It may be illustrated by reviewing the results from a quantum mechanical calculation of the electron orbitals in a H_2 molecule. There it is found, that in the ground state an electron will not be bound to a single nuclei, but does, to put it loosely, spend equal time around both. It is energetically favorable for the nuclei to "share" both electrons rather than to have one each. Generalized to crystals this accounts for the presence of conduction electrons in metals and semiconductors. In a single isolated atom, the core electrons are bound more tightly to the nuclei than are the valence electrons in the outermost orbitals. When an atom is placed in a crystal, the core electrons are usually still bound to the nuclei, but the valence electrons are often detached and move around as conduction electrons in the solid.

Bloch's theorem

To assume that these itinerant electrons can be described as non-interacting electrons in a static periodic potential is a rather crude simplification. The atomic ions do no sit still in lattice points, but vibrate in thermal motion. Even at zero temperature they vibrate. In real materials there will be impurities and imperfections in the crystal, and of course the conduction electrons interact with each other. Nevertheless, a sensible starting point is to consider a system of non-interacting electrons in a periodic potential, described by the Bloch Hamiltonian

$$H(\mathbf{r}) = -\frac{\hbar^2\nabla^2}{2m} + V(\mathbf{r}), \tag{2.21}$$

where $-\hbar^2\nabla^2/2m$ is the free electron kinetic energy operator, and $V(\mathbf{r})$ is the periodic potential of an electron in the static ionic lattice potential.

The fundamental theorem for such a system is Bloch's theorem, which traditionally can be stated in two equivalent formulations (for convenience the spin index is suppressed in the following).

THEOREM 2.1.2 *The eigenstates of the one-electron Hamiltonian* $H = -\hbar^2\nabla^2/2m + V(\mathbf{r})$*, where* $V(\mathbf{r}) = V(\mathbf{r}+\mathbf{R})$ *for all lattice vectors* $\mathbf{R}$*, can be written as*

$$\psi_{n\mathbf{k}}(\mathbf{r}) = u_{n\mathbf{k}}(\mathbf{r})\, e^{i\mathbf{k}\cdot\mathbf{r}}, \tag{2.22}$$

where $u_{n\mathbf{k}}(\mathbf{r}) = u_{n\mathbf{k}}(\mathbf{r}+\mathbf{R})$ *for all lattice vectors* $\mathbf{R}$*.*

THEOREM 2.1.3 *Every eigenstate, ψ, of the one-electron Hamiltonian $H = -\hbar^2\nabla^2/2m + V(\mathbf{r})$, where $V(\mathbf{r}) = V(\mathbf{r}+\mathbf{R})$ for all lattice vectors $\mathbf{R}$, can be chosen so a wave vector $\mathbf{k}$ exist such that*

$$\psi(\mathbf{r}+\mathbf{R}) = e^{i\mathbf{k}\cdot\mathbf{R}}\,\psi(\mathbf{r}), \tag{2.23}$$

for all lattice vectors $\mathbf{R}$.

The band index n is introduced in theorem 2.1.2 because the eigenvalue problem, after inserting the Bloch solution into $H(\mathbf{r})$, reduces to a Shrődinger equation restricted to a single primitive cell. In analogy to a particle in a box, this spatial restriction of the problem results in the existence of many different eigenfunctions for every $\mathbf{k}$, each labelled with a band index n and with eigenvalues $\varepsilon_{n\mathbf{k}}$ discretely spaced. This can be shown rigourously when proving theorem 2.1.2, but we choose a simpler proof and refer readers to Ashcroft and Mermins standard textbook [1] in solid state physics for further details.

Proving that the two formulations of Bloch's theorem are equivalent (without discussing the band index) is easy. That theorem 2.1.2 implies theorem 2.1.3 follows from

$$\psi(\mathbf{r}+\mathbf{R}) = u_{n\mathbf{k}}(\mathbf{r}+\mathbf{R})\,e^{i\mathbf{k}\cdot(\mathbf{r}+\mathbf{R})} = e^{i\mathbf{k}\cdot\mathbf{R}}u_{n\mathbf{k}}(\mathbf{r})\,e^{i\mathbf{k}\cdot\mathbf{r}} = e^{i\mathbf{k}\cdot\mathbf{R}}\psi(\mathbf{r}). \tag{2.24}$$

The opposite implication is shown by defining $u(\mathbf{r}) = \psi(\mathbf{r})\,e^{-i\mathbf{k}\cdot\mathbf{r}}$, so that $\psi(\mathbf{r}) = u(\mathbf{r})e^{i\mathbf{k}\cdot\mathbf{r}}$, and using (2.23) to see that

$$u(\mathbf{r}+\mathbf{R}) = \psi(\mathbf{r}+\mathbf{R})\,e^{-i\mathbf{k}\cdot(\mathbf{r}+\mathbf{R})} = e^{i\mathbf{k}\cdot\mathbf{R}}\psi(\mathbf{r})\,e^{-i\mathbf{k}\cdot\mathbf{r}}e^{-i\mathbf{k}\cdot\mathbf{R}} = u(\mathbf{r}). \tag{2.25}$$

We proceed by proving theorem 2.1.3.

PROOF. Define, for all lattice vectors $\mathbf{R}$, a translation operator, $T_{\mathbf{R}}$, by $T_{\mathbf{R}}f(\mathbf{r}) = f(\mathbf{r}+\mathbf{R})$. We see that $T_{\mathbf{R}}$ is conserving the norm of $f(\mathbf{r})$. Since $H(\mathbf{r}+\mathbf{R}) = H(\mathbf{r})$ when $\mathbf{R}$ is a lattice vector, we find that

$$T_{\mathbf{R}}H\psi = H(\mathbf{r}+\mathbf{R})\psi(\mathbf{r}+\mathbf{R}) = H(\mathbf{r})\psi(\mathbf{r}+\mathbf{R}) = HT_{\mathbf{R}}\psi \tag{2.26}$$

so $T_{\mathbf{R}}$ and H are commutating operators. For any two lattice vectors $\mathbf{R}$ and $\mathbf{R}'$, we have

$$T_{\mathbf{R}}T_{\mathbf{R}'} = T_{\mathbf{R}+\mathbf{R}'} = T_{\mathbf{R}'}T_{\mathbf{R}} \tag{2.27}$$

showing, together with (2.26), that the Hamiltonian, H, and the total set of operators, $\{T_{\mathbf{R}} \mid \mathbf{R}$ is a lattice vector$\}$, are mutual commutating and therefore have common eigenstates ψ, fulfilling

$$H\psi = E\psi, \quad T_{\mathbf{R}}\psi = C(\mathbf{R})\psi. \tag{2.28}$$

Using the identities in (2.27) it is clear that

$$C(\mathbf{R}+\mathbf{R}') = C(\mathbf{R})C(\mathbf{R}') \tag{2.29}$$

for all lattice vectors $\mathbf{R}$ and $\mathbf{R}'$, and since $T_{\mathbf{R}}$ is conserving the norm we have that $|C(\mathbf{R})| = 1$. For given three primitive vectors, $\mathbf{a}_1$, $\mathbf{a}_2$, $\mathbf{a}_3$, there therefore exist three real numbers, x_1, x_2, x_3, so that $C(\mathbf{a}_i) = exp(i2\pi x_i)$. Since a lattice vector, $\mathbf{R}$, can be written $\mathbf{R} = n_1\mathbf{a}_1 + n_2\mathbf{a}_2 + n_3\mathbf{a}_3$, use of (2.29) gives that

$$C(\mathbf{R}) = C(\mathbf{a}_1)^{n_1}C(\mathbf{a}_2)^{n_2}C(\mathbf{a}_3)^{n_3} = e^{i2\pi(n_1x_1+n_2x_2+n_3x_3)}. \tag{2.30}$$

Defining $\mathbf{k} = x_1\mathbf{b}_1 + x_2\mathbf{b}_2 + x_3\mathbf{b}_3$, where $\mathbf{b}_1$, $\mathbf{b}_2$, $\mathbf{b}_3$ are the reciprocal lattice vectors from (2.20), and using that $\mathbf{a}_i \cdot \mathbf{b}_j = 2\pi\delta_{ij}$, we find $\mathbf{k}\cdot\mathbf{R} = 2\pi(n_1x_1 + n_2x_2 + n_3x_3)$, meaning that $C(\mathbf{R}) = exp(i\mathbf{k}\cdot\mathbf{R})$. This gives that

$$\psi(\mathbf{r}+\mathbf{R}) = T_{\mathbf{R}}\psi = C(\mathbf{R})\psi = e^{i\mathbf{k}\cdot\mathbf{R}}\psi(\mathbf{r}), \tag{2.31}$$

which proves theorem 2.1.3.

Energy bands

The "free particle" form of the Bloch functions (2.22) is reflected in the dispersion relation $\varepsilon_{n\mathbf{k}}$. We shall not describe the various methods used to calculate the energy bands in solids, but merely sketch the principal behavior. An example for a one dimensional lattice with atom spacing a in a weak periodic potential is shown in figure 2.6.

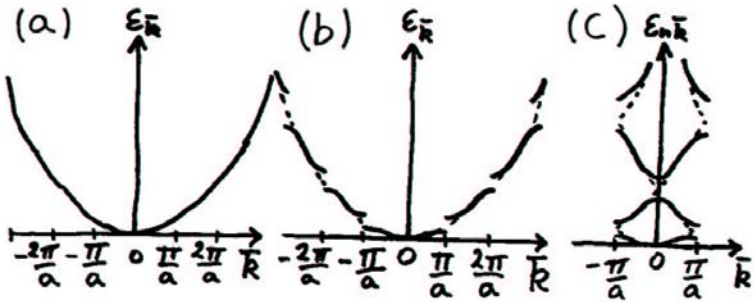

Figure 2.6: (a) The free electron parabolic energy band. (b) The Bloch bands split up near the Brillouin zone boundaries. (c) All wavevectors are equivalent to those in the first Brillouin zone, and often the energy bands are translated into this zone (this is called the reduced zone scheme).

This simple model provides all that is needed to understand the fundamental difference between metals, semiconductors and insulators.

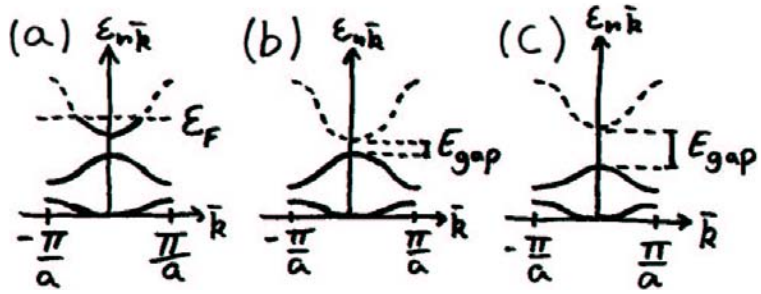

Figure 2.7: (a) In a metal the conduction band is a only partly filled with electrons. (b) The energy gap in a semiconductor is sufficiently small compared to k_BT, so that electrons can be exited into the empty conduction band. (c) In an insulator the energy gap is large compared to k_BT, preventing electrons to be exited into the empty conduction band.

One consequence of the Pauli principle is that a totally filled energy band can carry no current (if interband transitions are neglected), so in order for the solid to conduct electricity a partly filled band is needed. Each band contains exactly 2N states (including spin), where N is the number of primitive cells in the crystal. Assuming that all valence electrons are itinerant, then if the crystal has an odd number of valence electrons in each primitive cell, the highest lying band containing electrons will be half full (figure 2.7a) and the solid is a metal.

On the other hand, if the number of valence electrons in a primitive cell is even, all bands will either be completely full or empty (figure 2.7b and c) at $T = 0$ K. When the size of the energy gap between the highest lying filled band and the lowest lying empty band is small, electrons can be thermally exited into the empty band at room temperatures. The two bands are therefore partly filled and can conduct electrical currents, making the solid a semiconductor. This does not happen if the gap is larger, and the solid will be an insulator. Often the conduction band minimum and the valence band maximum are situated directly above each other and the band gap is called direct. When this is not the case the gap is called indirect.

In real three dimensional materials, the band structures are very complex and may "overlap" in energy, meaning that even solids with an even number of itinerant electrons per primitive cell may be metals. For an insulator all bands must be filled. Since this never occur with an odd number of conduction electrons in every primitive cell, no matter how the band structure might be, all insulators and semiconductors must have an even number of conduction electrons per primitive cell. Reassuringly, this is confirmed experimentally.

Another important feature that is indicated by figure 2.7 is the fact that the conduction electrons and holes often will be situated close to the gaps. The curvature of the energy band, $\varepsilon_{n\mathbf{k}}$, at these points determines the electrons "effective mass" m^* in analogue with the free energy dispersion relation $\varepsilon_{\mathbf{k}} = \hbar^2 k^2/2m$. In three dimensional materials the energy bands are often anisotropic and one may need to specify up to 3 different $\mathbf{k}$-direction dependent effective masses. Luckily, in the materials of interest to us, the relevant effective masses are isotropic. We will more often than not choose to write the effective mass as m instead of m^*.

Finally we mention that it can be shown quite generally [1], using second order perturbation theory, that an electron in a level specified by band index n and wave vector $\mathbf{k}$ has a mean velocity

$$v_{n\mathbf{k}} = \frac{1}{\hbar}\frac{\partial \varepsilon_{n\mathbf{k}}}{\partial \mathbf{k}}. \tag{2.32}$$

2.1.4 The semiclassical model

A free classical particle with charge, q, position, $\mathbf{r}$, and momentum, $\mathbf{p}$, in an applied electrical field, $\mathbf{E}$, and magnetic field, $\mathbf{B}$, will between collisions follow a trajectory given by

$$\dot{\mathbf{r}} = \frac{\mathbf{p}}{m}, \quad \dot{\mathbf{p}} = q(\mathbf{E} + \mathbf{v} \times \mathbf{B}), \tag{2.33}$$

with $\mathbf{v} = \dot{\mathbf{r}}$.

This approach can not be generalized to a quantum mechanical particle, since a simultaneous determination of $\mathbf{r}$ and $\mathbf{p}$ is prohibited by Heisenberg's uncertainty relation. However, if it is not necessary to localize the particle on a scale comparable to the de Broglie wavelength $\lambda_{deBroglie}$, the particle may be described by a wave package of free particle states

$$\Psi(\mathbf{r}, t) = \sum_{\mathbf{k}'} g(\mathbf{k}') e^{i(\mathbf{k}'\cdot\mathbf{r} - \hbar k'^2 t/2m)}, \quad g(\mathbf{k}') \approx 0 \text{ for } |\mathbf{k}' - \mathbf{k}| > \Delta k. \tag{2.34}$$

Here $\mathbf{r}$ is the mean position and $\hbar\mathbf{k}$ the mean momentum around which the wave package is distributed and the spatial width, $\Delta x \gg \lambda_{deBroglie}$, and momentum width, Δk, of the package obviously fulfills $\Delta x \Delta k > 1$. For particles described by such wave packages, the mean values $\mathbf{r}$ and $\mathbf{p} = \hbar\mathbf{k}$ are governed by the equations (2.33) between collisions.

Describing electrons confined in a general periodic potential between collisions is often done using a method called the semiclassical model. We shall not try to justify it from first principles, but will merely outline the method.

The semiclassical model generalize the approach for the free electron wave packages (2.34) to Bloch electron wave packages. These are assumed to be constructed from a superposition of Bloch functions from a given band, and can in analogy with (2.34) be written as

$$\Psi_n(\mathbf{r}, t) = \sum_{\mathbf{k}'} g(\mathbf{k}') \Psi_{n\mathbf{k}'}(\mathbf{r}) e^{-i\varepsilon_{n\mathbf{k}'} t/\hbar}, \quad g(\mathbf{k}') \approx 0 \text{ for } |\mathbf{k}' - \mathbf{k}| > \Delta k. \tag{2.35}$$

The wave packages in (2.35) are constructed with sufficiently small Δk, giving $\omega_{n\mathbf{k}'} \approx \varepsilon_{n\mathbf{k}}/\hbar$ for the components in the package, so the group velocities

$$\frac{\partial \omega}{\partial \mathbf{k}} = \frac{1}{\hbar}\frac{\partial \varepsilon_{n\mathbf{k}}}{\partial \mathbf{k}}, \tag{2.36}$$

are consistent with the mean velocity of an electron in a definite Bloch state, $\Psi_{n\mathbf{k}}$, given by (2.32).

Referring to (2.35) as an electron with position $\mathbf{r}$ and wave vector $\mathbf{k}$, the semiclassical model predicts how $\mathbf{r}$ and $\mathbf{k}$ of each electron evolve between collisions in the presence of externally applied fields, and calculations

are based entirely upon the band structure $\varepsilon_{n\mathbf{k}}$. The model is not concerned about how $\varepsilon_{n\mathbf{k}}$ are found, but presupposes that these functions are known.

PROPOSITION 2.1.4 *The semiclassical model ascribes to each electron a position* $\mathbf{r}$*, a wave vector* $\mathbf{k}$ *and a band index* n*. In the presence of external electrical and magnetic fields,* $\mathbf{E}(\mathbf{r},t)$ *and* $\mathbf{B}(\mathbf{r},t)$*, the parameters evolve in time according to the following rules*

1. *The band index,* n*, is constant.*
2. *The following equations of motion hold*

$$\dot{\mathbf{r}} = \mathbf{v}_n(\mathbf{k}) = \frac{1}{\hbar}\frac{\partial \varepsilon_{n\mathbf{k}}}{\partial \mathbf{k}}, \tag{2.37}$$

$$\hbar\dot{\mathbf{k}} = -e\Big[\mathbf{E}(\mathbf{r},t) + \mathbf{v}_n(\mathbf{k}) \times \mathbf{B}(\mathbf{r},t)\Big]. \tag{2.38}$$

3. *The wave vector* $\mathbf{k}$ *is only defined within an additive reciprocal lattice vector* $\mathbf{K}$*, meaning that, for all reciprocal lattice vectors* $\mathbf{K}$*, the labels* n*,* $\mathbf{r}$*,* $\mathbf{k}$ *and* n*,* $\mathbf{r}$*,* $\mathbf{k}+\mathbf{K}$ *are completely equivalent ways of describing the same electron.*
4. *In thermal equilibrium (defined in section 2.2) the Bloch electrons are Fermi-Dirac distributed*

$$f(\varepsilon_{n\mathbf{k}}) = \frac{1}{e^{\beta(\varepsilon_{n\mathbf{k}}-\mu)}+1}, \tag{2.39}$$

where $\beta = (k_B T)^{-1}$ *and* μ *is the chemical potential.*

Introducing the effective mass, m_n, for the n'th band, we write for the Bloch electrons

$$\varepsilon_{n\mathbf{k}} = \frac{\hbar^2 k^2}{2m_n}, \tag{2.40}$$

and see that (2.37) can be written

$$\dot{\mathbf{r}} = \mathbf{v}_n(\mathbf{k}) = \frac{\hbar\mathbf{k}}{m_n}, \tag{2.41}$$

in analogue with the free electron result $\mathbf{v} = \hbar\mathbf{k}/m_e$.

2.1.5 Lattice vibrations and phonons

The atomic nuclei will, as mentioned previously, not sit still in lattice points, but vibrate in thermal motion around their equilibrium position. The vibrations of the individual nuclei couple to each other and create quantized lattice vibrations. In analogue with the quantum mechanical treatment of the harmonic oscillator, the quantized lattice vibrations can be described by creation- and annihilation operators. These socalled second quantization operators formally describe the lattice vibrations as particles, known as phonons. The description is carried further, since phonons not only interact with each other, but also with other particles in the system like for instance electrons.

A detailed view on the phonons and their interactions requires many theoretical considerations, typically one uses quantum field theoretical methods. However, in this thesis we will not take phonons into account. The reason is simply that the effect of phonons decrease at low temperatures and we assume it may be neglected at the temperatures of interest to us. The dissatisfied reader is referred to the quantum field theoretically based descriptions made for instance in [3, 23].

Neglecting the effect of phonons in low-temperature experiments is not always a good approximation, as we shall discuss in section 3.1.2, but is sufficient for our purpose.

2.2 The Boltzmann equation

A thermodynamic system is defined as an arbitrary amount of matter with properties that can be completely described by a number of macroscopic quantities called state variables, like the energy, E, volume, V, temperature, T, pressure, P, and so on. When a thermodynamical system is left undisturbed for a sufficient amount of time it automatically settles in a macroscopic state where all the state quantities no longer change with time. This is called the state of thermal equilibrium. A system in thermal equilibrium is completely described by a few independent state quantities, and all other state quantities are related to these through a number of empirical equations and the laws of thermodynamics.

A metal or semiconductor in which a electrical current is flowing is not in thermal equilibrium. When a system is not in thermal equilibrium methods beyond those of elementary thermodynamics are needed. In this section we introduce the Boltzmann equation, which is often used in semiclassical transport theory.

2.2.1 The Boltzmann equation for dilute gasses

We start by considering a dilute gas of classical particles, by which we mean a gas where the average separation between the particles is much larger than the range of their interactions. A complete mechanical treatment of a system with N particles would require the position and momentum of all N particles. Since the number of particles in a gas is astronomical, the bookkeeping, not to mention the treatment, of these 6N coordinates is an impossible task and another approach must be found.

Introducing the one particle distribution function, $f(\mathbf{r},\mathbf{p},t)$, where $f(\mathbf{r},\mathbf{p},t)(2\pi\hbar)^{-3}d\mathbf{r}d\mathbf{p}$ is the mean number of particles in the phase space element $d\mathbf{r}d\mathbf{p}$ around $(\mathbf{r},\mathbf{p})$ at the time t, lay the foundation towards a statistical description. The continuity equation, known from electro- or hydrodynamics, generalized to a 6 dimensional phase space, gives the following equation for the one particle distribution

$$\frac{\partial f}{\partial t}+\frac{\partial}{\partial x_\nu}(\dot{x}_\nu f)=0, \tag{2.42}$$

where $x_\nu=(\mathbf{r},\mathbf{p})$. Equation (2.42) does not take into account that a particle can be "instantaneously" scattered into or out of the phase space point $(\mathbf{r},\mathbf{p})$ by collisions. These effects are collected in a source term, $(\partial f/\partial t)_{coll}$, called the collision integral and (2.42) is generalized as

$$\frac{\partial f}{\partial t}+\frac{\partial}{\partial x_\nu}(\dot{x}_\nu f)=\left(\frac{\partial f}{\partial t}\right)_{coll}. \tag{2.43}$$

It is possible to rewrite (2.43) using Hamiltons equations

$$\dot{\mathbf{r}}=\frac{\partial H}{\partial \mathbf{p}},\qquad \dot{\mathbf{p}}=-\frac{\partial H}{\partial \mathbf{r}}, \tag{2.44}$$

known from classical mechanics, since

$$\frac{\partial}{\partial x_\nu}(\dot{x}_\nu f)=\dot{x}_\nu\frac{\partial f}{\partial x_\nu}+\Big(\frac{\partial \dot{\mathbf{r}}}{\partial \mathbf{r}}+\frac{\partial \dot{\mathbf{p}}}{\partial \mathbf{p}}\Big)f=\dot{x}_\nu\frac{\partial f}{\partial x_\nu}+\Big(\frac{\partial^2 H}{\partial \mathbf{r}\partial \mathbf{p}}-\frac{\partial^2 H}{\partial \mathbf{p}\partial \mathbf{r}}\Big)f=\dot{x}_\nu\frac{\partial f}{\partial x_\nu}. \tag{2.45}$$

Using (2.45) in (2.43) we find the Boltzmann equation

$$\frac{\partial f}{\partial t}+\dot{\mathbf{r}}\cdot\frac{\partial f}{\partial \mathbf{r}}+\dot{\mathbf{p}}\cdot\frac{\partial f}{\partial \mathbf{p}}=\left(\frac{\partial f}{\partial t}\right)_{coll}. \tag{2.46}$$

We finally mention that although $\mathbf{p}$ in (2.46) is the canonical momentum, the Boltzmann equation is easily proven to be form invariant under change from the canonical to the kinetic momentum.

The collision integral

The collision term, $(\partial f/\partial t)_{coll}$, is a sum of integrals, one for each considered type of scattering process. Two processes, that we assume to be of primary importance in the systems we shall be dealing with, are elastic collisions of a particle on an impurity and mutual two particle collisions.

The rate of change in $f(\mathbf{r}, \mathbf{p}, t)$ due to impurity scattering, can, suppressing the variables $\mathbf{r}$ and t for convenience, be written as

$$\left(\frac{\partial f}{\partial t}\right)_{coll} = -\int \frac{d\mathbf{p}'}{(2\pi\hbar)^3}\big[w(\mathbf{p}', \mathbf{p})f(\mathbf{p}) - w(\mathbf{p}, \mathbf{p}')f(\mathbf{p}')\big], \tag{2.47}$$

and is understood as follows. The probability that a particle with momentum $\mathbf{p}$ scatters into the phase space element $d\mathbf{p}'$ around $\mathbf{p}'$ (this is from now on referred to as "scattered into $d\mathbf{p}'$") during a time interval of length dt, is $w(\mathbf{p}', \mathbf{p})d\mathbf{p}'dt$, and the probability of finding a particle with momentum $\mathbf{p}$, is $(2\pi\hbar)^{-3}f(\mathbf{p})$. Therefore the rate of change due to impurity scattering out of $\mathbf{p}$, is

$$\left(\frac{\partial f}{\partial t}\right)_{coll,out} = -\int \frac{d\mathbf{p}'}{(2\pi\hbar)^3} w(\mathbf{p}', \mathbf{p})f(\mathbf{p}). \tag{2.48}$$

In a similar fashion we find that the rate of change due to particles scattered into $\mathbf{p}$ is

$$\left(\frac{\partial f}{\partial t}\right)_{coll,in} = \int \frac{d\mathbf{p}'}{(2\pi\hbar)^3} w(\mathbf{p}, \mathbf{p}')f(\mathbf{p}'), \tag{2.49}$$

and adding (2.48) and (2.49) gives (2.47).

The collision integral corresponding to particle-particle scattering is found in an equivalent manner, giving the result

$$\left(\frac{\partial f}{\partial t}\right)_{coll} = -\int \frac{d\mathbf{p}_1}{(2\pi\hbar)^3}\int \frac{d\mathbf{p}'}{(2\pi\hbar)^3}\int \frac{d\mathbf{p}_1'}{(2\pi\hbar)^3}\big[w(\mathbf{p}', \mathbf{p}_1'; \mathbf{p}, \mathbf{p}_1)f(\mathbf{p})f(\mathbf{p}_1) - w(\mathbf{p}, \mathbf{p}_1, \mathbf{p}', \mathbf{p}_1')f(\mathbf{p}')f(\mathbf{p}_1')\big]. \tag{2.50}$$

Here the first term corresponds to processes where a particle with momentum $\mathbf{p}$ and one in $d\mathbf{p}_1$ scatters on each other, resulting in one particle in $d\mathbf{p}'$ and another in $d\mathbf{p}_1'$. The second term refers to the "opposite" process. We should mention that (2.50) is not an exact equation, since the two particle distribution $f^{(2)}(\mathbf{p}, \mathbf{p}_1)$ should have been used instead of the product $f(\mathbf{p})f(\mathbf{p}_1)$. It is justifiable to use $f(\mathbf{p})f(\mathbf{p}_1)$ for dilute gasses, since the large interparticle distance decrease the correlations between particles, making an independent distribution approximation acceptable.

Often the process rates fulfil $w(\mathbf{p}', \mathbf{p}) = w(\mathbf{p}, \mathbf{p}')$ or $w(\mathbf{p}', \mathbf{p}_1'; \mathbf{p}, \mathbf{p}_1) = w(\mathbf{p}, \mathbf{p}_1; \mathbf{p}', \mathbf{p}_1')$ and the equations (2.47) and (2.50) are simplified accordingly.

2.2.2 The Boltzmann equation for metals and semiconductors

A surprising feature is that the Boltzmann equation can be used to calculate the semiclassical transport properties in many three and two dimensional metals and semiconductors. It is beyond the scope of this thesis to investigate why the Boltzmann equation works in these high density systems of strongly interacting electrons, this would require some degree of Fermi Liquid theory. Here we simply state the Boltzmann equation used in semiclassical electronic transport theory, and use it "on face value".

Having the semiclassical model in mind, the Boltzmann equation for Bloch electrons is written

$$\frac{\partial f}{\partial t} + \dot{\mathbf{r}} \cdot \frac{\partial f}{\partial \mathbf{r}} + \dot{\mathbf{k}} \cdot \frac{\partial f}{\partial \mathbf{k}} = \left(\frac{\partial f}{\partial t}\right)_{coll}, \tag{2.51}$$

where, according to proposition 2.1.4,

$$\dot{\mathbf{r}} = \mathbf{v}(\mathbf{k}) = \frac{1}{\hbar}\frac{\partial \varepsilon_{\mathbf{k}}}{\partial \mathbf{k}}, \tag{2.52}$$

and

$$\hbar\dot{\mathbf{k}} = -e\big(\mathbf{E} + \mathbf{v} \times \mathbf{B}\big). \tag{2.53}$$

The scattering probability

Electron scattering on impurities is a dominant scattering process at low temperatures, since neither the impurity concentration nor the Coulomb interaction between an electron and an impurity is particular temperature dependant. This stand in contrast to scattering on lattice vibrations which "freeze" out at low temperatures (section 2.1.5) and electron-electron scattering where the available phase space due to the Pauli principle goes as T^2 in a 3DEG and as $T^2 \ln T$ in a 2DEG [16]. The energy gap between the impurity ground state and the lowest exited state is usually of the order eV and therefore large compered to $k_B T$. This means that no energy is transferred between the electron and the impurity, and the collision is elastic.

One often uses Fermi's Golden Rule, well known from quantum mechanics, to evaluate the scattering probabilities. For instance one will find that for weak electron-impurity interaction, U, and low impurity concentrations, n_i, the scattering probability is given by

$$w(\mathbf{k}, \mathbf{k}') = \frac{2\pi}{\hbar} n_i \delta(\varepsilon_k - \varepsilon_{k'}) \left| \langle \mathbf{k}' | U | \mathbf{k} \rangle \right|^2. \tag{2.54}$$

Here the δ-function explicitly indicates that the impurity scattering is elastic.

In this thesis we also consider the effect of electron-electron scattering. For such processes Fermi's Golden Rule gives that

$$\begin{aligned} w(\mathbf{k}, \mathbf{k}'; \mathbf{k}+\mathbf{q}, \mathbf{k}'-\mathbf{q}) &= \frac{2\pi}{\hbar} |\langle \mathbf{k}+\mathbf{q}, \mathbf{k}'-\mathbf{q} | e\phi | \mathbf{k}, \mathbf{k}' \rangle|^2 \delta(\varepsilon_{\mathbf{k}} + \varepsilon_{\mathbf{k}'} - \varepsilon_{\mathbf{k}+\mathbf{q}} - \varepsilon_{\mathbf{k}'-\mathbf{q}}) \\ &= \frac{2\pi}{\hbar} \left| e\phi(q) \right| \delta(\varepsilon_{\mathbf{k}} + \varepsilon_{\mathbf{k}'} - \varepsilon_{\mathbf{k}+\mathbf{q}} - \varepsilon_{\mathbf{k}'-\mathbf{q}}) \equiv w(q) \delta(\varepsilon_{\mathbf{k}} + \varepsilon_{\mathbf{k}'} - \varepsilon_{\mathbf{k}+\mathbf{q}} - \varepsilon_{\mathbf{k}'-\mathbf{q}}), \end{aligned} \tag{2.55}$$

where the introduction of $\mathbf{q}$ ensures momentum conservation and the δ-function ensures energy conservation. In analytical calculations to come (section 4.7 and 4.8.1) we shall use the Thomas-Fermi expressions (2.92) and (2.103) found in section 2.3 for the screened electrical potential, $\phi(q)$, between electrons in an electron gas.

The collision integral

The collision integrals used in (2.102) can easily be generalized from (2.48) and (2.50). Since we are dealing with fermions we have to be sure that the electrons are scattered into vacant states. This is done by introducing terms of the form $(1 - f_s(\mathbf{k}))$, giving the probability of the state $\mathbf{k}$ being vacant, before the process scatter an electron into state $\mathbf{k}$.

We only consider systems where the scattering probability fulfils what is known as detailed balance

$$w(\mathbf{k}, \mathbf{k}') = w(\mathbf{k}', \mathbf{k}), \quad w(\mathbf{k}, \mathbf{k}_1; \mathbf{k}', \mathbf{k}_1') = w(\mathbf{k}', \mathbf{k}_1'; \mathbf{k}, \mathbf{k}_1). \tag{2.56}$$

Assuming that detailed balance applies is not particular restricting. We immediately see that (2.56) upholds for (2.55), and it can be shown that if the crystal and impurity potentials are real and invariant under spatial inversions detailed balance also hold for (2.54).

As mentioned above, impurity scattering is considered to be elastic. There are in principle two types of impurity scattering; spin conserving and spin-inverting (spin-flip) impurity scattering. They have the following collision integrals.

Spin conserving elastic impurity scattering has a collision integral, H_0, given by

$$H_0[f_s](\mathbf{k}) = -\int \frac{d\mathbf{k}'}{(2\pi)^d} w_s^0(\mathbf{k},\mathbf{k}')[f_s(\mathbf{k})(1-f_s(\mathbf{k}')) - f_s(\mathbf{k}')(1-f_s(\mathbf{k}))]\delta(\varepsilon_{ks}-\varepsilon_{k's}) \\ = -\int \frac{d\mathbf{k}'}{(2\pi)^d} w_s^0(\mathbf{k},\mathbf{k}')[f_s(\mathbf{k}) - f_s(\mathbf{k}')]\delta(\varepsilon_{ks}-\varepsilon_{k's}). \tag{2.57}$$

Here the energy conservation is written explicitly as a δ-function and d is the dimension of the system.

The expression for the spin-flip elastic impurity collision integral, H_{sf}, is

$$H_{sf}[f_s,f_{-s}](\mathbf{k}) = -\int \frac{d\mathbf{k}'}{(2\pi)^d} w_{sf}(\mathbf{k},\mathbf{k}')[f_s(\mathbf{k})(1-f_{-s}(\mathbf{k}')) - f_{-s}(\mathbf{k}')(1-f_s(\mathbf{k}))]\delta(\varepsilon_{ks}-\varepsilon_{k'-s}) \\ = -\int \frac{d\mathbf{k}'}{(2\pi)^d} w_{sf}(\mathbf{k},\mathbf{k}')[f_s(\mathbf{k}) - f_{-s}(\mathbf{k}')]\delta(\varepsilon_{ks}-\varepsilon_{k'-s}), \tag{2.58}$$

once again explicitly writing the energy conservation.

We also need the collision integral, H_{ee}, arising from electron-electron scattering processes between spin s and s' electrons. This is given as

$$H_{ee}[f_s,f_{s'}](\mathbf{k}) = -\int\frac{d\mathbf{k}'}{(2\pi)^d}\int\frac{d\mathbf{q}}{(2\pi)^d} w(q)\delta(\varepsilon_{ks}+\varepsilon_{k's'}-\varepsilon_{\mathbf{k}+\mathbf{q}s}-\varepsilon_{\mathbf{k}'-\mathbf{q}s'}) \\ \times\left[f_s(k)f_{s'}(k')(1-f_s(\mathbf{k}+\mathbf{q}))(1-f_{s'}(\mathbf{k}'-\mathbf{q})) - f_s(\mathbf{k}+\mathbf{q})f_{s'}(\mathbf{k}'-\mathbf{q})(1-f_s(k))(1-f_{s'}(k'))\right], \tag{2.59}$$

where we have incorporated momentum conservation by introducing the quantity $\mathbf{q}$ and also has introduced

$$w(\mathbf{k},\mathbf{k}';\mathbf{k}+\mathbf{q},\mathbf{k}'-\mathbf{q}) = w(q)\delta(\varepsilon_{\mathbf{k}}+\varepsilon_{\mathbf{k}'}-\varepsilon_{\mathbf{k}+\mathbf{q}}-\varepsilon_{\mathbf{k}'-\mathbf{q}}),$$

in equivalence with (2.55).

2.2.3 A property of the Fermi-Dirac distribution

The Fermi-Dirac distribution has an interesting property, which is used when the electron-electron collision integral (2.59) is linearized in the electrical field (chapter 4).

The Fermi-Dirac distribution is defined by (2.7) as

$$f_{FD}(\varepsilon) = \frac{1}{e^{\beta\varepsilon}+1}, \tag{2.60}$$

and therefore

$$(1-f_{FD}(\varepsilon)) = 1-\frac{1}{e^{\beta\varepsilon}+1} = \frac{e^{\beta\varepsilon}}{e^{\beta\varepsilon}+1}. \tag{2.61}$$

From (2.60) and (2.61) we immediately see that

$$f_{FD}(\varepsilon_1)f_{FD}(\varepsilon_2)(1-f_{FD}(\varepsilon_1+\varepsilon))(1-f_{FD}(\varepsilon_2-\varepsilon)) = \frac{e^{\beta(\varepsilon_1+\varepsilon)}e^{\beta(\varepsilon_2-\varepsilon)}}{(e^{\beta\varepsilon_1}+1)(e^{\beta\varepsilon_2}+1)(e^{\beta\varepsilon_1+\varepsilon}+1)(e^{\beta\varepsilon_2+\varepsilon}+1)} \\ = \frac{e^{\beta\varepsilon_1}e^{\beta\varepsilon_2}}{(e^{\beta\varepsilon_1}+1)(e^{\beta\varepsilon_2}+1)(e^{\beta\varepsilon_1+\varepsilon}+1)(e^{\beta\varepsilon_2+\varepsilon}+1)} = f_{FD}(\varepsilon_1+\varepsilon)f_{FD}(\varepsilon_2-\varepsilon)(1-f_{FD}(\varepsilon_1))(1-f_{FD}(\varepsilon_2)). \tag{2.62}$$

Consider a process where two electrons, one with energy ε and spin s, the other with ε_1 and spin s', scatter on each other, the spin s electron ending up with energy ε' and the spin s' electron with ε_1'. Since the total energy of the process is conserved, we have that $\varepsilon - \mu_s + \varepsilon_1 - \mu_{s'} = \varepsilon' - \mu_s + \varepsilon_1' - \mu_{s'}$, and using (2.62) gives that

$$f_s^0(\mathbf{k}) f_{s'}^0(\mathbf{k}_1)[1 - f_s^0(\mathbf{k}')][1 - f_{s'}^0(\mathbf{k}_1')] = f_s^0(\mathbf{k}') f_{s'}^0(\mathbf{k}_1')[1 - f_s^0(\mathbf{k})][1 - f_{s'}^0(\mathbf{k}_1)]. \tag{2.63}$$

This is the property we wanted to prove.

Besides being used to linearize the electron-electron collision integral, we can use (2.63) to indicate why the Fermi-Dirac distribution is considered to be the equilibrium distribution for the system. In thermal equilibrium the electron distribution, f_{eq}, must fulfil that the collision integral, $(\partial_t f_{eq})_{coll}$, is zero. If this were not the case then for a uniform ($\partial_x f_{eq} = 0$) electron gas without external forces ($\dot{\mathbf{k}} = 0$), the Boltzmann equation would read

$$\frac{\partial f_{eq}}{\partial t} = \left(\frac{\partial f_{eq}}{\partial t}\right)_{coll} \neq 0, \tag{2.64}$$

in contrast to the definition of thermal equilibrium which requires a time independent distribution. It is immediately seen that the Fermi-Dirac distribution fulfils

$$H_0[f_s^0](\mathbf{k}) = H_{sf}[f_s^0, f_{-s}^0](\mathbf{k}) = 0, \tag{2.65}$$

and

$$\begin{aligned} H_{ee}[f_s^0, f_{s'}^0](\mathbf{k}) = &- \int \frac{d\mathbf{k}'}{(2\pi)^2} \int \frac{d\mathbf{q}}{(2\pi)^2} w(\mathbf{k}, \mathbf{k}'; \mathbf{k}+\mathbf{q}, \mathbf{k}-\mathbf{q}) \delta(\varepsilon_{ks} + \varepsilon_{k's'} - \varepsilon_{\mathbf{k}+\mathbf{q}s} - \varepsilon_{\mathbf{k}'-\mathbf{q}s'}) \\ &\times \left[f_s^0(k) f_{s'}^0(k')(1 - f_s^0(\mathbf{k}+\mathbf{q}))(1 - f_{s'}^0(\mathbf{k}'-\mathbf{q})) - f_s^0(\mathbf{k}+\mathbf{q}) f_{s'}^0(\mathbf{k}'-\mathbf{q})(1 - f_s^0(k))(1 - f_{s'}^0(k')) \right] = 0, \end{aligned} \tag{2.66}$$

according to (2.63). It can also be shown (appendix A) that the entropy rates, $(\partial_t S)_{coll}$, due to elastic impurity and electron-electron collisions are zero for a distribution that satisfies (2.63). That f^0 fulfil these for the true equilibrium distribution, f_{eq}, two necessary requirements indicate that our fundamental assumption $f_{eq} = f^0$ is correct (of course this is not a rigorous proof, since we have not shown if there are other suitable distributions, f, that fulfil $(\partial_t f)_{coll} = 0$ and $(\partial_t S)_{coll} = 0$).

2.3 Screening

In order to find an expression for the Coulomb interaction between electrons in the structures we are dealing with, it is necessary to know how an electrical field is effected by dielectric materials, metals and semiconductors. The charges in the solid react to the electrical field, weakening the internal effective field. We say that the electrical field is screened by the response of the system.

2.3.1 Dielectric screening

Let us begin with the elementary electrostatic treatment of dielectric materials. In the presence of an external field the electronic cloud surrounding each atom is slightly displaced and the dielectric will be polarized. This is expressed by introducing a polarization field, $\mathbf{P}$, induced inside the solid. It is well known that the polarization originates from an induced charge density, ρ_{ind}, via the relation

$$\rho_{ind} = -\nabla \cdot \mathbf{P}. \tag{2.67}$$

For linear materials and not to large fields, the polarization, $\mathbf{P}$, is proportional to the electrical field, $\mathbf{E}$, and the susceptibility, χ, is defined by

$$\mathbf{P} = \varepsilon_0 \chi \mathbf{E}, \tag{2.68}$$

where ε_0 is the vacuum permittivity. Using (2.67) in Gauss law, leads to

$$\nabla \cdot \mathbf{E} = \frac{\rho_{tot}}{\varepsilon_0} = \frac{\rho_{ext} + \rho_{ind}}{\varepsilon_0} = \frac{\rho_{ext} - \nabla \cdot \mathbf{P}}{\varepsilon_0} \Rightarrow \nabla \cdot \mathbf{D} = \nabla \cdot (\varepsilon_0 \mathbf{E} + \mathbf{P}) = \rho_{ext}, \tag{2.69}$$

which also serves as definition of the electric displacement, $\mathbf{D} = \varepsilon_0 \mathbf{E} + \mathbf{P}$. Using (2.68) we find that

$$\mathbf{D} = \varepsilon_0 \mathbf{E} + \mathbf{P} = \varepsilon_0 (1 + \chi) \mathbf{E} = \varepsilon_0 \varepsilon_r \mathbf{E}, \tag{2.70}$$

defining the relative permittivity, ε_r, also called the dielectric constant, as

$$\varepsilon_r = 1 + \chi. \tag{2.71}$$

2.3.2 Screening in 3 dimensional metals and semiconductors

An important feature of dielectric materials is the fact that charges are not itinerant, and the screening is exclusively caused by distorting the bound electron cloud surrounding each atomic nuclei. In metals and semiconductors, however, itinerant conduction electrons are present. Their response to the electrical field contributes significantly to the screening, making screening much more efficient than in a dielectric.

Let us consider a semiconductor where there is a "dielectric" screening due to the polarization of background ions. Introducing a dielectric constant, ε_b, even before adding the contribution of the itinerant electrons accounts for this polarization. Next, the effect of the itinerant electrons must be found.

A generalized form of (2.70) can be written as a time and space convolution

$$\mathbf{D}(\mathbf{r}, t) = \int_{-\infty}^{t'} dt' \int d\mathbf{r} \varepsilon(\mathbf{r} - \mathbf{r}', t - t') \mathbf{E}(\mathbf{r}', t'), \tag{2.72}$$

with $\varepsilon(\mathbf{r}, t) = \varepsilon_0 \varepsilon_b \varepsilon_r(\mathbf{r}, t)$. Here $\varepsilon_r(\mathbf{r}, t)$ refers to the contribution from the itinerant electrons. Using the convolution theorem from Fourier theory, we immediately write

$$\mathbf{D}(\mathbf{q}, \omega) = \varepsilon(\mathbf{q}, \omega) \mathbf{E}(\mathbf{q}, \omega), \tag{2.73}$$

with $\varepsilon(\mathbf{q}, \omega) = \varepsilon_0 \varepsilon_b \varepsilon_r(\mathbf{q}, \omega)$.

Suppose an excess electron is placed in a point, $\mathbf{0}$, inside the electron gas and is somehow held there. Other electrons in the vicinity are repulsed by this electron, which is therefore surrounded by a "cloud" of positive charge density, screening its field. At this point it is convenient to introduce three electrostatic scalar potentials, ϕ_{ext}, ϕ_{tot} and ϕ_{ind}. The external potential, ϕ_{ext}, is the potential induced solely by the excess electron and satisfy the Poisson equation, that reads

$$\nabla^2 \phi_{ext}(\mathbf{r}, t) = -\frac{\rho_{ext}(\mathbf{r}, t)}{\varepsilon_0 \varepsilon_b}, \tag{2.74}$$

when radiation is neglected. Here $\rho_{ext}(\mathbf{r}, t) = -e\delta(\mathbf{r})$ is the charge density of the electron, and ε_b accounts for the dielectric screening. Fourier transforming (2.74) gives

$$-q^2 \phi_{ext}(\mathbf{q}, \omega) = -\frac{\rho_{ext}(\mathbf{q}, \omega)}{\varepsilon_0 \varepsilon_b} = \frac{e}{\varepsilon_0 \varepsilon_b} \Rightarrow \phi_{ext}(\mathbf{q}, \omega) = -\frac{e}{\varepsilon_0 \varepsilon_b q^2} \delta(\omega), \tag{2.75}$$

which has the the well known Fourier transform

$$\phi_{ext}(\mathbf{r}, t) = -\frac{e}{4\pi \varepsilon_0 \varepsilon_b r}, \tag{2.76}$$

as it should. The total potential, ϕ_{tot}, produced by the total charge density, i.e. both the excess electron and the surrounding cloud, and the induced potential, ϕ_{ind}, produced by the cloud alone, satisfy

$$\nabla^2\phi_{tot}(\mathbf{r},t) = -\frac{\rho_{tot}(\mathbf{r},t)}{\varepsilon_0\varepsilon_b}, \quad \nabla^2\phi_{ind}(\mathbf{r},t) = -\frac{\rho_{ind}(\mathbf{r},t)}{\varepsilon_0\varepsilon_b}, \tag{2.77}$$

in analogue with (2.74). Since $\rho_{tot} = \rho_{ext} + \rho_{ind}$, we can choose that $\phi_{tot} = \phi_{ext} + \phi_{ind}$.

Using

$$\nabla \cdot \mathbf{E}(\mathbf{r},t) = \frac{\rho_{tot}(\mathbf{r},t)}{\varepsilon_0\varepsilon_b} \Rightarrow i\mathbf{q}\cdot\mathbf{E}(\mathbf{q},\omega) = \frac{\rho_{tot}(\mathbf{q},\omega)}{\varepsilon_0\varepsilon_b}, \tag{2.78}$$

$$\nabla \cdot \mathbf{D}(\mathbf{r},t) = \rho_{ext}(\mathbf{r},t) \Rightarrow i\mathbf{q}\cdot\mathbf{D}(\mathbf{q},\omega) = \rho_{ext}(\mathbf{q},\omega), \tag{2.79}$$

together with (2.73), gives

$$\begin{aligned} \rho_{ext}(\mathbf{q},\omega) = i\mathbf{q}\cdot\mathbf{D}(\mathbf{q},\omega) = \varepsilon(\mathbf{q},\omega)i\mathbf{q}\cdot\mathbf{E}(\mathbf{q},\omega) = \varepsilon(\mathbf{q},\omega)\frac{\rho_{tot}(\mathbf{q},\omega)}{\varepsilon_0\varepsilon_b} = \varepsilon_r(\mathbf{q},\omega)\rho_{tot}(\mathbf{q},\omega) \\ \Rightarrow \varepsilon_r(\mathbf{q},\omega) = \frac{\rho_{ext}(\mathbf{q},\omega)}{\rho_{tot}(\mathbf{q},\omega)}. \end{aligned} \tag{2.80}$$

From the Fourier transformed versions of the Poisson equations, (2.74) and (2.77),

$$-q^2\phi_{tot}(\mathbf{q},\omega) = -\frac{\rho_{tot}(\mathbf{q},\omega)}{\varepsilon_0\varepsilon_b}, \quad -q^2\phi_{ext}(\mathbf{q},\omega) = -\frac{\rho_{ext}(\mathbf{q},\omega)}{\varepsilon_0\varepsilon_b}, \tag{2.81}$$

we find, that

$$\frac{\rho_{ext}(\mathbf{q},\omega)}{\rho_{tot}(\mathbf{q},\omega)} = \frac{\phi_{ext}(\mathbf{q},\omega)}{\phi_{tot}(\mathbf{q},\omega)}, \tag{2.82}$$

and write (2.80) as

$$\varepsilon_r(\mathbf{q},\omega) = \frac{\rho_{ext}(\mathbf{q},\omega)}{\rho_{tot}(\mathbf{q},\omega)} = \frac{\phi_{ext}(\mathbf{q},\omega)}{\phi_{tot}(\mathbf{q},\omega)}. \tag{2.83}$$

Using (2.75) and (2.83), we find that the total potential is

$$\phi_{tot}(\mathbf{q},\omega) = \frac{\phi_{ext}(\mathbf{q},\omega)}{\varepsilon_r} = -\frac{e}{\varepsilon_0\varepsilon_b\varepsilon_r(\mathbf{q},\omega)q^2}\delta(\omega), \tag{2.84}$$

in the considered case where an extra electron is placed in $\mathbf{0}$. We now need to find an expression for the relative permittivity, $\varepsilon_r(\mathbf{q},\omega)$.

The Thomas-Fermi approximation

There are many approximative ways to find the relative permittivity, $\varepsilon_r(\mathbf{q},\omega)$. When evaluating the potential between two electrons we choose to use the simplest, called the Thomas-Fermi approximation, which describes the static response ($\omega = 0$) to a long wavelength ($q \ll k_F$) influence. This approximation can be introduced in various ways, here we take an approach that use the Boltzmann equation.[1]

Suppose that the electrical field varies in time and space as $\mathbf{E}(\mathbf{r},t) = \mathbf{E}e^{i(\mathbf{q}\cdot\mathbf{r}-\omega t)}$. Since the electrical field can be written[2] $\mathbf{E} = -\nabla\phi$, we know that $\nabla \times \mathbf{E} = 0$, and see that $\mathbf{q} \times \mathbf{E} = 0$. This means that the electromagnetic field is longitudinal, i.e. $\mathbf{E} \parallel \mathbf{q}$. Let us write the non-equilibrium electron distribution, $f(\mathbf{k})$, as

[1] In the next section, concerning screening in a 2DEG, we derive the Thomas-Fermi expression in a slightly different manner. The approach used there could equally well have been applied in the three dimensional case.

[2] Again radiation effects are neglected.

$$f(\mathbf{k}) = f_0(k) + \delta f(\mathbf{k}) e^{i(\mathbf{q}\cdot\mathbf{r}-\omega t)}, \tag{2.85}$$

where $\delta f(\mathbf{k})$ to linear order in E is proportional to E. The Boltzmann equation, going to linear order in E and neglecting the effect of collisions, gives

$$\begin{aligned}\frac{\partial f(\mathbf{k})}{\partial t} + \mathbf{v}\cdot\frac{\partial f(\mathbf{k})}{\partial \mathbf{r}} - \frac{e\mathbf{E}}{\hbar}\cdot\frac{\partial f^0(\mathbf{k})}{\partial \mathbf{k}} e^{i(\mathbf{q}\cdot\mathbf{r}-\omega t)} = 0 \Rightarrow \big[(-i\omega + i\mathbf{v}\cdot\mathbf{q})\delta f(\mathbf{k}) - \frac{e\mathbf{E}}{\hbar}\cdot\frac{\partial f^0(k)}{\partial \mathbf{k}}\big] e^{i(\mathbf{q}\cdot\mathbf{r}-\omega t)} = 0 \\ \Rightarrow \delta f(\mathbf{k}) = -i\frac{e\mathbf{E}}{\hbar}\cdot\frac{\partial f^0(k)}{\partial \mathbf{k}}\frac{1}{\mathbf{v}\cdot\mathbf{q}-\omega}.\end{aligned} \tag{2.86}$$

In the Thomas-Fermi approximation we set $\omega = 0$. Using $\mathbf{E} \parallel \mathbf{q}$ together with $\partial f^0/\partial \mathbf{k} = \hbar\mathbf{v}\partial f^0/\partial\varepsilon$, (2.86) is written

$$\delta f(\mathbf{k}) = -\frac{ie\mathbf{E}}{\hbar}\cdot\frac{\partial f^0(k)}{\partial k}\frac{1}{\mathbf{q}\cdot\mathbf{v}} = -ie\frac{\mathbf{E}\cdot\mathbf{v}}{\mathbf{q}\cdot\mathbf{v}}\frac{\partial f^0(\varepsilon)}{\partial\varepsilon} = -\frac{ieE}{q}\frac{\partial f^0(\varepsilon)}{\partial\varepsilon}. \tag{2.87}$$

Using that the induced polarization charge density, $\delta\rho_{pol} = -\nabla\cdot\mathbf{P}$, in Fourier space is connected to δf, we write

$$-i\mathbf{q}\cdot\mathbf{P} = \delta\rho_{pol}(\mathbf{q}) = -2e\int\frac{d\mathbf{k}}{(2\pi)^3}\delta f(\mathbf{k}), \tag{2.88}$$

where the factor 2 accounts for spin summation. Since $\mathbf{P}(\mathbf{q}) = \varepsilon_0\varepsilon_b(\varepsilon_r(\mathbf{q})-1)\mathbf{E}(\mathbf{q})$, and using (2.87) together with $\mathbf{E} \parallel \mathbf{q} \Rightarrow \mathbf{E}\cdot\mathbf{q} = qE$, we immediately rewrite (2.88) as

$$i\varepsilon_0\varepsilon_b(\varepsilon_r(\mathbf{q})-1)qE(\mathbf{q}) = -\frac{ieE}{q}2e\int\frac{d\mathbf{k}}{(2\pi)^3}\frac{\partial f^0}{\partial\varepsilon} \Rightarrow \varepsilon_r(\mathbf{q}) = 1 - \frac{2e^2}{\varepsilon_0\varepsilon_b q^2}\int\frac{d\mathbf{k}}{(2\pi)^3}\frac{\partial f^0}{\partial\varepsilon}.$$

Since

$$\int\frac{d\mathbf{k}}{(2\pi)^3}\frac{\partial f^0}{\partial\varepsilon} = \frac{4\pi}{(2\pi)^3}\int dk k^2\frac{\partial f^0}{\partial\varepsilon} = \frac{1}{2\pi^2}\int d\varepsilon\frac{mk}{\hbar^2}\frac{\partial f^0}{\partial\varepsilon} = -\frac{mk_F}{2\pi^2\hbar^2},$$

we find that

$$\varepsilon_r(\mathbf{q}) = 1 + \frac{k_{TF}^2}{q^2}, \tag{2.89}$$

where the three dimensional Thomas Fermi wave number, k_{TF}, is given by

$$k_{TF}^2 = \frac{me^2k_F}{\pi^2\hbar^2\varepsilon_0\varepsilon_b} = \frac{4k_F}{\pi a_b}. \tag{2.90}$$

Here

$$a_b = \frac{me^2}{4\pi\hbar^2\varepsilon_0\varepsilon_b} \tag{2.91}$$

is the effective Bohr radius and k_F the Fermi wave number for the electron gas. As a cautionary note, we mention once again that m is the effective electron mass and not m_e.

The screened potential in a 3DEG is given by (2.84), and using (2.89), we find that in the Thomas-Fermi approximation

$$\phi_{tot}(q) = -\frac{e}{\varepsilon_0\varepsilon_b(q^2+k_{TF}^2)}. \tag{2.92}$$

2.3.3 Screening in a 2DEG

The screening of an electron in a 2DEG is a bit more complicated, since the electrical field is not restricted to the plane of the 2DEG and must still be treated in all three dimensions. Once again we want to derive the Thomas-Fermi expression, now for a 2DEG, that describes the static response to a long wavelength influence.

Ignoring the finite thickness of the 2DEG, we write the charge density of the 2DEG as $\rho(x,y,z) = \sigma(x,y)\delta(z)$, where the z-axis is chosen to be perpendicular to the plane of the electron gas, and $\sigma(x,y)$ is the area charge density. Let us consider the case where an excess electron is situated at a distance d from the z=0 plane. The unscreened (external) potential, $\phi_{ext}(x,y)$, in the z=0 plane, originating from this electron can be written as

$$\phi_{ext}(x,y) = -\frac{e}{4\pi\varepsilon_0\varepsilon_b\sqrt{r^2+d^2}}, \tag{2.93}$$

where $\mathbf{r} = (x,y)$. The two dimensional Fourier transform of (2.93) involves a Bessel function, $J_0(x)$, but can be done analytically. We have

$$\begin{aligned}\phi_{ext}(\mathbf{q}) &= \int d\mathbf{r}\phi_{ext}(\mathbf{r})e^{-i\mathbf{q}\cdot\mathbf{r}} = -\frac{e}{4\pi\varepsilon_0\varepsilon_b}\int_0^\infty rdr\int_0^{2\pi}d\theta\frac{e^{-iqr\cos\theta}}{\sqrt{r^2+d^2}} \\ &= -\frac{e}{4\pi\varepsilon_0\varepsilon_b}\int_0^\infty\frac{2\pi J_0(qr)rdr}{\sqrt{r^2+d^2}} = -\frac{e}{2\varepsilon_0\varepsilon_b q}e^{-qd},\end{aligned} \tag{2.94}$$

where $\mathbf{q} = (q_x, q_y)$.

The excess electron induces a surface charge density, σ_{ind}, in the 2DEG, that induce a potential

$$\phi_{ind}(\mathbf{r}, z=0) = \phi_{ind}(\mathbf{q})e^{i\mathbf{q}\cdot\mathbf{r}}, \tag{2.95}$$

in the plane of the 2DEG. This potential spread over all space as

$$\phi_{ind}(\mathbf{r}, z) = \phi_{ind}(\mathbf{q})e^{i\mathbf{q}\cdot\mathbf{r}}e^{-q|z|}, \tag{2.96}$$

since (2.96) satisfy the Laplace equation for $z \neq 0$ and falls off for large $|z|$. According to ordinary electromagnetism the charge density satisfies the condition

$$\frac{\sigma_{ind}}{\varepsilon_0\varepsilon_b} = E_z(0_+) - E_z(0_-) = -\left.\frac{\partial\phi_{ind}}{\partial z}\right|_{0_+} + \left.\frac{\partial\phi_{ind}}{\partial z}\right|_{0_-}. \tag{2.97}$$

Using (2.96), it is clear that (2.97) can be written as

$$\frac{\sigma_{ind}(q)}{\varepsilon_0\varepsilon_b} = 2q\phi_{ind}(q), \tag{2.98}$$

so the dielectric function becomes

$$\varepsilon_r(q) = \frac{\phi_{ext}(q)}{\phi_{tot}(q)} = 1 - \frac{\phi_{ind}(q)}{\phi_{tot}(q)} = 1 - \frac{1}{2\varepsilon_0\varepsilon_b q}\frac{\sigma_{ind}(q)}{\phi_{tot}(q)}. \tag{2.99}$$

Writing the induced charge density, $\sigma_{ind} = -edn$, where dn is the change in the electron density, and defining the change in the potential energy of these electrons as $d\varepsilon = -e\phi_{tot}$, we have that

$$\frac{\sigma_{ind}(q)}{\phi_{tot}(q)} = e^2\frac{dn}{d\varepsilon} = \frac{me^2}{\pi\hbar^2}. \tag{2.100}$$

Here we have used that the state density $dn/d\varepsilon = m/\pi\hbar^2$ (see table 2.1) in a 2DEG.

All in all, we have that

$$\varepsilon_r(q) = 1 + \frac{q_{TF}}{q}, \tag{2.101}$$

where the two-dimensional Thomas-Fermi wave number, q_{TF}, is given as

$$q_{TF} = \frac{me^2}{2\pi\hbar^2\varepsilon_0\varepsilon_b} = \frac{2}{a_b}. \tag{2.102}$$

Here a_b once again is the effective Bohr radius (2.91). For d=0 we find the screened potential to be

$$\phi_{tot}(q) = \frac{\phi_{ext}(q)}{\varepsilon_r(q)} = -\frac{e}{2\varepsilon_0\varepsilon_b(q + q_{TF})}. \tag{2.103}$$

2.4 Elementary transport theory

Many of the concepts used in transport theory can be introduced by the following simplified approach to an electron gas model. Assume that an electric field, **E**, is applied causing a current density, **J**, to run in the electron gas. In linear isotropic systems **E** and **J**, are proportional and the conductivity, σ, is defined by

$$\mathbf{J} = \sigma\mathbf{E}. \tag{2.104}$$

In non-isotropic systems the conductivity is described by a tensor, but here we concentrate on isotropic materials. The inverse relation

$$\mathbf{E} = \rho\mathbf{J}, \tag{2.105}$$

define the resistivity, ρ, and of course $\sigma = \rho^{-1}$.

Suppose that the effect of the applied electric field, E, in the x-direction is to shift the distribution in momentum space an amount $p_D = mv_D$ away from the equilibrium Fermi-Dirac distribution (figure 2.8a). The velocity, v_D, is called the drift velocity. The interactions in the system will attempt to drive such a non-equilibrium distribution toward the equilibrium distribution. This is described by introducing a relaxation rate, τ, and writing

$$\dot{p}_D = -eE - \frac{p_D}{\tau}. \tag{2.106}$$

When the initial transient effects have died out, and the system is in a steady state $\dot{p}_D = 0$, and therefore

$$p_D = mv_D = -e\tau E \Rightarrow v_D = -\frac{e\tau}{m}E = -\mu E. \tag{2.107}$$

Here we have introduced the mobility $\mu = e\tau/m$, which must not be confused with the chemical potential, μ, defined earlier. The mobility is an often used measure of the electron gas "quality", and in experiments "good" 2DEG's typically have mobilities of several hundreds $m^2V^{-1}s^{-1}$. The current density is given by

$$J = -nev_D = \frac{ne^2\tau}{m}E, \tag{2.108}$$

and comparing (2.104) with (2.108) gives the Drude conductivity

$$\sigma = \frac{ne^2\tau}{m}. \tag{2.109}$$

The resistivity, $\rho(T)$, measured in a normal metal at low temperatures, is sketched in figure 2.8b. The zero temperature contribution can be shown to arise from impurities and imperfections in the crystal, and the additional contribution primarily from electron-phonon scattering. This latter contribution is readily seen to vanish at low temperatures, indicating that phonon scattering can be neglected at very low temperatures. This assumption is used to simplify many of the low temperature calculations that follows.

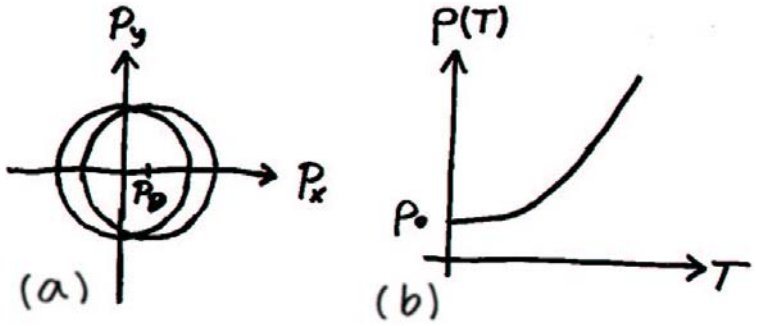

Figure 2.8: (a) The assumed shift from the Fermi-Dirac distribution (centered around $\mathbf{0}$) to the current carrying distribution (centered around p_D). (b) The resistivity, $\rho(T)$, of a metal, sketched at low temperatures.

2.5 Ferromagnetism

The magnetic properties of solids vary widely from one material to another. Placed in an external magnetic field most materials are magnetized. The size of this magnetization can be found by measuring the change in the magnetic field at some point in space when a sample of the solid is placed in the vicinity. A vast pallet of ingenious experimental setups are used to probe various other magnetic properties, but in this introductionary survey it is sufficient to consider the magnetization. In the following we concentrate, although not attempting to give a thorough description, on ferromagnetic materials.

2.5.1 Basic magnetic properties

Some solids will, after having been subjected to an external magnetic field, retain a macroscopic magnetization when the external field is removed. Such materials are called ferromagnetic and typical examples are iron, cobalt and nickel.

If a sample of unmagnetized iron is placed in a small increasing magnetic field, the magnetization will at first grow slowly in a reversible manner. When the field surpasses a critical value the process stops being reversible and is described by a hysteresis curve showing a non-zero magnetization in the absence of an external field. Increasing the magnetic field further enhance the hysteresis loop until the magnetization eventually becomes saturated. The hysteresis loop from saturation (figure 2.9a) is characteristic for the sample and determines a number of parameters for the specimen. For instance the remanence is defined as the magnetization remaining when the field is switched off from saturation, and the coercivity as the field necessary to reduce the magnetization from saturation to zero.

The hysteresis properties are mainly consequences of the presence of ferromagnetic domains in the solid. These divide the ferromagnet into domains, each with an intrinsic homogeneous magnetization. This magnetization is of equal magnitude, but may vary in direction from domain to domain. The effect of the external field is primarily to change the size of the different domains, making domains with a magnetization in the field direction larger and domains with opposing magnetization smaller. The external field may also alter the magnitude of the intrinsic magnetization slightly. The magnitude of the intrinsic magnetization in absence of an external field is called the spontaneous magnetization, and is investigated in the next section. It decreases with increasing temperature (figure 2.9b) and becomes zero at temperatures above a certain critical temperature called the ferromagnetic Curie temperature. Above the Curie temperature ferromagnetics become paramagnetic[3].

The shape and size of the ferromagnetic domains (figure 2.10a) are determined by minimizing the total energy. A specimen gains energy when having many domains, but at the expense of creating domain boundaries, and the resulting equilibrium configuration is highly dependant on the physical shape of the sample

[3]We do not describe the various other forms of magnetism. The reader is refered to [4, 19, 35]

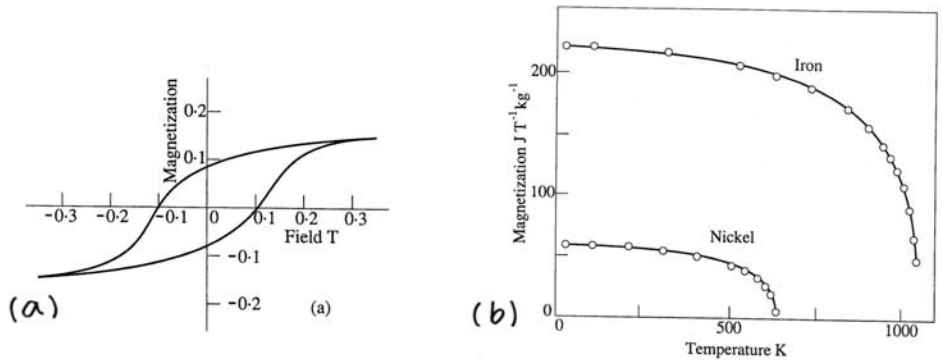

Figure 2.9: (a) Magnetization hysteresis loop from saturation. (b) Spontaneous magnetization against temperature for iron and nickel.

and the external magnetic field. Many experimental methods are used to observe the domain boundaries, the simplest are Bitter patterns created by spreading a magnetic powder upon the sample surface. The particles in the powder are attracted toward regions with high magnetic field gradients. Since these occur where the domain boundaries intersect the sample surface, the powder creates a pattern that depict the domains.

When the size of a magnetic body is sufficiently small it it not energetically favorable to have more than one domain. In the remaining thesis we consider such single domain ferromagnets.

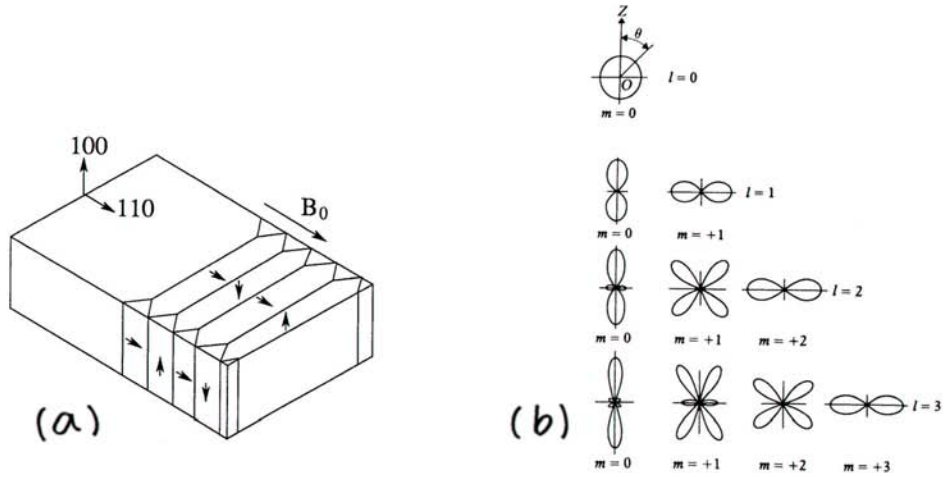

Figure 2.10: (a) Ferromagnetic domain structure in a single crystal specimen of iron. (b) Polar plots of the probability distributions of lm spatial orbitals (note that here m is written instead of m_l).

2.5.2 The origins of spontaneous magnetization

The magnetic moments in any solid primarily originate from electrons. An electron has a magnetic moment, $\mu = -g\mu_B \mathbf{s}$, attached to its spin, $\mathbf{s}$, where $g = 2$ and the Bohr magneton $\mu_B = e\hbar/2m = 9,27 \cdot 10^{-24} JT^{-1}$. The nuclei also have a spin, $\mathbf{I}$, and therefore an associated magnetic moment, $g_N \mu_N \mathbf{I}$. This moment, however, is seldom significant since the mass of a nucleus is several thousand times larger than the electron mass making the nuclear magneton, $\mu_N = e\hbar/2M$, much smaller than μ_B.

There are two main reasons to the spontaneous ferromagnetic magnetization. The first is when the coupling between magnetic ions favors a parallel ion spin configuration. The second when itinerant electrons

present in the system prefer to have their spin aligned.

Magnetic ions

Often the electronic cloud in an atom has a total spin and subsequently a magnetic moment. This follows from quantum physics where the electronic orbitals are described with spatial quantum numbers n, l, m_l and spin quantum number m_s. The single electron energy levels are primarily determined by the main quantum number, $n = 1, 2, \ldots$. The angular momentum quantum number, $l = 0, 1, \ldots, n-1$, and the ordering of these nl levels (shells) can be listed with increasing energy as

$$1s \quad 2s \quad 2p \quad 3s \quad 3p \quad (4s \quad 3d) \quad 4p \quad (5s \quad 4d) \quad 5p \quad \ldots$$

Here levels inside the parentheses have almost the same energy and their ordering may vary from element to element. The two remaining quantum numbers split the energy levels further, but only on a small scale compared to the difference between the shells. Every shell can at most room $2(2l+1)$ electrons, and a filled shell has a total spin of zero and therefore no magnetic momentum. Partly filled shells on the other hand may have a magnetic moment. This moment is often determined by two empirical rules, called Hund's rules, stating how the electrons usually occupy a shell.

Hund's first rule states that the electron configuration with the largest total spin S is lower in energy.

Hund's second rule states that, for a given S, the term with the largest total angular momentum L is lower in energy.

Here $L(L+1)\hbar^2$ and $S(S+1)\hbar^2$ are eigenvalues to the operators $\mathbf{L}^2$ and $\mathbf{S}^2$ where $\mathbf{L} = \sum \mathbf{l}_i$ is the total angular momentum operator and $\mathbf{S} = \sum \mathbf{s}_i$ is the total spin operator. $\mathbf{l}_i$ and $\mathbf{s}_i$ are the angular momentum and spin operators of the i'th electron.

Hunds first rule is a consequence of the Pauli principle that force electrons with the same spin to have different spatial orbitals. These have a smaller overlap in space compared to electrons with identical spatial quantum numbers (see figure 2.10b), and therefore have a smaller electrostatic repulsion. For that reason configurations with maximum total spin is preferred. The second rule follows since electrons with same sign of m_l orbit the nuclei "in the same sense" spending more time apart than electrons with m_l's of opposite sign.

The magnetic ions in the material interact with each other through their spin. This is responsible for a coupling term

$$-\sum_{ij} J_{ij} \mathbf{S}_i \cdot \mathbf{S}_j, \tag{2.110}$$

in the Hamiltonian. When J_{ij} is positive the coupling term favors ferromagnetism, but in general J_{ij} may have either sign. Of the several coupling mechanism between magnetic ions we mention the following three.

Direct exchange is an electrostatic effect. When the relative charge of two interacting spins are changed, so is the the spatial distribution of charge. The result is a coupling that can have either sign for J_{ij}, but is very short ranged. It is considered unlikely that direct exchange play a significant role except in very few materials.

Superexchange is a coupling that favors antiferromagnetism. It can act directly between the magnetic ions via a coupling described by an electron from one ion jumping to another, followed by an electron jumping back from this second ion to the first (figure 2.11a) This second order process favors an antiparallel configuration as is immediately illustrated on figure 2.11a, when the jumping electrons are in an s-state. Superexchange can also act in ionic crystals like MnO where nonmagnetic anions are situated between the magnetic ions. Spins of the magnetic cations are coupled indirectly through the intervening anions by a mixing of the outermost cation orbitals with the orbitals in the anion. Only mixing of the same spin is possible (figure 2.11b). Due to the Pauli-principle the anion orbital

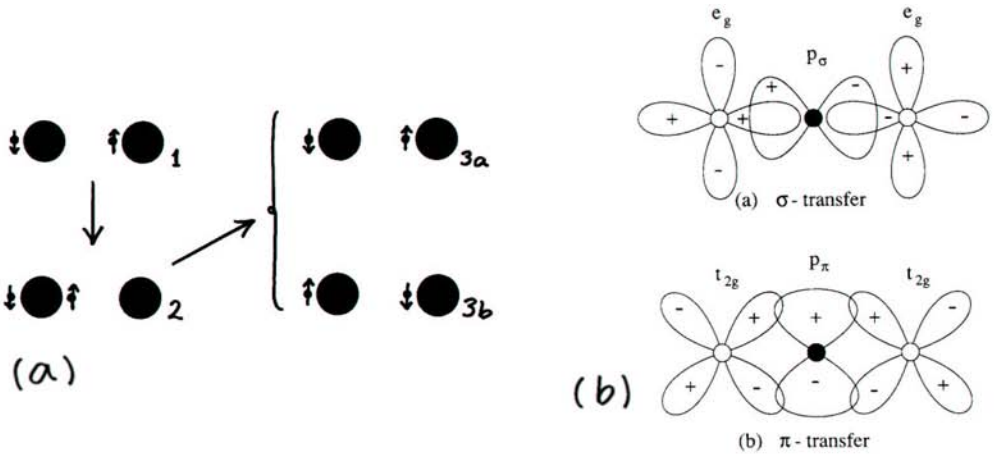

Figure 2.11: (a) Superexchange where an electron jumps from one ion to another, followed by one electron jumping back. If the electrons are in an s-state, then the intermediate state (2) is only possible when the electrons have opposite spin. (b) Superexchange through anion-cation mixing of orbitals. Each loop represents an electron, and only electrons with same spin (+ or -) are allowed to mix. This favors antiferromagnetism as seen in MnO. We shall not go into detail of the two different kinds of superexchange, illustrated by the upper and lower figure.

mixing with one cation has opposite spin to the anion orbital mixing with the other cation, and the process therefore favor an antiferromagnetic configuration. Superexchange is thought to be responsible for the antiferromagnetism of the compound MnO, illustrated in figure 2.12a.

The RKKY coupling is a long range coupling mechanism between localized magnetic moments important in metals and dilute magnetic alloys like CuMn. It is mediated through itinerant conduction electrons (or holes) interacting with the localized magnetic ions. The itinerant electron wave functions are distorted, resulting in a conduction electron spin density that oscillates throughout the crystal. Whether the RKKY coupling favors ferro- or antiferromagnetic behavior depends on the distance between the magnetic ions compared to the wave length of the distorted spin density oscillation. Even an overall spin polarization of the conduction electrons can be caused by the RKKY coupling. This results in a conduction electron dispersion relation resembling the one found by the Stoner model (described below) and is illustrated in figure 2.13. For most materials the conduction electrons are not overall spin-polarized [35], but for diluted magnetic semiconductors like GaMnAs, which are often used in spin-injection experiments (section 3.2.3), the itinerant electrons are often polarized and contribute to the ferromagnetism of these materials [21].

Figure 2.12: (a) The spin configuration of MnO. Mn^{2+} is represented by the filled circles and O^{2-} by the open. (b) The function $(1+\zeta)^{2/3}-(1-\zeta)^{2/3}$ appearing in the Stoner model.

Ferromagnetism of conduction electrons, the Stoner model

The magnetic properties of many real materials can not alone be explained by the presence of magnetic ions. The itinerant electrons sometimes have an overall spin polarization, caused basically by the Pauli principle (as Hund's first rule), that gives a ferromagnetic contribution, and this must be incorporated in the description. We illustrate the effect by considering a simple model, the Stoner model, of interacting electrons in a box with volume $\mathcal{V}$.

So far we have avoided the use of second quantization, but in this section we assume this formulation of quantum mechanics to be well known. We refer the reader to [3, 30] for an easily accessible introduction to second quantization or to [29] for a more detailed description. The Stoner calculations can be done without use of second quantization, see for instance [4], but here we follow the route taken in [3].

The starting point is a simplified Hamiltonian, the Hubbard Hamiltonian, for the electrons

$$H = H_0 + H_{int} = \sum_{\mathbf{k}s} \varepsilon_k c^\dagger_{\mathbf{k}s} c_{\mathbf{k}s} + \frac{U}{2\mathcal{V}} \sum_{\mathbf{k}\mathbf{k}'\mathbf{q}ss'} c^\dagger_{\mathbf{k}+\mathbf{q}s} c^\dagger_{\mathbf{k}'-\mathbf{q}s'} c_{\mathbf{k}'s'} c_{\mathbf{k}s}. \tag{2.111}$$

Here $c^\dagger_{\mathbf{k}s}$ and $c_{\mathbf{k}s}$ are the creation- respectively annihilation operators for electrons in a state with definite wave vector $\mathbf{k}$ and spin s. The number operator is given by $c^\dagger_{\mathbf{k}s} c_{\mathbf{k}s}$, and since $c^\dagger_{\mathbf{k}s}$ and $c_{\mathbf{k}s}$ describe fermions the anti-commutator relation

$$\{c^\dagger_{\mathbf{k}s}, c_{\mathbf{k}'s'}\} = c^\dagger_{\mathbf{k}s} c_{\mathbf{k}'s'} + c_{\mathbf{k}'s'} c^\dagger_{\mathbf{k}s} = \delta_{\mathbf{k}\mathbf{k}'}\delta_{ss'}, \quad \{c_{\mathbf{k}s}, c_{\mathbf{k}'s'}\} = \{c^\dagger_{\mathbf{k}s}, c^\dagger_{\mathbf{k}'s'}\} = 0, \tag{2.112}$$

applies. The second sum in (2.111) is due to the Coulomb interaction between electrons, which for simplicity is taken to be point-like (a delta-function) in real space and therefore is constant in momentum space.

We define the thermal average of any operator, A, as

$$\langle A \rangle = \frac{Tr\{e^{-\beta(H-\mu N)}A\}}{Tr\{e^{-\beta(H-\mu N)}\}} = \frac{\sum \langle \nu | e^{-\beta(H-\mu N)} A | \nu \rangle}{\sum \langle \nu | e^{-\beta(H-\mu N)} | \nu \rangle}, \tag{2.113}$$

where $\beta = (k_B T)^{-1}$, μ is the chemical potential and N is the particle number operator. Introducing the quantum field operators

$$\psi^\dagger_s(\mathbf{r}) = \frac{1}{\mathcal{V}} \sum_{\mathbf{k}} e^{-i\mathbf{k}\cdot\mathbf{r}} c^\dagger_{\mathbf{k}s}, \quad \psi_s(\mathbf{r}) = \frac{1}{\mathcal{V}} \sum_{\mathbf{k}} e^{i\mathbf{k}\cdot\mathbf{r}} c_{\mathbf{k}s}, \tag{2.114}$$

that creates respectively annihilates an electron with spin s in the space point $\mathbf{r}$, we have

$$\langle c^\dagger_{\mathbf{k}s} c_{\mathbf{k}'s'} \rangle = \int d\mathbf{r} \int d\mathbf{r}' e^{-i\mathbf{k}'\cdot\mathbf{r}'} e^{i\mathbf{k}\cdot\mathbf{r}} \langle \psi^\dagger_s(\mathbf{r}) \psi_{s'}(\mathbf{r}') \rangle. \tag{2.115}$$

In a homogenous system without spin-flip mechanisms the thermal averages fulfils

$$\langle \psi^\dagger_s(\mathbf{r}) \psi_{s'}(\mathbf{r}') \rangle = h(\mathbf{r} - \mathbf{r}')\delta_{ss'}, \tag{2.116}$$

and therefore

$$\langle c^\dagger_{\mathbf{k}s} c_{\mathbf{k}'s'} \rangle = \langle n_{\mathbf{k}s} \rangle \delta_{\mathbf{k}\mathbf{k}'}\delta_{ss'} \equiv n_{\mathbf{k}s}\delta_{\mathbf{k}\mathbf{k}'}\delta_{ss'}. \tag{2.117}$$

The next step is to reduce the Coulomb term, H_{int}, in the Hubbard hamiltonian to a sum of $c^\dagger c$ components. We use the mean field approximation, which assumes that the operators $c^\dagger_{\mathbf{k}s} c_{\mathbf{k}'s'}$ deviate only slightly from their thermal averages $\langle c^\dagger_{\mathbf{k}s} c_{\mathbf{k}'s'} \rangle$. If this is the case, then

$$\begin{aligned} c^\dagger_\mu c_{\mu'} c^\dagger_\nu c_{\nu'} &= c^\dagger_\mu c_{\mu'} (c^\dagger_\nu c_{\nu'} - \langle c^\dagger_\nu c_{\nu'} \rangle) + c^\dagger_\mu c_{\mu'} \langle c^\dagger_\nu c_{\nu'} \rangle = (c^\dagger_\mu c_{\mu'} - \langle c^\dagger_\mu c_{\mu'} \rangle)(c^\dagger_\nu c_{\nu'} - \langle c^\dagger_\nu c_{\nu'} \rangle) \\ &+ \langle c^\dagger_\mu c_{\mu'} \rangle (c^\dagger_\nu c_{\nu'} - \langle c^\dagger_\nu c_{\nu'} \rangle) + c^\dagger_\mu c_{\mu'} \langle c^\dagger_\nu c_{\nu'} \rangle = c^\dagger_\mu c_{\mu'} \langle c^\dagger_\nu c_{\nu'} \rangle + \langle c^\dagger_\mu c_{\mu'} \rangle c^\dagger_\nu c_{\nu'} - \langle c^\dagger_\mu c_{\mu'} \rangle \langle c^\dagger_\nu c_{\nu'} \rangle, \end{aligned} \tag{2.118}$$

when we go to linear order in the deviation $c^\dagger c - \langle c^\dagger c\rangle$. Using (2.112) and (2.118), we find that (2.111) in the mean field approximation can be written

$$\begin{aligned} H_{MF} =& \sum_{\mathbf{k}s} \varepsilon_k c^\dagger_{\mathbf{k}s} c_{\mathbf{k}s} + \frac{U}{2\mathcal{V}} {\sum}' c^\dagger_{\mathbf{k}+\mathbf{q}s} c_{\mathbf{k}s} c^\dagger_{\mathbf{k}'-\mathbf{q}s'} c_{\mathbf{k}'s'} - \frac{U}{2\mathcal{V}} {\sum}'' c^\dagger_{\mathbf{k}+\mathbf{q}s} c_{\mathbf{k}'s'} c^\dagger_{\mathbf{k}'-\mathbf{q}s'} c_{\mathbf{k}s} = \sum_{\mathbf{k}s} \varepsilon_k c^\dagger_{\mathbf{k}s} c_{\mathbf{k}s} \\ &+ \frac{U}{2\mathcal{V}} {\sum}' \left[c^\dagger_{\mathbf{k}+\mathbf{q}s} c_{\mathbf{k}s} \langle c^\dagger_{\mathbf{k}'-\mathbf{q}s'} c_{\mathbf{k}'s'}\rangle + \langle c^\dagger_{\mathbf{k}+\mathbf{q}s} c_{\mathbf{k}s}\rangle c^\dagger_{\mathbf{k}'-\mathbf{q}s'} c_{\mathbf{k}'s'} - \langle c^\dagger_{\mathbf{k}+\mathbf{q}s} c_{\mathbf{k}s}\rangle \langle c^\dagger_{\mathbf{k}'-\mathbf{q}s'} c_{\mathbf{k}'s'}\rangle \right] \\ &- \frac{U}{2\mathcal{V}} {\sum}'' \left[c^\dagger_{\mathbf{k}+\mathbf{q}s} c_{\mathbf{k}'s'} \langle c^\dagger_{\mathbf{k}'-\mathbf{q}s'} c_{\mathbf{k}s}\rangle + \langle c^\dagger_{\mathbf{k}+\mathbf{q}s} c_{\mathbf{k}'s'}\rangle c^\dagger_{\mathbf{k}'-\mathbf{q}s'} c_{\mathbf{k}s} - \langle c^\dagger_{\mathbf{k}+\mathbf{q}s} c_{\mathbf{k}'s'}\rangle \langle c^\dagger_{\mathbf{k}'-\mathbf{q}s'} c_{\mathbf{k}s}\rangle \right], \end{aligned} \tag{2.119}$$

where $\sum'$ is a sum over $\mathbf{k}, \mathbf{k}', \mathbf{q}, s, s'$ under the condition that $(\mathbf{k}, s) \neq (\mathbf{k}'-\mathbf{q}, s')$, and $\sum''$ under the condition $(\mathbf{k}, s) = (\mathbf{k}'-\mathbf{q}, s')$.

Introducing the mean field parameters (2.117) and defining the spin dependent densities

$$n_s = \frac{1}{\mathcal{V}} \sum_{\mathbf{k}} \langle c^\dagger_{\mathbf{k}s} c_{\mathbf{k}s}\rangle, \tag{2.120}$$

we write (2.119) as

$$H_{MF} = \sum_{\mathbf{k}s} E_{\mathbf{k}s} c^\dagger_{\mathbf{k}s} c_{\mathbf{k}s} - \frac{U\mathcal{V}}{2} \sum_{ss'} n_s n_{s'} + \frac{U\mathcal{V}}{2} \sum_s n_s^2, \tag{2.121}$$

where the spin dependant energy, $E_{\mathbf{k}s}$, is given as

$$E_{\mathbf{k}s} = \varepsilon_k + U n_{-s}. \tag{2.122}$$

Minimizing the energy gives

$$\frac{\partial \langle H_{MF}\rangle}{\partial n_{-s}} = 0 \Rightarrow n_s = \frac{1}{\mathcal{V}} \sum_k \langle c^\dagger_{\mathbf{k}s} c_{\mathbf{k}s}\rangle_{MF} = \frac{1}{\mathcal{V}} \sum_k f_{FD}(E_{\mathbf{k}s} - \mu). \tag{2.123}$$

Now, at zero temperature, $f_{FD}(E_{\mathbf{k}s} - \mu) = \theta(\varepsilon_{Fs} - \varepsilon_k)$, where the spin dependant Fermi energy $\varepsilon_{Fs} = \mu - U n_{-s}$. This means that we have two coupled self-consistent equations

$$n_s = \int \frac{d\mathbf{k}}{(2\pi)^3} \theta(\varepsilon_{Fs} - \varepsilon_k) = \frac{1}{6\pi^2} k_{Fs}^3, \tag{2.124}$$

where

$$\frac{\hbar^2 k_{Fs}^2}{2m} + U n_{-s} = \mu. \tag{2.125}$$

We insert k_{Fs} from (2.124) in (2.125) and find

$$\frac{\hbar^2}{2m} (6\pi^2 n_s)^{2/3} + U n_{-s} = \mu \Rightarrow n_\uparrow^{2/3} - n_\downarrow^{2/3} = \frac{2mU}{\hbar^2} (6\pi^2)^{-2/3} (n_\uparrow - n_\downarrow). \tag{2.126}$$

Defining the quantities

$$\zeta = \frac{n_\uparrow - n_\downarrow}{n}, \quad \gamma = \frac{2mU n^{1/3}}{(3\pi^2)^{2/3}\hbar^2}, \quad n = n_\uparrow + n_\downarrow, \tag{2.127}$$

we write the last equation in (2.126) as

$$\gamma\zeta = (1+\zeta)^{2/3} - (1-\zeta)^{2/3}. \tag{2.128}$$

There are three types of solutions to this equation (see figure 2.12 and figure 2.13). When $\gamma < 4/3$ then $\zeta = 0$ and the electron gas is in a normal unpolarized state. The system is weakly ferromagnetic when

$4/3 < \gamma < 2^{2/3}$, since in this case the spin density is partially polarized ($0 < \zeta < 1$). When $\gamma > 2^{2/3}$ the system is strongly ferromagnetic since the spin density is fully polarized ($\zeta = 1$).

The spin polarization is illustrated in figure 2.13, showing the dispersion relation, $E_{\mathbf{k}s}$, corresponding to the three principal solutions to the Stoner model.

Figure 2.13: The three different types of solutions in the Stoner model.

2.6 Linear response and the Kubo formula

Consider a system with a time dependent Hamiltonian

$$H(t) = H_0 + H'(t)\theta(t), \tag{2.129}$$

where H_0 is constant in time, and $H'(t)$ is a small perturbation turned on at time $t = 0$. From statistical physics it is known that the thermal average of an operator, A, is given by

$$\langle A(t)\rangle = Tr\{\rho(t)A\}, \tag{2.130}$$

with the density operator, ρ, for the systems we consider being

$$\rho = \frac{e^{-\beta(H-\mu N)}}{Tr\{e^{-\beta(H-\mu N)}\}}. \tag{2.131}$$

Here N is the particle number operator and μ the chemical potential. From quantum mechanics we know that the density operator fulfil the equation of motion

$$i\hbar\frac{\partial\rho}{\partial t} = [H, \rho]. \tag{2.132}$$

It is convenient to introduce the interaction picture where states and operators are defined from their Schrődinger counterparts as

$$|\hat{\psi}(t)\rangle = e^{\frac{i}{\hbar}H_0 t}|\psi(t)\rangle, \tag{2.133}$$

$$\hat{A}(t) = e^{\frac{i}{\hbar}H_0 t}Ae^{-\frac{i}{\hbar}H_0 t}. \tag{2.134}$$

The 'hat' is applied to mark states and operators in the interaction picture while states and operators without a 'hat' originate from the Schrődinger picture.

Defining the density operator, $\hat{\rho}$, in the interaction picture

$$\hat{\rho}(t) = e^{\frac{i}{\hbar}H_0 t}\rho(t)e^{-\frac{i}{\hbar}H_0 t}, \tag{2.135}$$

we get that

$$\frac{\partial \rho(t)}{\partial t} = \frac{\partial}{\partial t}\left(e^{-\frac{i}{\hbar}H_0 t}\hat{\rho}(t)e^{\frac{i}{\hbar}H_0 t}\right) = -\frac{i}{\hbar}e^{-\frac{i}{\hbar}H_0 t}[H_0, \hat{\rho}(t)]e^{\frac{i}{\hbar}H_0 t} + e^{-\frac{i}{\hbar}H_0 t}\frac{\partial \hat{\rho}(t)}{\partial t}e^{\frac{i}{\hbar}H_0 t}. \tag{2.136}$$

Comparing (2.132) and (2.136) we find

$$i\hbar\frac{\partial \hat{\rho}(t)}{\partial t} = e^{\frac{i}{\hbar}H_0 t}[H(t), \rho(t)]e^{-\frac{i}{\hbar}H_0 t} - [H_0, \hat{\rho}(t)] = [\hat{H}'(t), \hat{\rho}(t)], \tag{2.137}$$

after using that $1 = e^{-\frac{i}{\hbar}H_0 t}e^{\frac{i}{\hbar}H_0 t}$ and $\hat{H}_0 = H_0$. Defining

$$\rho_0 \equiv \frac{e^{-\beta(H_0-\mu N)}}{Tr\{e^{-\beta(H_0-\mu N)}\}} = \rho(t=0) = \hat{\rho}(t=0), \tag{2.138}$$

we have

$$\hat{\rho}(t) = \rho_0 - \frac{i}{\hbar}\int_0^t dt'[\hat{H}'(t'), \hat{\rho}(t')]. \tag{2.139}$$

In linear response, (2.139) is solved to linear order in the perturbation, H', and we have

$$\hat{\rho}(t) = \rho_0 - \frac{i}{\hbar}\int_0^t dt'[\hat{H}'(t'), \rho_0], \tag{2.140}$$

giving

$$\rho(t) = \rho_0 - \frac{i}{\hbar}e^{-\frac{i}{\hbar}H_0 t}\int_0^t dt'[\hat{H}'(t'), \rho_0]e^{\frac{i}{\hbar}H_0 t}. \tag{2.141}$$

Using (2.130), (2.141) and the well known rule

$$Tr\{A_1 A_2 \dots A_n\} = Tr\{A_n A_1 \dots A_{n-1}\} = \dots = Tr\{A_2 A_3 \dots A_1\}, \tag{2.142}$$

we find

$$\langle A(t)\rangle = Tr\{\rho(t)A\} = Tr\{\rho_0 A\} - \frac{i}{\hbar}Tr\left\{\hat{A}(t)\int_0^t dt'[\hat{H}'(t'), \rho_0]\right\} = \langle A\rangle_0 - \frac{i}{\hbar}\int_0^t dt'\langle[\hat{A}(t'), \hat{H}'(t')]\rangle_0. \tag{2.143}$$

Here the notation

$$\langle A\rangle_0 = Tr\{\rho_0 A\}, \tag{2.144}$$

is introduced for the thermal expectation value in the unperturbed system. Defining $\delta\langle A(t)\rangle$ as the deviation from the unperturbed value, we find the Kubo formula expressing that the linear response of $\langle A\rangle$ to the perturbation, H', is

$$\delta\langle A(t)\rangle = \langle A(t)\rangle - \langle A\rangle_0 = \int_0^\infty dt' G^R_{AH'}(t,t')e^{-\eta(t-t')}, \tag{2.145}$$

with the retarded Greens function, $G^R_{AH'}$, defined as

$$G^R_{AH'}(t,t') = -\frac{i}{\hbar}\theta(t-t')\langle[\hat{A}(t), \hat{H}'(t')]\rangle_0. \tag{2.146}$$

The infinitesimal positive parameter, η, introduced in (2.145) is a mathematical artifact included so that the response behaves physically correct, i.e. decays for times $t \gg 0$. At the end of calculations η is removed from all expressions by taking the limit $\eta \to 0_+$.

2.6.1 The polarizability

For a system with a weak applied electric field there is a linear connection between the Fourier components of the induced charge density, ρ_{ind}, and the external potential, ϕ_{ext}. This is written as

$$\rho_{ind}(\mathbf{q},\omega) = \chi(\mathbf{q},\omega)\phi_{ext}(\mathbf{q},\omega), \tag{2.147}$$

where χ is called the polarizability. The polarizability is not identical to the susceptibility defined by (2.68), even though (2.147) often in the literature also is named the susceptibility. In this thesis the polarizability is χ defined by (2.147), and the susceptibility is χ defined by (2.68).

Let $\rho(\mathbf{r},t) \equiv \rho_{tot}(\mathbf{r},t)$ be the total charge density. A weak external field that is applied will cause a perturbation term

$$H'(t) = \int d\mathbf{r}\rho(\mathbf{r},t)\phi_{ext}(\mathbf{r},t), \tag{2.148}$$

in the Hamiltonian. Inserting (2.148) into the Kubo formula (2.145) gives

$$\rho_{ind}(\mathbf{r},t) = \delta\langle\rho(\mathbf{r},t)\rangle = \int d\mathbf{r}' \int_0^\infty dt' G^R_{\rho\rho}(\mathbf{r}t,\mathbf{r}'t')e^{-\eta(t-t')}\phi_{ext}(\mathbf{r}',t'), \tag{2.149}$$

and comparing with (2.147) after a certain amount of Fourier transforming, we find that the polarizability is given by

$$\chi(\mathbf{r}t,\mathbf{r}'t') = G^R_{\rho\rho}(\mathbf{r}t,\mathbf{r}'t') = -\frac{i}{\hbar}\theta(t-t')\langle[\hat{\rho}(\mathbf{r},t),\hat{\rho}(\mathbf{r}',t')]\rangle_0, \tag{2.150}$$

i.e. the charge-charge Greens (or correlation) function.

The connection between the polarizability function, χ, and the relative permittivity, ε_r, can easily be found. Knowing the induced charge density, $\rho_{ind}(\mathbf{r},t)$, we use (2.149) and find that

$$\phi_{ind}(\mathbf{r},t) = \int d\mathbf{r}' V(\mathbf{r}-\mathbf{r}')\rho_{ind}(\mathbf{r}',t) = \int d\mathbf{r}' \int d\mathbf{r}'' \int dt' V(\mathbf{r}-\mathbf{r}')\chi(\mathbf{r}'t,\mathbf{r}''t')\phi_{ext}(\mathbf{r}'',t'), \tag{2.151}$$

where

$$V(\mathbf{r}) = \frac{1}{4\pi\varepsilon_0 r}, \tag{2.152}$$

is the unscreened Coulomb potential. This means that

$$\phi_{tot}(\mathbf{r},t) = \phi_{ext}(\mathbf{r},t) + \phi_{ind}(\mathbf{r},t) = \phi_{ext}(\mathbf{r},t) + \int d\mathbf{r}' \int d\mathbf{r}'' \int dt' V(\mathbf{r}-\mathbf{r}')\chi(\mathbf{r}'t,\mathbf{r}''t')\phi_{ext}(\mathbf{r}'',t'), \tag{2.153}$$

which in Fourier space becomes

$$\phi_{tot}(\mathbf{q},\omega) = \left(1 + V(\mathbf{q})\chi(\mathbf{q},\omega)\right)\phi_{ext}(\mathbf{q},\omega). \tag{2.154}$$

Comparing (2.154) with (2.80) the connection between the polarizability, χ, and the relative permittivity, ε_r, is found to be

$$\varepsilon_r(\mathbf{q},\omega) = \frac{1}{1 + V(\mathbf{q})\chi(\mathbf{q},\omega)}. \tag{2.155}$$

In condensed matter physics an often used approximation, the Random Phase Approximation (RPA), ties the polarizability, χ, together with the polarizability, χ^0, of a free electron gas, via

$$\chi^{RPA}(\mathbf{q},\omega) = \frac{\chi^0(\mathbf{q},\omega)}{1 - V(q)\chi^0(\mathbf{q},\omega)}. \tag{2.156}$$

To show (2.156) rigorously one uses quantum field theoretical calculations, illustrated by the Feynmann diagram in figure 2.14. Feynmann diagrams are developed in quantum field theory and is a diagrammatical representation of the integrals and Greens functions that arise in the theory. They often have pleasing physical interpretations, but we will not investigate this further.

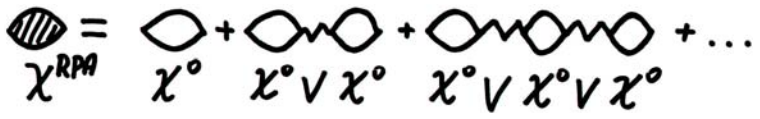

Figure 2.14: Feynmann diagram where the RPA polarizability, χ^{RPA}, (the filled bobble), is approximated by the non-interacting polarizability, χ_0, (the open bobbles) connected by the unscreened Coulomb interaction V (the wiggled lines).

Instead we show (2.156) using the following considerations. We have already stated (2.147) expressing that the electrons in the gas react to the external field. Here the mutual electron-electron interactions are taken into account by the polarizability χ. Another way of expressing the same situation would be to include the electron-electron interactions into the field, thus replacing the external potential, ϕ_{ext}, with the total field, ϕ_{tot}, and write

$$\rho_{ind}(\mathbf{q},\omega) = \chi^0(\mathbf{q},\omega)\phi_{tot}(\mathbf{q},\omega). \tag{2.157}$$

Since the electron-electron interactions are taken into account by $\phi_{tot}(\mathbf{q},\omega)$, the quantity $\chi^0(\mathbf{q},\omega)$ must be the polarizability of the free electron gas. Now it is simple, using (2.83) and 2.155, to see that

$$\rho_{ind} = \chi^0(1+V\chi)\phi_{ext}, \tag{2.158}$$

which compared with (2.147) gives

$$\chi = \chi^0(1+V\chi), \tag{2.159}$$

which is equivalent to (2.156).

Inserting (2.156) into (2.155) gives the RPA result

$$\varepsilon_r^{RPA}(\mathbf{q},\omega) = \frac{1}{1+V(\mathbf{q})\chi^{RPA}(\mathbf{q},\omega)} = 1 - V(\mathbf{q},\omega)\chi^0(\mathbf{q},\omega), \tag{2.160}$$

which is often used in calculations.

2.6.2 The Lindhard function

The polarizability function, χ^0, in a gas of non-interacting electrons can be calculated using either time dependent perturbation theory or the second quantization formulation of quantum mechanics. We shall not go through all the details, but will sketch the main points following the derivation found in [3] using second quantization. The result is expressed by an often encountered function called the Lindhard function or Lindhard polarizability.

The second quantized Hamiltonian for a gas of non-interacting electrons can be written

$$H = \sum_{\mathbf{k}s} \varepsilon_{\mathbf{k}s} c^\dagger_{\mathbf{k}s} c_{\mathbf{k}s} \tag{2.161}$$

where $c^\dagger_{\mathbf{k}s}$ and $c_{\mathbf{k}s}$ are the Schrődinger creation- respectively annihilation operators introduced in section 2.5.2. Since $c_{\mathbf{k}s}(t) = e^{\frac{i}{\hbar}Ht} c_{\mathbf{k}s} e^{-\frac{i}{\hbar}Ht}$ and $\partial_t c_{\mathbf{k}s} = 0$, we find that

$$\dot{c}_{\mathbf{k}s}(t) = \frac{i}{\hbar} e^{\frac{i}{\hbar}Ht}[H, c_{\mathbf{k}s}] e^{-\frac{i}{\hbar}Ht}. \tag{2.162}$$

Using (2.112) and the commutator relation, $[AB,C] = A\{B,C\} - \{A,C\}B$, we have

$$[H, c_{\mathbf{k}s}] = \sum_{\mathbf{k}'s'} \varepsilon_{\mathbf{k}'s'} [c^\dagger_{\mathbf{k}'s'} c_{\mathbf{k}'s'}, c_{\mathbf{k}s}] = \sum_{\mathbf{k}'s'} \varepsilon_{\mathbf{k}'s'} (c^\dagger_{\mathbf{k}'s'} \{c_{\mathbf{k}'s'}, c_{\mathbf{k}s}\} - \{c_{\mathbf{k}'s'\dagger}, c_{\mathbf{k}s}\} c_{\mathbf{k}'s'}) = -\varepsilon_{\mathbf{k}s} c_{\mathbf{k}s}, \tag{2.163}$$

which inserted in (2.162) shows

$$c_{\mathbf{k}s}(t) = e^{-\frac{i}{\hbar}\varepsilon_{\mathbf{k}s} t} c_{\mathbf{k}s}, \tag{2.164}$$

and also, taking the hermitian conjugate of (2.164), that

$$c^\dagger_{\mathbf{k}s}(t) = e^{\frac{i}{\hbar}\varepsilon_{\mathbf{k}s} t} c^\dagger_{\mathbf{k}s}. \tag{2.165}$$

Introducing the quantum field operators given by (2.114) and the spin, we immediately can write the charge operator as

$$\rho_s(\mathbf{r}, t) = -e \int d\mathbf{r} \psi^\dagger_s(\mathbf{r}, t) \psi_s(\mathbf{r}, t), \tag{2.166}$$

which has the Fourier transform

$$\rho_s(\mathbf{q}, t) = -e \sum_{\mathbf{k}} c^\dagger_{\mathbf{k}s}(t) c_{\mathbf{k}+\mathbf{q}s}(t) = -e \sum_{\mathbf{k}} c^\dagger_{\mathbf{k}s} c_{\mathbf{k}+\mathbf{q}s} e^{\frac{i}{\hbar}(\varepsilon_{\mathbf{k}s} - \varepsilon_{\mathbf{k}+\mathbf{q}s})t}. \tag{2.167}$$

Using (2.167) it is straightforward to show that the Fourier transform of (2.150) can be written as

$$\chi^0_s(\mathbf{q}, t - t') = -\frac{i}{\hbar(2\pi)^d} \theta(t - t') \langle [\rho_s(\mathbf{q}, t), \rho_s(-\mathbf{q}, t')] \rangle_0, \tag{2.168}$$

where d is the dimension of the non-interacting electron gas. From (2.168), the commutator relation $[c^\dagger_\nu c_\mu, c^\dagger_{\nu'} c_{\mu'}] = c^\dagger_\nu c_{\mu'} \delta_{\mu,\nu'} - c^\dagger_{\nu'} c_\mu \delta_{\mu',\nu}$, and $\langle c^\dagger_{\mathbf{k}s} c_{\mathbf{k}s} \rangle = f^0_s(\mathbf{k})$, we then find that

$$\begin{aligned} \chi^0_s(\mathbf{q}, \omega) =& -\frac{ie^2}{\hbar} \int_{t'}^{\infty} dt e^{i\omega(t-t')} \int \frac{d\mathbf{k}}{(2\pi)^d} (f^0_s(\mathbf{k}) - f^0_s(\mathbf{k}+\mathbf{q})) e^{\frac{i}{\hbar}(\varepsilon_{\mathbf{k}s} - \varepsilon_{\mathbf{k}+\mathbf{q}s})(t-t')} e^{-\frac{\eta}{\hbar}(t-t')} \\ =& e^2 \lim_{\eta \to 0_+} \int \frac{d\mathbf{k}}{(2\pi)^d} \frac{f^0_s(\mathbf{k}) - f^0_s(\mathbf{k}+\mathbf{q})}{\varepsilon_{\mathbf{k}s} - \varepsilon_{\mathbf{k}+\mathbf{q}s} + \hbar\omega + i\eta} \equiv -e^2 \chi^{lind}_s(\mathbf{q}, \omega), \end{aligned} \tag{2.169}$$

The sign in the definition of the Lindhard function, $\chi^{lind}_s(\mathbf{q}, \omega)$, is a matter of choice, and both possibilities are found in the literature. Here we define the Lindhard function as

$$\chi^{lind}_s(\mathbf{q}, \omega) = \lim_{\eta \to 0_+} \int \frac{d\mathbf{k}}{(2\pi)^d} \frac{f^0_s(\mathbf{k}+\mathbf{q}) - f^0_s(\mathbf{k})}{\varepsilon_{\mathbf{k}s} - \varepsilon_{\mathbf{k}+\mathbf{q}s} + \hbar\omega + i\eta}, \tag{2.170}$$

and note that the Lindhard function and the polarizability have opposite signs. In the rest of this thesis we write the Lindhard function as $\chi_s(\mathbf{q}, \omega)$ or $\chi(\mathbf{q}, \omega)$ instead of $\chi^{lind}_s(\mathbf{q}, \omega)$.

2.6.3 The zero temperature Lindhard function

We want to calculate, at T=0K, the imaginary part of the Lindhard function given in (2.155) in respectively a 3DEG and a 2DEG. Suppressing the spin index, we summarize the results in the following proposition.

PROPOSITION 2.6.1 *The imaginary part of the zero temperature Lindhard function in a 3DEG is given by*

$$Im\chi(q,\omega)=\begin{cases}-Im\chi(q,-\omega) \quad for\ \omega<0,\\ \\ \frac{m^2}{4\pi\hbar^3}\frac{\omega}{q} \quad for\ q<2k_F,\ 0<\omega<qv_F(1-q/2k_F),\\ \frac{m}{8\pi\hbar^2 q}\left[k_F^2-(\frac{m}{\hbar^2 q})^2(\hbar\omega-\varepsilon_q)^2\right] \quad for\ q<2k_F,\ qv_F(1-q/2k_F)<\omega<qv_F(1+q/2k_F),\\ \frac{m}{8\pi\hbar^2 q}\left[k_F^2-(\frac{m}{\hbar^2 q})^2(\hbar\omega-\varepsilon_q)^2\right] \quad for\ q>2k_F,\ qv_F(-1+q/2k_F)<\omega<qv_F(1+q/2k_F),\\ 0 \quad otherwise.\end{cases} \tag{2.171}$$

The imaginary part of the zero temperature Lindhard function in a 2DEG is given by

$$Im\chi(q,\omega)=\begin{cases}-Im\chi(q,-\omega) \quad for\ \omega<0,\\ \\ \frac{mk_F}{2\pi\hbar^2 q}\left[\sqrt{1-\left(\frac{\omega}{v_F q}-\frac{q}{2k_F}\right)^2}-\sqrt{1-\left(\frac{\omega}{v_F q}+\frac{q}{2k_F}\right)^2}\right] \quad for\ q<2k_F,\ 0<\omega<qv_F(1-q/2k_F),\\ \frac{mk_F}{2\pi\hbar^2 q}\sqrt{1-\left(\frac{\omega}{v_F q}-\frac{q}{2k_F}\right)^2} \quad for\ q<2k_F,\ qv_F(1-q/2k_F)<\omega<qv_F(1+q/2k_F),\\ \frac{mk_F}{2\pi\hbar^2 q}\sqrt{1-\left(\frac{\omega}{v_F q}-\frac{q}{2k_F}\right)^2} \quad for\ q>2k_F,\ qv_F(-1+q/2k_F)<\omega<qv_F(1+q/2k_F),\\ 0 \quad otherwise.\end{cases} \tag{2.172}$$

PROOF. We omit the proof of the two dimensional result (2.172) and only prove the 3 dimensional case (2.171). Since

$$\lim_{\eta\to 0_+}\mathrm{Im}\left(\frac{1}{x+i\eta}\right)=-\pi\delta(x), \tag{2.173}$$

then the imaginary part of (2.170) can be written as

$$\mathrm{Im}\chi(q,\omega)=\frac{1}{8\pi^2}\int d\mathbf{k}[f^0(\varepsilon_{\mathbf{k}})-f^0(\varepsilon_{\mathbf{k+q}})]\delta(\varepsilon_{\mathbf{k}}-\varepsilon_{\mathbf{k+q}}+\hbar\omega). \tag{2.174}$$

Using that $f^0(\varepsilon_k)=f^0(\varepsilon_{-k})$ we change the variable $\mathbf{k}\to-\mathbf{k}-\mathbf{q}$ in the second term in (2.174) corresponding to $f^0(\varepsilon_{\mathbf{k+q}})\to f^0(\varepsilon_k)$. Since at T=0K the Fermi-Dirac distribution $f^0(\varepsilon_k)=\theta(k_F-k)$ we get that

$$\begin{aligned}\mathrm{Im}\chi(q,\omega)&=\frac{1}{8\pi^2}\int d\mathbf{k}f^0(\varepsilon_k)[\delta(\varepsilon_k-\varepsilon_{\mathbf{k+q}}+\hbar\omega)-\delta(\varepsilon_k-\varepsilon_{\mathbf{k+q}}-\hbar\omega)]\\ &=\frac{1}{4\pi}\int_0^\infty dkk^2f^0(\varepsilon_k)\int_{-1}^1 d\nu[\delta(\varepsilon_q+\frac{\hbar^2kq\nu}{m}-\hbar\omega)-\delta(\varepsilon_q+\frac{\hbar^2kq\nu}{m}+\hbar\omega)]\\ &=\frac{1}{4\pi}\int_0^{k_F}dkk^2\int_{-1}^1 d\nu[\delta(\varepsilon_q+\frac{\hbar^2kq\nu}{m}-\hbar\omega)-\delta(\varepsilon_q+\frac{\hbar^2kq\nu}{m}+\hbar\omega)],\end{aligned} \tag{2.175}$$

where $\nu = \cos\theta$ is the angle between $\mathbf{k}$ and $\mathbf{q}$. From (2.175) it is obvious that

$$\mathrm{Im}\chi(q,\omega) = -\mathrm{Im}\chi(q,-\omega), \tag{2.176}$$

and it is therefore only necessary to calculate $\mathrm{Im}\chi(q,\omega)$ for $\omega > 0$.
Using that $k \geq 0$ we find that

$$\begin{aligned}\exists \nu \in [-1,1]:\ \varepsilon_q + \frac{\hbar^2 kq\nu}{m} \pm \hbar\omega = 0 \Leftrightarrow \exists \nu \in [-1,1]:\ \nu k = \mp\frac{m}{\hbar^2 q}(\hbar\omega \pm \varepsilon_q)\\ \Leftrightarrow k \geq \frac{m}{\hbar^2 q}|\hbar\omega \pm \varepsilon_q| \equiv k_\pm,\end{aligned} \tag{2.177}$$

and so

$$\int_{-1}^{1} d\nu \delta(\varepsilon_q + \frac{\hbar^2 kq\nu}{m} \pm \hbar\omega) = \frac{m}{\hbar^2 kq}\theta(k - k_\pm), \tag{2.178}$$

where

$$k_\pm = \frac{m}{\hbar^2 q}|\hbar\omega \pm \varepsilon_q|. \tag{2.179}$$

Using (2.178) in (2.175) we find that

$$\begin{aligned}\mathrm{Im}\chi(q,\omega) &= \frac{1}{4\pi}\int_0^{k_F} dk k^2 \frac{m}{\hbar^2 kq}\big[\theta(k-k_-) - \theta(k-k_+)\big]\\ &= \frac{m}{8\pi\hbar^2 q}\big[(k_F^2 - k_-^2)\theta(k_F - k_-) - (k_F^2 - k_+^2)\theta(k_F - k_+)\big].\end{aligned} \tag{2.180}$$

In the following we assume that $\omega > 0$ and evaluate $\mathrm{Im}\chi(q,\omega)$ for different combinations of q and ω. We note

- $k_F > k_+ \Leftrightarrow k_F > \frac{m}{\hbar^2 q}(\hbar\omega + \varepsilon_q) \Leftrightarrow qv_F - \varepsilon_q > \hbar\omega > 0,$ (2.181)
- $k_F > k_- \Leftrightarrow k_F^2 > k_-^2 \Leftrightarrow \varepsilon_q + qv_F > \hbar\omega > \max\{\varepsilon_q - qv_F, 0\}.$ (2.182)

Since $\varepsilon_q \gtrless qv_F \Leftrightarrow q \gtrless 2k_F$ it is easily seen that

$$\begin{aligned}&\bullet\ q < 2k_F \begin{cases} k_F > k_- \text{ for } \varepsilon_q + qv_F < \hbar\omega < 0, \\ k_F > k_+ \text{ for } qv_F - \varepsilon_q > \hbar\omega > 0 \end{cases},\\ &\bullet\ q > 2k_F \begin{cases} k_F > k_- \text{ for } \varepsilon_q + qv_F > \hbar\omega > \varepsilon - qv_F \\ k_+ > k_F \text{ for } \hbar\omega > 0 \end{cases}.\end{aligned} \tag{2.183}$$

Using that

$$\mathrm{Im}\chi(q,\omega) = \frac{m}{8\pi\hbar^2 q}\big[(k_F^2 - k_-^2) - (k_F^2 - k_+^2)\big] = \frac{m}{8\pi\hbar^2 q}\big[k_+^2 - k_-^2\big] = \frac{m^2}{4\pi\hbar^3}\frac{\omega}{q}, \tag{2.184}$$

when $k_F > k_+ > k_-$ and

$$\mathrm{Im}\chi(q,\omega) = \frac{m}{8\pi\hbar^2 q}\big[k_F^2 - k_-^2\big] = \frac{m}{8\pi\hbar^2 q}\big[k_F^2 - (\frac{m}{\hbar^2 q})^2(\hbar\omega - \varepsilon_q)^2\big], \tag{2.185}$$

when $k_+ > k_F > k_-$, proves (2.171).

In chapter 4 we use the low-frequency Lindhard function to evaluate the drag rates in respectively a 2DEG and a 3DEG. The three dimensional low-frequency Lindhard function, valid for $q \ll 2k_F$, is given in (2.171) as

$$\mathrm{Im}\chi(q,\omega) = \frac{m^2}{4\pi\hbar^3}\frac{\omega}{q}. \tag{2.186}$$

The two dimensional low-frequency Lindhard function, for $q \ll 2k_F$, is found, using

$$\sqrt{1-\left(\frac{\omega}{v_F q} \pm \frac{q}{2k_F}\right)^2} \approx 1 - \frac{1}{2}\left(\frac{\omega}{v_F q} \pm \frac{q}{2k_F}\right)^2 = 1 - \frac{1}{2}\left(\left(\frac{\omega}{v_F q}\right)^2 \pm \frac{\omega}{v_F k_F} + \left(\frac{q}{2k_F}\right)^2\right), \tag{2.187}$$

in (2.172), to be

$$\mathrm{Im}\chi(q,\omega) = \frac{m^2\omega}{2\pi\hbar^3 q k_F}. \tag{2.188}$$

2.7 The two dimensional electron gas

Naively, one may think that two dimensional structures in a three dimensional world are always approximative constructions in the sense "very thin three dimensional structures", but this is not the case. A physical system has as many dimensions as it has independent generalized coordinates (to use a word from classical mechanics) and often has properties that can not be explained by taking the limit of any appropriate 3D properties.

The nature of a "true" 2DEG originate from the quantization of energy levels and can be illustrated by the quantum mechanical case of a particle in a box with sides L_x, L_y and L_z. Elementary quantum mechanics tell us that the energies and wave-functions are given by

$$\psi_{n_x n_y n_z}(x,y,z) = \sqrt{\frac{8}{L_x L_y L_z}}\sin(\frac{n_x\pi x}{L_x})\sin(\frac{n_y\pi y}{L_y})\sin(\frac{n_z\pi z}{L_z}), \tag{2.189}$$

$$\varepsilon_{n_x n_y n_z} = \frac{\hbar^2}{8m}(\frac{n_x^2}{L_x^2} + \frac{n_y^2}{L_y^2} + \frac{n_z^2}{L_z^2}) \qquad , \; n_x, n_y, n_z = 1, 2\ldots \tag{2.190}$$

Seemingly this constitutes a three dimensional system, since it takes 3 independent generalized coordinates (or quantum numbers), n_x, n_y and n_z, to describe the state $\psi_{n_x n_y n_z}$, but this is not always the case. Suppose that $L_z \ll L_x, L_y$ and the energy, E, of the particle fulfils that

$$\frac{\hbar^2}{8mL_z^2} < E < \frac{4\hbar^2}{8mL_z^2},$$

then it is obvious that $n_z = 1$ and the system is at most two dimensional. In this fashion it is possible to create true two-, one- and even zero-dimensional electron systems. In the following sections we will consider the construction and the physics behind some of the structures used to create a 2DEG.

2.7.1 The field effect transistor

All the structures we have in mind are related to the field effect transistor (FET), which is a class of widely used semiconductor components where the active region is a 2DEG.

The basic principle in a field effect transistor is that of a simple capacitor. When a voltage, V, is imposed upon the capacitor there will be a positive charge, $Q = CV$, on one plate and a negative charge, $-Q$,

consisting of electrons on the other. The idea in a FET is to use the electrons on the negative charged "plate" as a current channel, i.e. to drive a current in the plane of this plate. The amount of electrons (the effect) in this channel is controlled by the voltage applied between the positive plate (the gate) and the negative plate (the channel). The channel electrons can, depending on the gate voltage, constitute a true 2DEG.

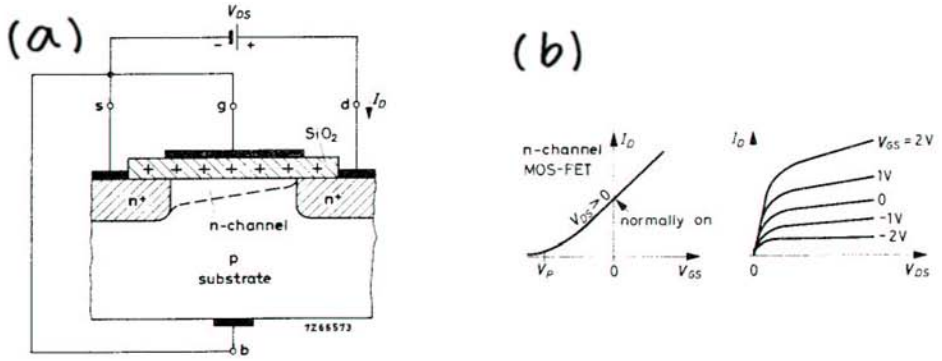

Figure 2.15: (a) Schematic cross-section through a MOSFET. (b) Example of the I-V characteristics of a field effect transistor.

One of the most used FET's in the industry is the Si MOSFET (metal oxide semiconductor FET) sketched in figure 2.15a. Silicon-oxide is a fairly good insulating material compared to the Si-substrate, so when a positive voltage, V_{GS}, is applied to the gate, an electron density is build up at the Si/SiO_2 interface, forming a 2DEG. There are different types of MOSFET's, the one pictured in figure 2.15a where a conducting channel is present even in the absence of a gate voltage is called a depletion type FET.

2.7.2 GaAs/AlGaAs heterostructures

The structures used in physical experiments are usually not Si MOSFET's, but rather GaAs/AlGaAs heterostructures which gives a higher quality 2DEG. It is appropriate to take a closer look on the compounds in question, how the structures are grown and some examples of components used in experiments.

GaAs, AlAs and AlGaAs

Before considering AlGaAs we look at GaAs and AlAs. They both crystalize in a zinc-blende structure (figure 2.16b) with almost identical lattice constants (5.65Å for GaAs and 5.66Å for AlAs), are both III-V semiconductors and their band structures are shown in figure 2.17a. The band gap is direct for GaAs ($E_g = 1.52\ meV$ at $T = 0K$), but is indirect for AlAs ($E_g = 2.23\ meV$ at $T = 0K$).

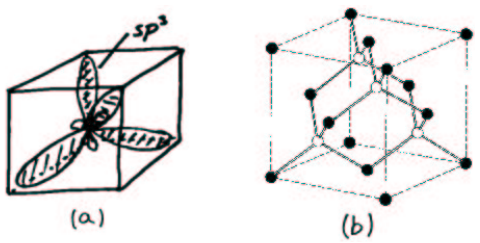

Figure 2.16: (a) Four independent sp^3 orbitals. (b) The zincblende crystal structure - two fcc-lattices interpenetrating each other, displaced 1/4 the diagonal length along the diagonal of the cubic cell.

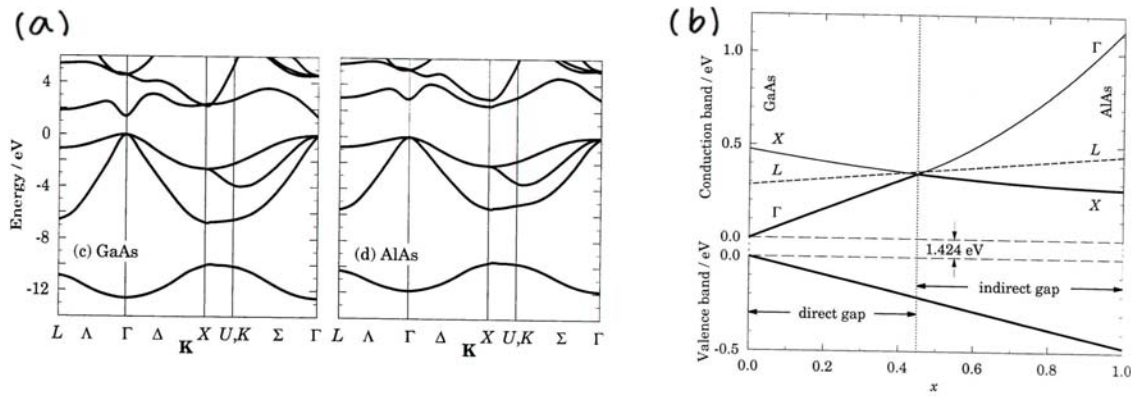

Figure 2.17: (a) Band structure of GaAs and AlAs. X, K, Γ etc. are standard points of symmetry in reciprocal space. (b) The band gap of $Al_xGa_{1-x}As$ as a function of x.

A rough understanding of the band structure can be obtained by chemical considerations. The zinc-blende lattice is not a Bravais lattice, and the primitive vectors can be chosen to be (a/2,a/2,0), (a/2,0,a/2) and (0,a/2,a/2), where a is the lattice constant. In this case the basis will consist of one atom (Ga or Al) situated in (0,0,0) and one atom (As) in $(a/4, a/4, a/4)$. Gallium and aluminum has 3 valence electrons (s^2p^1) and arsenic has 5 ($4s^24p^3$) so there is a total of 8 valence electrons per primitive cell. During crystallization the s and and p orbitals of each atom hybridize into four sp^3 orbitals sticking out from the corner of a tetrahedron (figure 2.16a) joining Ga and As together in the zinc-blende structure. Taking these eight orbitals from each primitive cell as basis functions, using Bloch's theorem and diagonalizing[4] results in 8 **k**-dependent energy levels. For every direction in reciprocal space these **k**-dependant energy levels form 8 bands as showed in figure 2.17a, each band containing 2 states (when spin is included) per primitive cell. Since there is a total of eight electrons per primitive cell, the four lowest lying bands are filled (the valence bands) and the four highest are empty (the conduction bands) at T=0 K. Naively, the valence bands can be viewed as being made from bonding combinations of sp^3 orbitals and the conductance band from antibonding combinations. This picture works better for the valence bands than for the conductance bands, since the conduction electrons are less localized and therefore retains only little of the atomic structure. It could be expected that there would be no gap between the four valence bands due to the hybridization, this is the case for silicon and germanium, but here a band gap is seen between the valence bands. This can be explained by noting that the electron density around the As atoms overshoots slightly, making the bond not only covalent, but also ionic. This weakens the hybridization and split the valence band up in a single s-like[5] and a triple p-like band.

AlGaAs is shorthand for the alloy $Al_xGa_{1-x}As$ and it is assumed that the Ga and the Al atoms are situated on corresponding lattice points, but in a random pattern. Luckily it is often adequate to treat the alloy as a crystal with properties interpolated from GaAs and AlAs. This is known as the virtual-crystal approximation. Since the band gap is direct for GaAs and indirect for AlAs, not only the size, but also the type of the gap varies with x. The gap characteristics are given in figure 2.17b, showing that the band gap for $Al_xGa_{1-x}As$ is direct for $x < 0.45$ and indirect (situated at point X in **k**-space) for $x > 0.45$.

The active regions in heterostructures lie typically close to interfaces, and in order to optimize the performance these interfaces must be nearly perfect. To achieve this not only refined growing technics are needed, but the interfacing materials must also have the same crystal structure and almost identical lattice constants. Furthermore, it is necessary that the energy gaps are somewhat different in order to create the

[4]This is called the tight-binding method of calculating band structures. There are other methods and real band calculations are of course much more complicated.

[5]The terms s- and p-like bands correspond to the band having the symmetry of s- and p-orbitals. For instance a p-like valence band will have one single 'light' hole branch and a double degenerated 'heavy' hole branch (when spin-orbit band splitting is neglected).

potential barriers used to trap the electrons in a 2DEG.

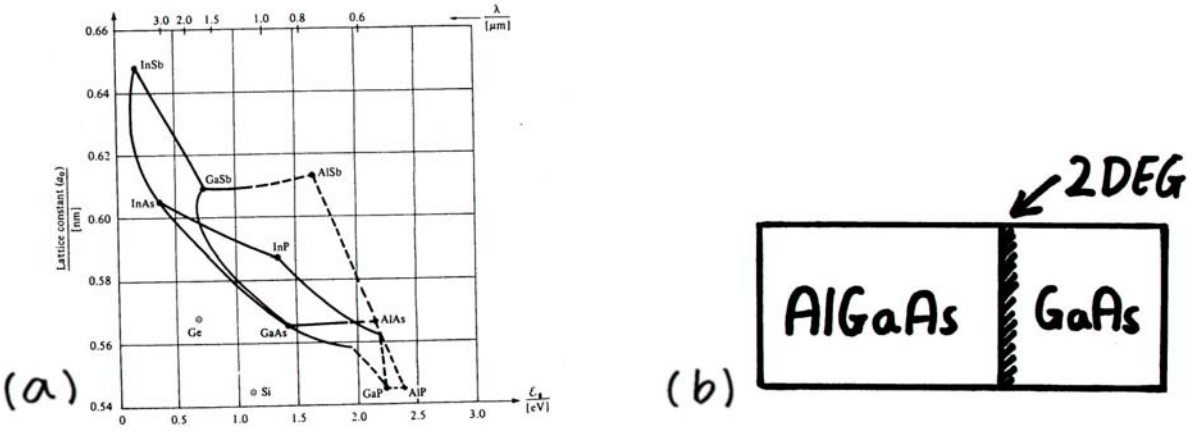

Figure 2.18: (a) Plot of the lattice constant of various semiconductors against their minimum band gap. Full lines show a direct band gap, dashed lines an indirect band gap. (b) Sketch of a GaAs/AlGaAs heterojunction.

Figure 2.18a show the energy gap as a function of lattice constants for some zinc-blende type semiconductors and we see that GaAs and AlAs fulfill the required conditions. Since it is often preferred that the materials have direct gaps, it is customary to choose GaAs/$Al_xGa_{1-x}As$ heterostructures with $x < 0.45$.

Modulation doped heterostructures

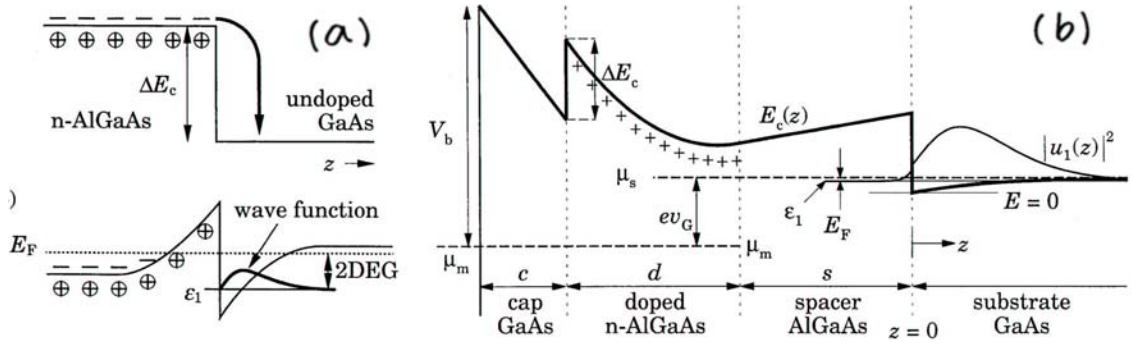

Figure 2.19: (a) Carriers from a non-active region form a 2DEG at the potential barrier between GaAs and AlGaAs. (b) The conduction band profile in a MODFET.

The obvious way to introduce carriers is to dope the regions were electrons or holes are desired. Unfortunately this leaves behind charged donors in the active regions where they generally will disturb the effects we wish to study, and the enhanced impurity scattering will also lower the mobility of the 2DEG. The solution to this problem is to grow the doping in a non-active region, from which the carriers subsequently migrate to the active region. This is called modulation doping and is illustrated in figure 2.19. Often an intrinsic spacer layer is placed between the doped- and the active region, an example is pictured in figure 2.19b. Such spacer layers diminish impurity scattering and enhance the mobility of the 2DEG.

The conduction band profile shown in figure 2.19b was calculated self-consistently by computer, using the Laplace and Schrődinger equation under the assumption that a metal gate with gate voltage V_G is placed upon the GaAs cap.

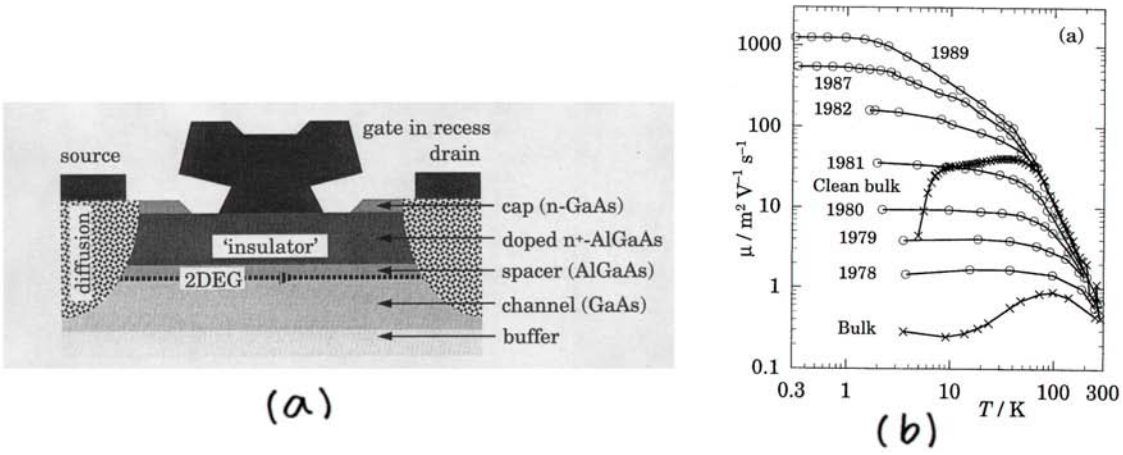

Figure 2.20: (a) Simplified cross section through a MODFET. (b) Mobility of various 2DEG as function of temperatures (circles), showing how the peak mobility has risen over 20 years. The mobility of bulk samples is shown for comparison (crosses), for old material (Bulk) and purer material (Clean bulk) [Stanley et. al (1991)].

After the heterostructure is grown, the density of the 2DEG can be controlled, as in the MOSFET, by forming a capacitor between the 2DEG and a metallic gate. Adding a source and drain completes the FET called a modulation doped field effect transistor (MODFET). A simplified sketch is shown in figure 2.20a. In figure 2.20b the development in mobilities of various 2DEG during the years is shown, the peak mobilities being higher than 1000 $m^2V^{-1}s^{-1}$, which is significantly higher than the best mobilities in Si-MOSFET's that lie around 4 $m^2V^{-1}s^{-1}$.

Molecular Beam Epitaxy

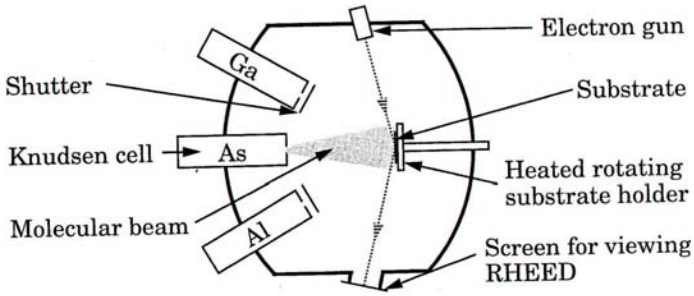

Figure 2.21: Highly simplified schematic diagram of a MBE machine.

One of the most customary methods of growing high quality AlGaAs/GaAs heterostructures is called Molecular Beam Epitaxy (MBE). In an ultra high vacuum chamber (fig 2.21) a GaAs substrate is placed in a heated holder. A number of cells (called Knudsen- or K cells) are incorporated in the chamber penetrating the walls. These each contain one source element in vaporized form and can be opened or closed by shutters. When one or several of the Knudsen cells are opened, their content diffuse into the chamber with a flux controlled by the temperature of the K cell, and a fraction fasten on the substrate. Since the substrate is heated the condensed atoms on the substrate will be able to move about on the surface, creating an homogenius atomic monolayer.

The growth can be monitored monolayer by monolayer by, for instance, a high energy electron diffraction

(RHEED) device, in which a beam of electrons are refracted upon the sample surface and analyzed on a fluorescent screen.

If dopants are needed, they are added by using additional cells. The usual donor in AlGaAs/GaAs heterostructures is Si, but at very high concentrations (around 10^{25} m^{-3}) Si can act as both donor and acceptor. The usual acceptor is Be.

Reference

We end this chapter by giving a short list of the primary references we have used in the different sections.

Section 2.1 : [1, 2, 3, 17, 22].
Section 2.2 : [1, 31].
Section 2.3 : [6, 19, 31].
Section 2.4 : [1].
Section 2.5 : [2, 3, 4, 35].
Section 2.6 : [1, 3, 23].
Section 2.7 : [6, 7].

Chapter 3

Looking back

> In physics, you don't have to go around making trouble for yourself - nature does it for you.
>
> *Frank Wilczek*

3.1 Coulomb drag in double quantum well systems

The fundamental idea behind a double quantum well (DQW) Coulomb drag experiment is as follows. Two high quality 2DEG, usually created in a GaAs/AlGaAs DQW heterostructure, are placed very close to each other. The system is then cooled down to temperatures below the Fermi temperatures of the electron gasses, and a current is driven through one of the wells (let us refer to this well as (1)). The electrons in (1) will influence the electrons in the other layer (called (2)) through momentum carrying interwell interactions like Coulomb, and phonon mediated scattering. These interactions tend to act as "frictional forces" between the electrons in the two layers and can be measured by letting (2) be part of either an open or a closed circuit. If the circuit is open, a current is induced in (2) because the electrons are dragged along by the current in (1) (figure 3.1a). If the circuit on the other hand is closed, then electrons in (2) accumulate at one end of the well, building up an electrical field that exactly cancels the drag induced force on the electrons, and a voltage across (2) can be measured (figure 3.1b).

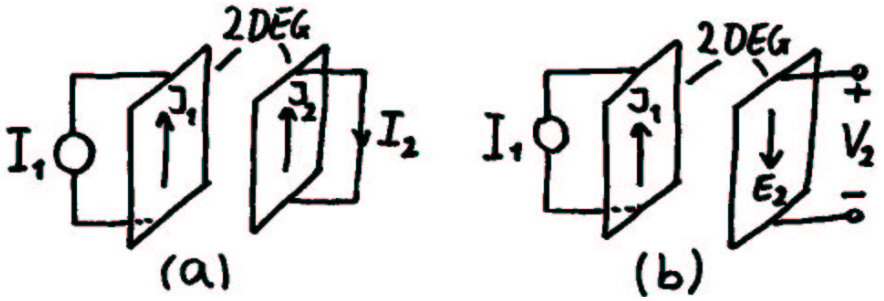

Figure 3.1: (a) When layer 2 is open an electrical current is induced by the current in layer 1. (b) When layer 2 is closed an electrical field is induced by the current in layer 1.

When the experiments are conducted at sufficiently low temperatures, it is assumed that the Coulomb interaction between electrons in the two layers is the dominating drag source. Calculations at low temperatures therefore typically take Coulomb interactions to be the only interwell interactions. We shall see in the next section that although this approximation is not accurate, it nevertheless reflects many of the characteristic features found in experiments.

3.1.1 Gramilas experiment

The first successful Coulomb drag experiments in 2DEG DQW systems was reported by T.J. Gramila et al. [12] in 1991. Previously, drag effects had been observed (Solomon et al. [32], 1989) between a 2DEG and a 3DEG system, but the results were complicated by subtle thermal effects and are not suitable for an introductional discussion.

Gramilas experiment was performed on modulation-doped GaAs/AlGaAs DQW structures grown by MBE. The active region of the two 2DEG was shaped in a Hall bar like geometry by a lithographic pattern on the sample front surface and diffusion indium contacts was placed at the end of each arm (figure 3.2a). Two aluminium gates straddled each arm, one on front and one on back of the sample. They were used to control the connection between the In contacts and the central bar of either quantum well. This was possible, since applying a suitable negative voltage on a gate depleted the arm of the 2DEG closest to the gate without significantly influencing the other.

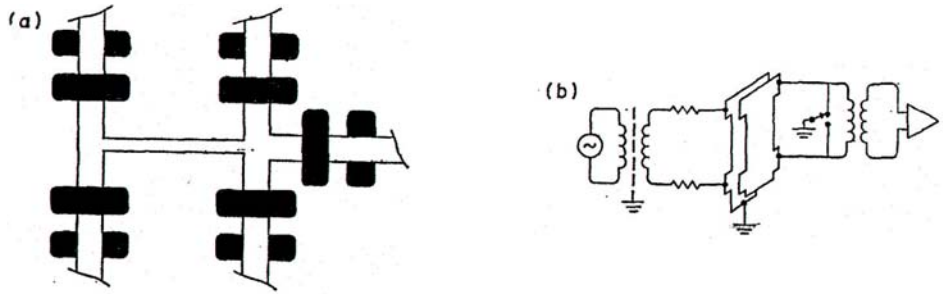

Figure 3.2: Figures taken from Gramila's article [12]. (a) The active 2DEG region shaped in a Hall bar sample geometry, including the front and back gates in black. Each arm of the Hall bar is terminated with an indium diffusion contact. (b) Schematic of the measurement configuration showing the same principal setup as figure 3.1b.

Two such samples were grown, both with $GaAs$ quantum wells of width 200 Å containing a 2DEG of mobility $350\,m^2/Vs$ and density $1.5 \cdot 10^{15}\,m^{-2}$, corresponding to a Fermi temperature of 60 K. The wells were separated by an undoped $AlGaAs$ layer which had a thickness of 175 Å in one sample and 225 Å in the other.

Each sample was submitted to the experiment illustrated in figure 3.1b. A constant current, I, was driven through one well while the other was connected to a voltmeter (figure 3.2b) measuring the induced "drag voltage" V_D. It is customary to depict the measured experimental result as a drag resistance $R_D = V_D/I$, or equivalently as a "drag rate", τ_D^{-1}, defined via the Drude-like resistivity

$$\rho_D = \frac{m}{ne^2\tau_D} = \frac{E}{J}, \tag{3.1}$$

where J is the current density corresponding to I and E the field corresponding to V. Figure 3.3 give the results obtained by Gramila, and it is readily seen that the drag rate has a near T^2 behavior. That τ_D^{-1} depends on the interwell distance is clearly seen in figure 3.3b, as is the drag rate's deviation from the T^2 proportionality. We note that the measured drag rate $\tau_D^{-1} \sim 10^6$ s^{-1}, which is small compared to the typically momentum scattering rates $\tau^{-1} \sim 10^{10}$ s^{-1} for GaAs.

3.1.2 The calculated drag rate

Jauho and Smith [16] calculated the drag rate in 1993, using a Boltzmann equation approach, assuming that interwell electron tunneling was negligible and that the only significant electron-electron interaction was Coulomb scattering. We will go through the calculations in detail at a later state (section 4.3), but will give the result here. The drag rate was found to be

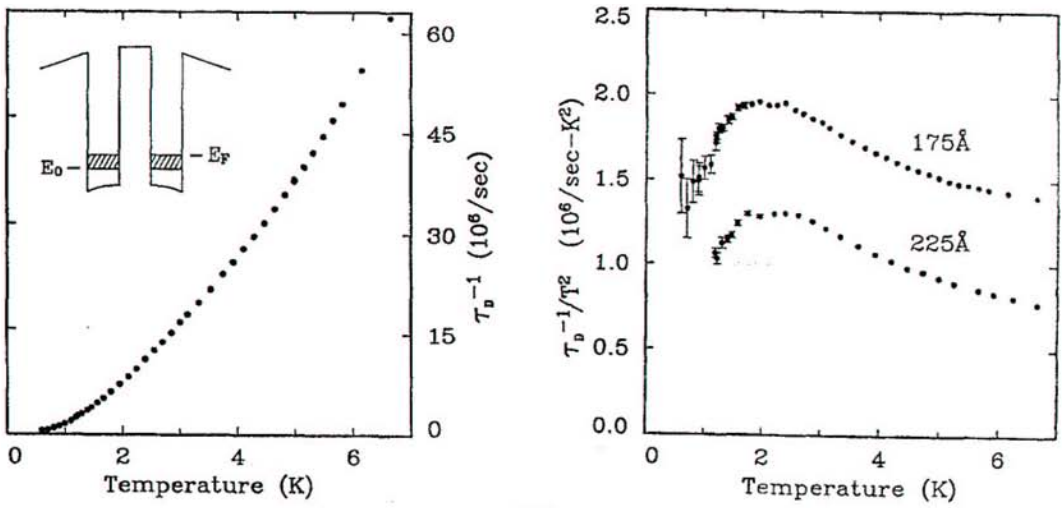

Figure 3.3: [12] (a) Temperature dependence of observed frictional drag between two 2DEG separated by 175 Å barrier. Inset: An idealized conduction band diagram for a DQW structure indicating the ground subband energy E_0 and Fermi energy E_F. (b) Temperature dependence of inter-well momentum-transfer rate divided by T^2 for both the 175- and 225 Å barrier samples.

$$\frac{1}{\tau_D} = \frac{\hbar^2}{2\pi^2 n_2 m_1 k_B T} \int_0^\infty dq \int_0^\infty d\omega \, q^3 |e\phi(q)|^2 \frac{Im\chi_1(q,\omega) Im\chi_2(q,\omega)}{\sinh^2(\hbar\omega/2k_B T)}, \tag{3.2}$$

where index 1 refer to the current carrying well and index 2 to the adjacent quantum well. The Fourier transform $e\phi(q)$ of the effective interaction was calculated self-consistently using the Poisson equation and treating screening by the Thomas-Fermi approximation (2.103). The Lindhard function, $\chi(q,\omega)$, used in (3.2), is the zero temperature two dimensional Lindhard function given by (2.172). Jauho and Smith made an analytical evaluation of the drag rate in the low temperature limit showing that $\tau_D^{-1} \propto T^2 d^{-4}$, d being the center-center distance between the quantum wells (in Gramilas experiment d was 375 and 425 Å), and also made a numerical calculation for higher temperatures (figure 3.4a).

There is a couple of notable discrepancies between the experimental and calculated drag rates. First of all, the observed drag rates are a factor of 2 larger that the calculated drag rates. This indicates that other scattering mechanism, like phonon scattering, may be important. Secondly, even though the calculated $1/\tau_D T^2$ curve was found to have a maximum that is in somewhat qualitative agreement with the observations, the temperature (T_{max} ≈10 K) at which these maxima appear is significantly larger than the experimentally measured values (T_{max} ≈2 K). These discrepancies were in 1998 fully explained by Bønsager et al. [24], taking phonon mediated drag effects into account. They used a quantum field linear response approach, developed by Flensberg et al. [9], that allows for arbitrary interlayer interactions, like phonon mediated interactions, to be included in the drag rate calculation.

In 1995, Flensberg and Hu [11] predicted a possible drag rate enhancement at intermediate temperatures ($T \approx T_F/2$) due to coupled interwell plasmons (figure 3.4b). Two different modes of coupled plasmons occur. One, called the optic mode, in which the electron densities in the two layers oscillate in phase, and one, referred to as the acoustic mode, where the oscillations are out of phase. This prediction, based on numerical calculations using a finite temperature form of $\chi(q,\omega)$ instead of the zero temperature polarizability, was confirmed experimentally by Hill et al. [14] in 1997.

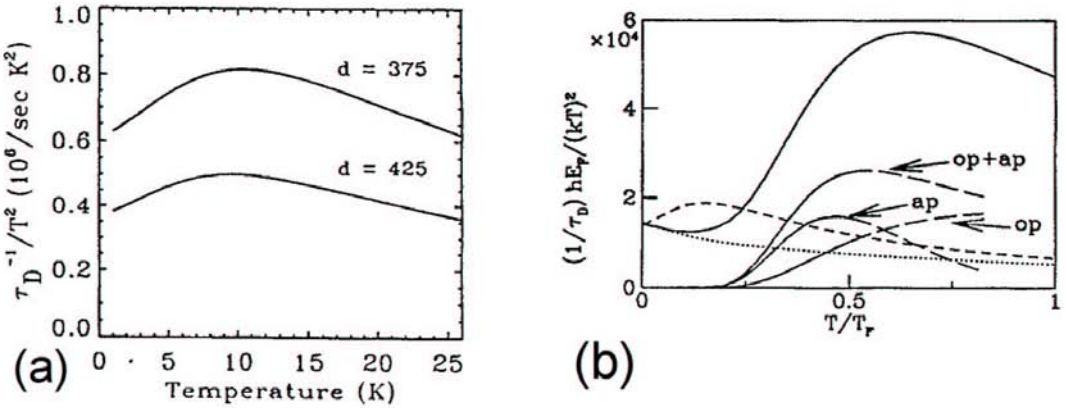

Figure 3.4: (a) [16] The values of $1/\tau_D T^2$ as function of the temperature calculated by Jauho and Smith with parameters appropriate to the experiment of Gramila. (b) [11] Temperature dependence of the drag rate scaled by T^2. The full bold curve corresponds to calculations using the finite-T form of χ (Flensberg) show the plasmon enhanced drag rate. The short-dashed (Jauho) and the dotted (not discussed) are calculations using the zero-T form, neither giving a plasmon enhancement. The curves (op) and (ap) depict the optic and the acoustic plasmon contribution in the plasmon-pole approximation (not discussed).

3.2 Spin polarized transport

Consider an electron gas in thermal equilibrium and suppose that the background system has ferromagnetic properties.

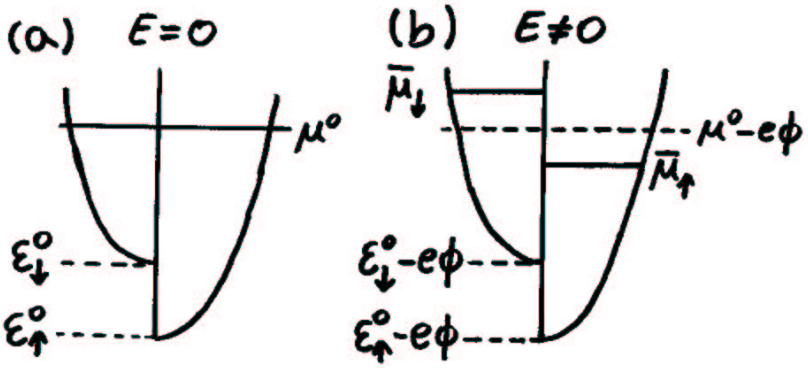

Figure 3.5: (a) Equilibrium dispersion relation, ε_{ks}, when $E = 0$. (b) Different spin dependent electrochemical potentials, $\bar{\mu}_s$, when $E \neq 0$.

We saw in section 2.5 that it may be energetically favorable for the system to have a predominance of spin conduction $\uparrow$ electrons (figure 3.5a). The equilibrium distribution, $f_s^0(k)$, is in this case a spin dependent Fermi-Dirac distribution

$$f_s^0(k) = f_0(\varepsilon_{ks}) = \frac{1}{e^{\beta(\varepsilon_{ks}-\mu^0)}+1}, \tag{3.3}$$

which returns to the usual Fermi-Dirac distribution ($\varepsilon_{k\uparrow} = \varepsilon_{k\downarrow}$) when the electron gas in un-polarized. The densities, n_s^0, of the spin s electrons is given by

$$n_s^0 = \int \frac{d\mathbf{k}}{(2\pi)^d} f_s^0(k), \tag{3.4}$$

with d being the dimension of the electron gas, and of course satisfy that $n_\uparrow^0 + n_\downarrow^0 = n^0$.

Assume that the system is placed in a circuit, and a current, $J = J_\uparrow(x) + J_\downarrow(x)$, is running in the x-direction. Here $J_s(x)$ is the electrical current carried by spin s electrons. Often the two spin dependent components, $J_\uparrow(x)$ and $J_\downarrow(x)$, are not identical, and we talk about spin polarized transport. The current-carrying electron gas is not in thermal equilibrium, and is described by a local, spin dependent distribution, $f_s(\mathbf{k}, x)$. By definition, the local spin dependent density, $n_s(x)$, and the current density, $J_s(x)$, is given by

$$n_s(x) = \int \frac{d\mathbf{k}}{(2\pi)^d} f_s(\mathbf{k}, x), \tag{3.5}$$

$$J_s(x) = \int \frac{d\mathbf{k}}{(2\pi)^d} (-ev_x) f_s(\mathbf{k}, x). \tag{3.6}$$

Outside depletion areas, the background ions and conduction electrons must be charge neutral and $n_\uparrow(x) + n_\downarrow(x) = n^0$ hold.

Suppose for a moment that $\partial J_s/\partial x \neq 0$, at some point, x_0, in space. This means that the current supplies or removes spin s electrons from x_0 at a given rate. The density, $n_s(x_0)$, will therefore increase or decrease compared to the equilibrium density, n_s^0. In systems with dominant spin flip processes these immediately restore (or almost restore) $n_s(x_0) = n_s^0$, but if the spin flip relaxation time, τ_{sf}, is long, $n_s(x_0)$ may very well differ from the equilibrium density.

It is convenient to define the local electrochemical potential, $\bar{\mu}_s(x)$, as

$$\bar{\mu}_s(x) = \mu_s(x) - e\phi(x), \tag{3.7}$$

(see figure 3.5b). Here the local chemical potential, $\mu_s(x)$, is defined by the spin dependent non-equilibrium electron density, $n_s(x)$, in equivalence with table 2.1, as

$$\text{In a 3DEG}: \quad n_s(x) = \frac{1}{6\pi^2}\left(\frac{2m(\mu_s(x) - \varepsilon_s^0)}{\hbar^2}\right)^{3/2}, \tag{3.8}$$

$$\text{In a 2DEG}: \quad n_s(x) = \frac{m(\mu_s(x) - \varepsilon_s^0)}{2\pi\hbar^2}, \tag{3.9}$$

and $\phi(x)$ is the electrical potential[1]. The spin dependency of the electrochemical potential, illustrated in figure 3.5b, occurs when $n_s(x)$ differs from n_s^0.

3.2.1 Valet and Fert's macroscopic transport equations

The calculation of $J_s(x)$ and $\bar{\mu}_s(x)$ is often based on the following two macroscopic equations

$$\frac{\partial J_s}{\partial x} = \frac{\sigma_s}{eD_s}\frac{\bar{\mu}_s - \bar{\mu}_{-s}}{\tau_{sf}}, \tag{3.10}$$

$$\frac{\partial \bar{\mu}_s}{\partial x} = \frac{e}{\sigma_s} J_s, \tag{3.11}$$

where the constants introduced in (3.10) and (3.11) depend on the system parameters. D_s is a diffusion constant, τ_{sf} is the spin flip relaxation time and σ_s is a spin dependent Drude conductivity.

[1] In chapter 4, definitions and calculations are considered in more detail.

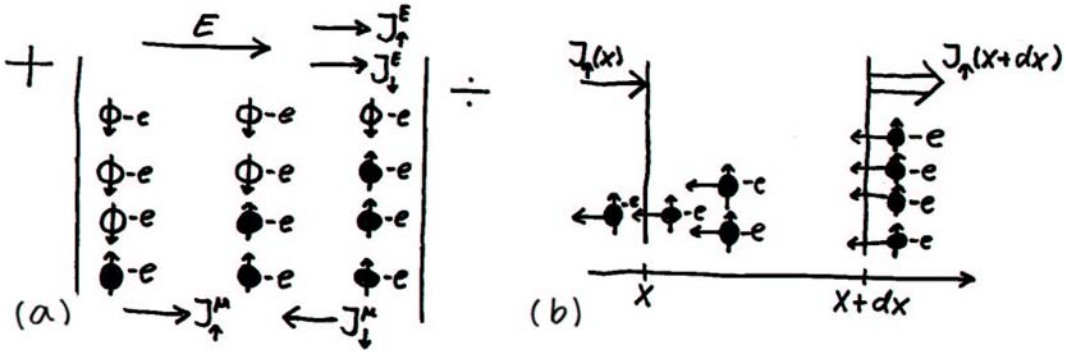

Figure 3.6: (a) The spin current is driven by an electrical field, but also by diffusion from areas with high spin s concentrations toward areas with low. (b) When the gradient of the spin current is positive, it is readily seen that the spin density is enhanced. This effect is counteracted by spin flip processes.

The physical interpretation of the equations is straightforward. (3.11) is a generalized form of Ohm's law, stating that the current, J_s, can be driven by as well an electrical field as a density gradient (figure 3.6a). Remembering that the density and the chemical potential are connected, we intuitively[2] write

$$J_s = J_s^E + J_s^\mu = \sigma_s(E + (-\frac{1}{e})(-\frac{\partial \mu_s}{\partial x})) = \frac{\sigma_s}{e}(\frac{\partial \mu_s}{\partial x} - e\frac{\partial \phi}{\partial x}) = \frac{\sigma_s}{e}\frac{\partial \bar{\mu}_s}{\partial x}, \tag{3.12}$$

which is Ohm's law, as stated in (3.11).

(3.10) is a steady state continuity equation, where the spin flip acts as an electron source or drain. The form can intuitively be understood as follows. From figure 3.6b it is clear that the spin density, n_s, is raised with a certain rate when $\partial_x J_s > 0$. Introducing the electrochemical potential, $\bar{\mu}_s$, instead of the density, and assuming a linear relation, we write this rate as

$$\frac{\partial \bar{\mu}_s^J}{\partial t} = A\frac{\partial J_s}{\partial x}. \tag{3.13}$$

The spin density rate due to spin flip processes can be written as

$$\frac{\partial \bar{\mu}_s^{sf}}{\partial t} = \frac{\bar{\mu}_{-s} - \bar{\mu}_s}{\tau_{sf}}. \tag{3.14}$$

This is just a standard balance equation, subtracting the rate of $s \to -s$ processes from the rate of $-s \to s$ processes. When the system is in a steady state, the net rate is zero, and

$$\frac{\partial \bar{\mu}_s^J}{\partial t} + \frac{\partial \bar{\mu}_s^{sf}}{\partial t} = 0 \Rightarrow \frac{\partial J_s}{\partial x} = \frac{1}{A}\frac{\bar{\mu}_s - \bar{\mu}_{-s}}{\tau_{sf}}. \tag{3.15}$$

Rewriting the proportionality factor A as eD_s/σ_s gives (3.10).

From (3.10) and (3.11) it is easy to derive the following two second order equations

$$\frac{\partial^2(\bar{\mu}_s - \bar{\mu}_{-s})}{\partial x^2} = \frac{\bar{\mu}_s - \bar{\mu}_{-s}}{l_{sf}^2}, \tag{3.16}$$

$$\frac{\partial^2}{\partial x^2}(\sigma_s\bar{\mu}_s + \sigma_{-s}\bar{\mu}_{-s}) = 0, \tag{3.17}$$

[2]The derivation of (3.12) and (3.15) is not to be understood as a rigorous proof, but is merely meant to give an an intuitive feeling of the transport equations.

and we recognize (3.16) as an ordinary diffusion equation with a diffusion constant l_{sf}^{-2}. The length l_{sf} is called the spin-flip length. We see that (3.17) has some resemblance to the electrostatic Laplace equation, $\nabla^2\phi = 0$, and could, in lack of a better name, call it a generalized Laplace equation.

The equations (3.11) and (3.16) were introduced and used by Son et al. in 1987 [34], but was not derived by first principles. This was done in 1993, when Valet and Fert [33] used a Boltzmann equation approach to show that $J_s(x)$ and $\bar{\mu}_s(x)$ fulfilled the two macroscopic transport equations, (3.10) and (3.11), and from them derived (3.16) and (3.17).

3.2.2 Transport through magnetic multilayers

Valet and Fert used their theory to calculate the spin-polarized current through a system of magnetic multilayers.

The second order equations (3.16) and (3.17) immediately give

$$\bar{\mu}_s(x) - \bar{\mu}_{-s}(x) = Ae^{x/l_{sf}} + Be^{-x/l_{sf}}, \tag{3.18}$$

$$\sigma_s\bar{\mu}_s(x) + \sigma_{-s}\bar{\mu}_{-s}(x) = Cx + D, \tag{3.19}$$

Solving these two equations and using (3.11), we find that

$$\bar{\mu}_s(x) = A_s e^{x/l_{sf}} + B_s e^{-x/l_{sf}} + C_s x + D_s, \tag{3.20}$$

$$J_s(x) = \frac{\sigma_s}{e}\frac{\partial\bar{\mu}_s}{\partial x} = \frac{\sigma_s}{e}\left(\frac{A_s}{l_{sf}}e^{x/l_{sf}} - \frac{B_s}{l_{sf}}e^{-x/l_{sf}} + C_s\right), \tag{3.21}$$

where the constants are determined by the relevant boundary conditions. Valet and Fert calculated $\Delta\mu = \bar{\mu}_s - \bar{\mu}_{-s}$ and J_s throughout different structures (figure 3.7), using the spin polarization of the layers as boundary conditions, and assuming no interfacial scattering.

The first of the three examples pictured in figure 3.7, describes transport from one semi-infinite magnetic layer to an other with antiparallel magnetization. The two following structures sketched in the figure, are multilayers of alternating magnetic and non-magnetic materials. In one case, the magnetic layers are in a antiparallel configuration, in the other case the configuration is parallel. Additional effects, like interfacial spin dependent scattering, can be included in the calculations. For further details the reader is refered to Valet and Fert's article [33].

It is seen that changes in the transport quantities typically takes place within the length, l_{sf}, from an interface. Here l_{sf} is the spin flip length introduced in (3.16), and the conversion of the spin $\uparrow$ into a spin $\downarrow$ current that takes place near the interface is responsible for an additional boundary resistance. This additional resistance has significant consequences, as discussed in the following section.

3.2.3 Injecting spin polarized currents into semiconductors

Injecting spin-polarized electron currents into semiconductors has been the center of a growing attention in the last decade. In 1990 Datta and Das suggested a device consisting of a 2DEG connected by two ferromagnetic metal contacts (figure 3.8a). The idea was to inject a spin polarized current into the 2DEG from one of the contacts (the source) and analyzed this current by the other contact (the drain). An applied electrical field perpendicular to the 2DEG-plane is seen as a magnetic field in the rest system of the moving electrons. This cause a precession of the current spin throughout the structure with a period depending on the field. The source-drain conductance was calculated to be proportional to the projection of the spin phase on the drain magnetization direction, and varying the field therefore modulates the diode conductance [18, 27]. Such "spintronic" devices would have many interesting applications, but unfortunately it is extremely

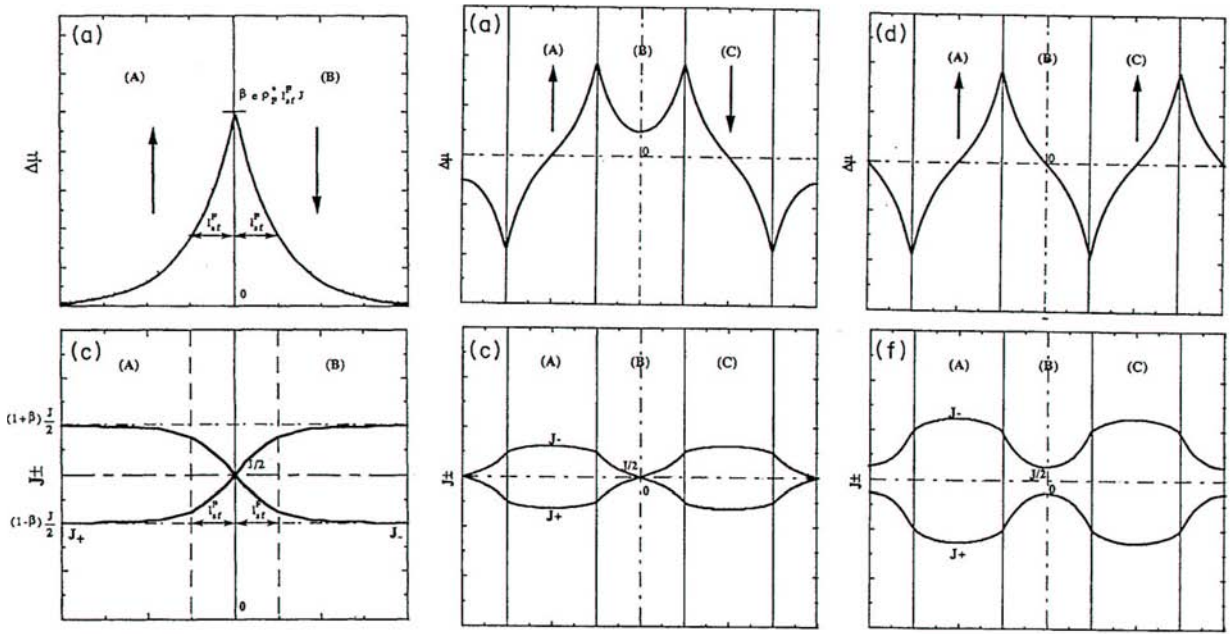

Figure 3.7: [33] Electrochemical potential difference, $\Delta\mu$ (upper figures), and corresponding spin currents, J_s (lower figures), in different systems of magnetic multilayers. The big arrows on the upper figures show the direction of the magnetization in the different layers. Layers without an arrow are non-magnetic. Note that β in this figure is used as a measure of the degree of magnetization and not as $(k_B T)^{-1}$.

difficult to inject a spin-polarized current from a ferromagnetic metal into a semiconductor. To this day no efficient Datta-Das diode has ever been constructed[3].

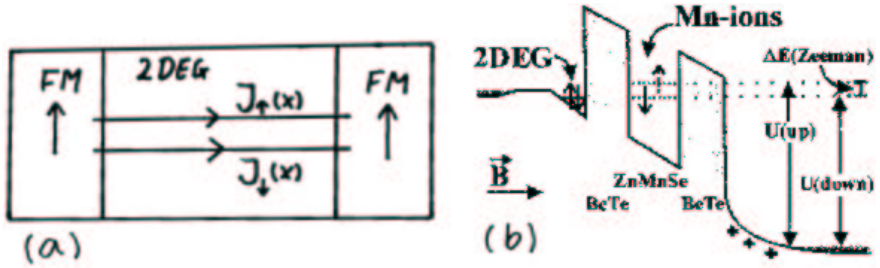

Figure 3.8: (a) A 2DEG connected to ferromagnetic metallic contacts. (b) [13] The resonant tunnelling injection diode.

To understand why it is difficult to to inject a spin-polarized current from a ferromagnetic metal into a semiconductor, one must analyze the effects of spin-polarized transport in detail. As early as 1987, Son et al. [34] used (3.11) and (3.16) to calculate the existence of an additional boundary resistance at the interface between a ferromagnetic metal and a non-ferromagnetic metal. The resistance is caused by the partly conversion of the spin $\uparrow$ current into a spin $\downarrow$ current taking place near the interface (see figure 3.7). A similar calculation for a two-dimensional electron gas with ferromagnetic metal contacts was made by Schmidt et al. [28] in 2000. They found that the polarization of the injected current depends critically on certain material parameters of the 2DEG and the contacts. Defining the spin-polarization, $\alpha(x)$, as

[3]At least not when the size of the 2DEG is in the diffusive regime. We do not in this thesis concern ourselves with the ballistic regime, i.e. systems where the width of the 2DEG is smaller than the electron mean free path.

$$\alpha(x) = \frac{J_\uparrow(x) - J_\downarrow(x)}{J_\uparrow(x) + J_\downarrow(x)}, \tag{3.22}$$

and using parameters typical for a such structures, the injected current was shown to have a polarization less than 1%.

This does not mean that it is impossible to inject a spin-polarized current into a semiconductor. Devices using ferromagnetic semiconductors such as GaMnAs [26, 20], or other non-metallic compounds [25] as contacts have shown promise, and recent experiments [8, 13] with resonant tunnelling spin injectors (figure 3.8b) indicate injected currents with 80-90% polarization. The principle behind the tunnelling injector, called a resonant tunnelling diode, is to use the energy difference between $\varepsilon_{\mathbf{k}\uparrow}$ and $\varepsilon_{\mathbf{k}\downarrow}$ caused by the Zeeman splitting. Applying a suitable voltage ensures that $\varepsilon_{k_F\uparrow}$ has an energy equal to the transmission resonance of the structure while $\varepsilon_{k_F\downarrow}$ has not. This means that only spin $\uparrow$ electrons tunnel through the structure and into the 2DEG. Altering the applied voltage causes the polarization of the injected current to change. The situation sketched in the figure has for instance $\varepsilon_{k_F\downarrow}$ lying at the resonance in stead of $\varepsilon_{k_F\uparrow}$.

The polarization degree of the current in a 2DEG is difficult to measure precisely. Usually this is done by optical means, measuring the electroluminescence, but the end result is only an estimate. Therefore, the true polarization in the experiment mentioned above may be significantly less than 80%. A polarization degree around 30% is often stated as the optimum polarization achieved with certainty to date.

3.3 Spin drag

The total current through a system is not affected by electron-electron scattering since the total momentum of the electrons is conserved in such processes. However if the current, $J = J_\uparrow + J_\downarrow$, is spinpolarized, then interactions between spin $\uparrow$ and $\downarrow$ electrons may transfer a net momentum from one spin current component to the other. The spin $\uparrow$ and $\downarrow$ electrons constitutes a two-component system and the momentum transfer between the two components cause a drag effect in analogue to the DQW drag described in section 3.1. To complete the DQW analogue, we mention that spin-flip mechanisms present in real materials and relevant to the spin 'case', is translated as non-negligible tunnelling between the two quantum wells in the DQW 'case'.

The electrons contributing to the spin drag effect are not spatially separated as are the electrons causing the DQW drag effect. Therefore spin drag is a considerably larger effect than DQW drag. In fact we will show (section 4.7 and 4.8) that the spin drag rate is comparable to the ordinary transport relaxation rate for many physical systems.

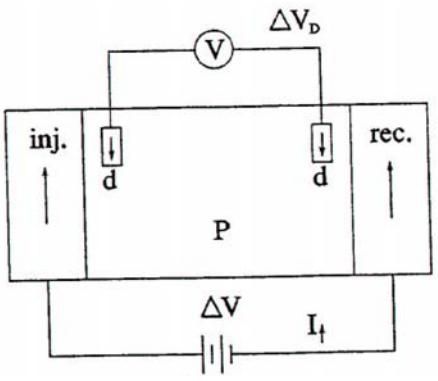

Figure 3.9: Figure taken from [5]. Experimental setup to detect the 3D spin drag effect, where the voltage ΔV is applied between two parallel half-metallic ferromagnets (injector (inj.) and receiver (rec.)) that sandwich a paramagnet (P). The voltage ΔV_D is detected using two ferromagnetic electrodes (d) similar to the injector and receiver, but polarized in the opposite direction.

In 2000 D'Amico and Vignale [5] calculated the spin drag rate, τ_s^{-1}, in a 3DEG. They found that the drag resistivity is proportional to T^2, and for many metals is comparable in size to the ordinary resistivity. The method they used was linear response, but their end result seems to differ slightly from the result one would expect to find generalizing the many previous DQW calculations to the spin 'case', and also from the one found in this thesis (section 4.5.1). The calculations in [5] must therefore be regarded with some caution, but the main idea behind the article, i.e. the presence of a spin drag effect, is nevertheless a good one. D'Amico and Vignale suggested an experiment, sketched in figure 3.9, that may be used to measure the spin drag rate. To this date such an experiment has not been carried out.

Evaluating the drag rate (section 4.7 and 4.8) shows that the effect is even more significant for a 2DEG than for a 3DEG, and a two dimensional version of the experiment sketched in figure 3.9 is a pleasing thought, although technical difficult to realize.

Chapter 4

Transport equations and spin drag in spin-polarized systems

> Insofar as mathematics is about reality, it is not certain, and insofar as it is certain, it is not about reality. *Albert Einstein*

Valet and Fert's transport equations (section 3.2.1) were derived without taking electron-electron interactions into account. In addition to that, the calculations did not always distinguish between different relaxation times, for instance between the spin-flip mean- and transport time. In this chapter we will generalize the transport equations by including electron-electron interactions, and by defining the various scattering times with more care.

Generalizing the transport equations was not an initial goal, but arose while answering a simple question. In the various treatments of Coulomb drag, much emphasis has been on the momentum transfer from one layer to the other (or in spin drag, from one spin component to the other). Such a momentum transfer affect the driving current, making it harder to run, and it is natural to ask how much the resistivity in the driving layer is enhanced. Surprisingly, this question has not been addressed in previous studies, and we set out to answer it. The approach was to combine Valet and Fert's transport equations with the Coulomb drag rate by taking electron-electron interactions into account, and resulted in the generalized transport equations. These, in turn, easily answer the originally asked question of the enhanced drag resistance, and has other implications as well (section 4.6).

One reason that the resistivity enhancement has avoided attention in the past, is the fact that interwell drag resistance in ordinary DQW Coulomb drag is very small compared to the ordinary impurity resistance. A simple calculation shows, however, that for spin polarized transport in a two- or three dimensional electron gas the spin drag resistance is comparable to, or even larger than, the impurity resistance (section 4.7 and 4.8.1). In this chapter we primarily concentrate on calculating the generalized transport equations governing a spin polarized current in a 2DEG. This could equally well have been done for other systems, like a spin-polarized 3DEG or a DQW structure with tunnelling between the two layers, the generalizing to a 3DEG is in fact done in section 4.9.

4.1 Linear transport in a 2DEG

We are considering a 2DEG in a semiconducting heterostructure, typically a GaAs/AlGaAs structure, with an applied electrical field. We restrict ourselves to weak electrical fields, but allow the background system to have ferromagnetic properties. In order to perform calculations a simple model of the system based on the knowledged gathered in chapter 2 is needed. This model is introduced below.

We emphasize at this point that we are considering electron gasses in the semiclassical limit, at temperatures well below the Fermi temperature, and where all applied fields are weak. These restrictions are

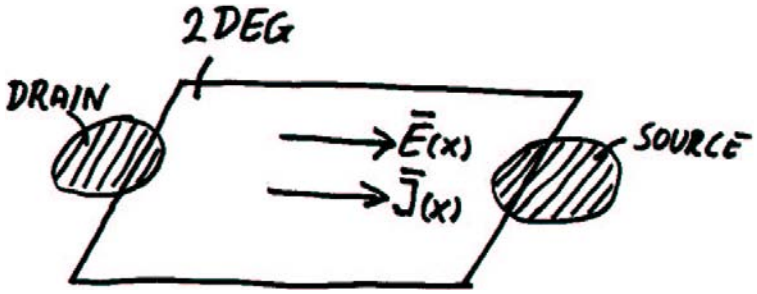

Figure 4.1: When an electrical field is applied, a current begins to run. The current spin polarization depend on the equilibrium polarization of the 2DEG, the source and the drain. The seemingly reversed use of the notion 'drain' and 'source' originate from the fact the the electron charge is negative.

asserted throughout this thesis unless stated otherwise.

4.1.1 The distribution and deviation

We assume that the carriers are conduction electrons situated near the bottom of an isotropic conduction band. The electrons have an equilibrium distribution, $f_s^0(k)$, being

$$f_s^0(k) = f^0(\varepsilon_{ks}) = \frac{1}{e^{\beta(\varepsilon_{ks}-\mu^0)}+1}, \tag{4.1}$$

allowing for the possibility of ferromagnetic systems. Introducing m as the effective electron mass near the conduction band minimum, and ε_s^0 as the spin dependent zero point energy of this minimum, we may write the conduction band as being parabolic

$$\varepsilon_{ks} = \varepsilon_k + \varepsilon_s^0 = \frac{(\hbar k)^2}{2m} + \varepsilon_s^0, \tag{4.2}$$

as discussed in chapter 2. The equilibrium spin dependent density, n_s^0, is given as

$$n_s^0 = \int \frac{d\mathbf{k}}{(2\pi)^2} f_s^0(k) = \frac{m}{2\pi\hbar^2}(\mu^0 - \varepsilon_s^0), \tag{4.3}$$

in analogy with table 2.1, and we define the spin dependent Fermi energy, $\varepsilon_{Fs} = \mu^0 - \varepsilon_s^0$.

Suppose that an electron source and drain is somehow connected to the electron gas. When an electrical field is applied in the x-direction, a spin polarized current density, $J(x)$, begins to run through the system (figure 4.1). The system is no longer in thermal equilibrium and is described by a spin dependent distribution, $f_s(\mathbf{k}, x)$. The local spin polarized density, $n_s(x)$, and the local current density, $J_s(x)$, is given by this distribution as

$$n_s(x) = \int \frac{d\mathbf{k}}{(2\pi)^2} f_s(\mathbf{k}, x), \tag{4.4}$$

$$J_s(x) = \int \frac{d\mathbf{k}}{(2\pi)^2} (-ev_x) f_s(\mathbf{k}, x). \tag{4.5}$$

Calculating the non-equilibrium distribution is complicated. If the applied field is weak, the distribution is a perturbation of the equilibrium distribution and a linear expansion in the electrical field is often adequate. When this is the case, we say that we are in the linear regime, or alternatively that we are considering linear transport. The applied electrical field is assumed to be proportional to the effective field, $\mathbf{E}$, and the linear expansion is usually made in $\mathbf{E}$.

It is useful to describe $f_s(\mathbf{k}, x)$ by a function called the deviation, $\Psi(\mathbf{k}, x)$.

DEFINITION 1 *The electron distribution for an isotropic 2DEG, in an applied electric field pointing in the x-direction, is written*

$$f_s(\mathbf{k}, x) = f_s^0(k) + f_s^0(k)(1 - f_s^0(k))\Psi_s(\mathbf{k}, x), \tag{4.6}$$

thus defining the deviation, $\Psi_s(\mathbf{k}, x) = \Psi_s(k, \cos\theta_{\mathbf{k}}, x)$. Here $\theta_{\mathbf{k}}$ is the angle between $\mathbf{k}$ and the k_x-axis. The deviation has rotational symmetry around the k_x-axis, and is in the linear regime proportional to the applied field.

Note that $\Psi_s(\mathbf{k}, x)$ has rotational symmetry around the x-axis due to the symmetry of the system, but is not necessarily isotropic in space. The system will be in equilibrium when the applied field is zero, so in the linear domain $\Psi_s(\mathbf{k}, x)$ is proportional to the field.

Any function can be described by a suitable (although not necessarily well behaved) deviation at non-zero temperatures, since at these temperatures $f_s^0(1 - f_s^0)$ is never identically equal to zero.

If the deviation is well behaved, then definition 1 has an interesting implication at temperatures below T_F. Since

$$f_s^0(k)(1 - f_s^0(k)) = -\frac{1}{\beta}\frac{\partial f_s^0}{\partial \varepsilon} \approx \frac{1}{\beta}\delta(\varepsilon_{ks} - \mu^0) \tag{4.7}$$

at these temperatures, the linear transport properties can be expected to depend solely on the behavior of the deviation near the Fermi surface, i.e. $\Psi_s(\mathbf{k}, x) = \Psi_s(k_{Fs}, \cos\theta_{\mathbf{k}}, x)$. Here k_{Fs} is the spin-dependent Fermi wave vector corresponding to ε_{Fs}. We shall see (section 4.4) that this is the case, even when electron spin drag interactions are taken into account.

4.1.2 The linearized Boltzmann equation

The steady state Boltzmann equation for the system can be written

$$v_x\frac{\partial f_s}{\partial x} + \dot{\mathbf{k}}\frac{\partial f_s}{\partial \mathbf{k}} = \left(\frac{\partial f_s}{\partial t}\right)_{coll}. \tag{4.8}$$

At low temperatures phonon scattering is normally ignored. We do not, however, ignore electron-electron scattering, since collisions between spin $\uparrow$ and $\downarrow$ electrons may effect $J_\uparrow$ and $J_\downarrow$. So in order to treat low temperature spin polarized transport with the Boltzmann equation, we use a collision integral

$$\left(\frac{\partial f_s}{\partial t}\right)_{coll}(\mathbf{k}, x) = H_0[f_s](\mathbf{k}, x) + H_{sf}[f_s, f_{-s}](\mathbf{k}, x) + H_{ee}[f_s, f_s](\mathbf{k}, x) + H_{ee}[f_s, f_{-s}](\mathbf{k}, x), \tag{4.9}$$

where H_0 and H_{sf} originate from elastic impurity scattering with spin conservation respectively spin flip, and $H_{ee}[f_s, f_{s'}]$ from electron-electron scattering between electrons with spin s and with s' (figure 4.2), as discussed in section 2.2.2.

In linear transport the Boltzmann equation must be linearized. Since $\hbar\dot{\mathbf{k}} = -e\mathbf{E}$, the left hand side (LHS) of (4.8) becomes

$$LHS = v_x\frac{\partial f_s}{\partial x} - \frac{eE}{\hbar}\frac{\partial f_s^0}{\partial k_x}, \tag{4.10}$$

to linear order i E.

For notational convenience the following function is introduced.

DEFINITION 2 *For a two-component system we define*

$$\Delta_{12}(\mathbf{k}_1, \mathbf{k}_2; \mathbf{k}_1', \mathbf{k}_2') = f_1^0(\mathbf{k}_1)f_2^0(\mathbf{k}_2)\big(1 - f_1^0(\mathbf{k}_1')\big)\big(1 - f_2^0(\mathbf{k}_2')\big)\delta(\varepsilon_{\mathbf{k}_1} + \varepsilon_{\mathbf{k}_2} - \varepsilon_{\mathbf{k}_1'} - \varepsilon_{\mathbf{k}_2'}). \tag{4.11}$$

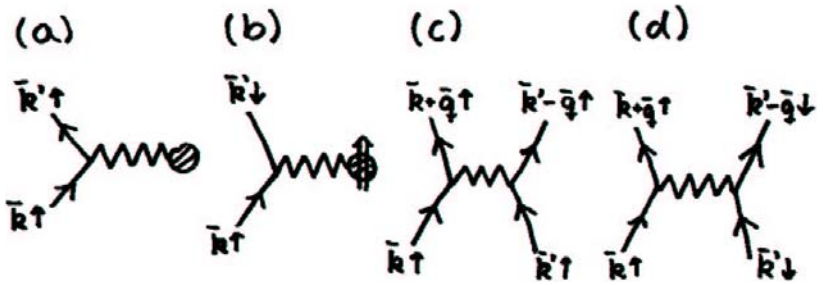

Figure 4.2: Feynman diagrams. (a) Spin conserving impurity scattering. (b) Spin flip impurity scattering. (c) Electron-electron scattering, same spin. (d) Electron-electron scattering, different spin.

The different terms in the collision integral (4.9) are linearized according to proposition 4.1.1.

PROPOSITION 4.1.1 *The linearized collision integrals, $H[\Psi_s, \Psi_{s'}](\mathbf{k}, x) \equiv H[f_s, f_{s'}](\mathbf{k}, x)$, can be written*

$$H_0[\Psi_s](\mathbf{k}, x) = \frac{1}{\beta}\frac{\partial f_s^0(k)}{\partial \varepsilon}\int \frac{d\mathbf{k}'}{(2\pi)^2} w_s^0(\mathbf{k}, \mathbf{k}')[\Psi_s(\mathbf{k}, x) - \Psi_s(\mathbf{k}', x)]\delta(\varepsilon_{ks} - \varepsilon_{k's}), \tag{4.12}$$

$$H_{sf}[\Psi_s, \Psi_{-s}](\mathbf{k}, x) = \frac{1}{\beta}\frac{\partial f_s^0(k)}{\partial \varepsilon}\int \frac{d\mathbf{k}'}{(2\pi)^2} w_{sf}(\mathbf{k}, \mathbf{k}')[\Psi_s(\mathbf{k}, x) - \Psi_{-s}(\mathbf{k}', x)]\delta(\varepsilon_{ks} - \varepsilon_{k'-s}), \tag{4.13}$$

$$\begin{aligned} H_{ee}[\Psi_s, \Psi_{s'}](\mathbf{k}, x) = &-\int \frac{d\mathbf{k}'}{(2\pi)^2}\int \frac{d\mathbf{q}}{(2\pi)^2} w(q)\Delta_{ss'}(\mathbf{k}, \mathbf{k}', \mathbf{k}+\mathbf{q}, \mathbf{k}'-\mathbf{q}) \\ &\times[\Psi_s(\mathbf{k}, x) + \Psi_{s'}(\mathbf{k}', x) - \Psi_s(\mathbf{k}+\mathbf{q}, x) - \Psi_{s'}(\mathbf{k}'-\mathbf{q}, x)]. \end{aligned} \tag{4.14}$$

Here the scattering rate for elastic spin conserving impurity scattering, $w_s^0(\mathbf{k}, \mathbf{k}')$, is allowed to be spin dependent, $w_{sf}(\mathbf{k}, \mathbf{k}')$ is the scattering rate for elastic impurity spin flipping scattering and $w(q)$ is the usual e-e scattering rate (2.55) found by Fermi's golden rule.

PROOF. The expressions (4.12) and (4.13) follows trivially when (4.6) is inserted in (2.57) and (2.58) while using that $f_s^0(k)\delta(\varepsilon_{ks}-\varepsilon_{k's'}) = f_{s'}^0(k')\delta(\varepsilon_{ks}-\varepsilon_{k's'})$. Proving (4.14) is straightforward, but a bit cumbersome. Omitting writing the x-dependance for convenience, $f_s = f_s^0 + f_s^0(1-f_s^0)\Psi_s$ is inserted into H_{ee} given by (2.59) and terms non-linear in Ψ are neglected. Using (2.63) (and omitting some trivial intermediate calculations), we find

$$
\begin{aligned}
H_{ee}[f_s, f_{s'}](\mathbf{k}) &= -\int\frac{d\mathbf{k}'}{(2\pi)^2}\int\frac{d\mathbf{q}}{(2\pi)^2}w(q)\delta(\varepsilon_{ks}+\varepsilon_{k's'}-\varepsilon_{\mathbf{k}+\mathbf{q}s}-\varepsilon_{\mathbf{k}'-\mathbf{q}s'})\\
&\quad\times\Big[f_s(k)f_{s'}(k')(1-f_s(\mathbf{k}+\mathbf{q}))(1-f_{s'}(\mathbf{k}'-\mathbf{q})) - f_s(\mathbf{k}+\mathbf{q})f_{s'}(\mathbf{k}'-\mathbf{q})(1-f_s(k))(1-f_{s'}(k'))\Big]\\
&= -\int\frac{d\mathbf{k}'}{(2\pi)^2}\int\frac{d\mathbf{q}}{(2\pi)^2}w(q)\delta(\varepsilon_{ks}+\varepsilon_{k's'}-\varepsilon_{\mathbf{k}+\mathbf{q}s}-\varepsilon_{\mathbf{k}'-\mathbf{q}s'})\Big[\big[f_s^0(k)+f_s^0(k)(1-f_s^0(k))\Psi_s(\mathbf{k})\big]\\
&\quad\times\big[f_s^0(k)'+f_s^0(k)'(1-f_s^0(k)')\Psi_s(\mathbf{k}')\big]\big[f_s^0(\mathbf{k}+\mathbf{q})+f_s^0(\mathbf{k}+\mathbf{q})(1-f_s^0(\mathbf{k}+\mathbf{q}))\Psi_s(\mathbf{k}+\mathbf{q})\big]\\
&\quad\times\big[f_{s'}^0(\mathbf{k}'-\mathbf{q})+f_{s'}^0(\mathbf{k}'-\mathbf{q})(1-f_{s'}^0(\mathbf{k}'-\mathbf{q}))\Psi_{s'}(\mathbf{k}'-\mathbf{q})\big] - \big[k\leftrightarrow\mathbf{k}+\mathbf{q}, k'\leftrightarrow\mathbf{k}'-\mathbf{q}\big]\Big]\\
&= \ldots = -\int\frac{d\mathbf{k}'}{(2\pi)^2}\int\frac{d\mathbf{q}}{(2\pi)^2}w(q)f_s^0(k)f_{s'}^0(k')(1-f_s^0(\mathbf{k}+\mathbf{q}))(1-f_{-s}^0(\mathbf{k}'-\mathbf{q}))\\
&\quad\times\big[\Psi_s(\mathbf{k})+\Psi_{s'}(\mathbf{k}')-\Psi_s(\mathbf{k}+\mathbf{q})-\Psi_{s'}(\mathbf{k}'-\mathbf{q})\big]\delta(\varepsilon_{ks}+\varepsilon_{k's'}-\varepsilon_{\mathbf{k}+\mathbf{q}s}-\varepsilon_{\mathbf{k}'-\mathbf{q}s'}),
\end{aligned}
$$

which concludes the proof.

4.2 The linearized shifted Fermi-Dirac distribution

In this section we define and investigate a particular type of distributions called shifted Fermi-Dirac (SFD) distributions. They are the simplest linearized distributions that describe the main transport properties in a spin-polarized system, and are, in some systems, solutions to the linearized Boltzmann equation.

4.2.1 Introducing the SFD distribution

Let $\delta\mathbf{k}_s = \delta k_s\hat{\mathbf{e}}_x$ be a $\mathbf{k}$-independent wave vector and $\delta\mu_s$ be a $\mathbf{k}$-independent energy. The function

$$f_s(\mathbf{k};\delta k_s,\delta\mu_s) = f_{FD}(\varepsilon_{\mathbf{k}+\delta\mathbf{k}_s} - (\mu^0+\delta\mu_s)), \tag{4.15}$$

is obviously a Fermi-Dirac distribution centered around $\mathbf{k} = -\delta\mathbf{k}_s$, with a Fermi surface as sketched in figure 4.3. We say that f_s is a shifted Fermi-Dirac distribution.

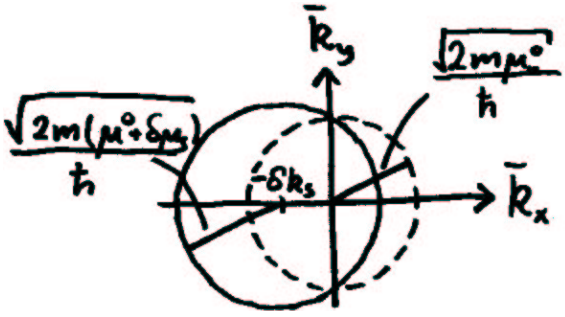

Figure 4.3: The equilibrium (dotted) and SFD Fermi surface.

We are looking for distributions, $f_s(\mathbf{k})$, that solve the Boltzmann equation with an effective electrical field $\mathbf{E} = E\hat{\mathbf{e}}_x$ and would like $f_s(\mathbf{k}; \delta k_s, \delta\mu_s)$ to be a candidate. For this to be realistic, δk_s and $\delta\mu_s$, has to be functions of E and, since they describe a deviation from equilibrium, must fulfill that $\delta k_s|_{E=0} = 0$ and $\delta\mu_s|_{E=0} = 0$. This means that δk_s and $\delta\mu_s$ are proportional to E in the linear regime.

Assuming that the equilibrium distribution, $f_s^0(k) = f_{FD}(\varepsilon_{ks} - \mu^0)$, and expanding $f_s(\mathbf{k})$ around $\varepsilon_{ks} - \mu^0$, we find

$$f_s(\mathbf{k}; \delta k_s, \delta\mu_s) = f_s^0(k) + \frac{\partial f_s^0(k)}{\partial\varepsilon}\big(\hbar v_x \delta k_s + \frac{\hbar^2}{2m}\delta k_s^2 - \delta\mu_s\big) + \frac{1}{2}\frac{\partial^2 f_s^0(k)}{\partial\varepsilon^2}\big(\hbar v_x \delta k_s + \frac{\hbar^2}{2m}\delta k_s^2 - \delta\mu_s\big)^2 + \dots. \quad (4.16)$$

Since δk_s and $\delta\mu_s$ are proportional to E in the linear regime, (4.16) gives that

$$f_s(\mathbf{k}; \delta k_s, \delta\mu_s) = f_s^0(k) + \frac{\partial f_s^0(k)}{\partial\varepsilon}\big(\hbar v_x \delta k_s - \delta\mu_s\big), \quad (4.17)$$

to linear order in E. Allowing δk_s and $\delta\mu_s$ to be x-dependent is trivial, and we have therefore proven proposition 4.2.1.

PROPOSITION 4.2.1 *Let $f_s^0(k)$ be the equilibrium distribution for an isotropic 2DEG and assume that an external electrical field is applied. In the linear regime, the function*

$$f_s(\mathbf{k}; \delta k_s(x), \delta\mu_s(x)) = f_s^0(k) + \frac{\partial f_s^0(k)}{\partial\varepsilon}\big(\hbar v_x \delta k_s(x) - \delta\mu_s(x)\big), \quad (4.18)$$

is a shifted Fermi-Dirac distribution if δk_s and $\delta\mu_s$ are proportional to the applied field.

Comparing (4.18) with (4.6) show corollary 4.2.2.

COROLLARY 4.2.2
The deviation corresponding to the linearized SFD distribution, (4.15), is

$$\Psi_s(\mathbf{k}, x) = \beta(\delta\mu_s(x) - \hbar v_x \delta k_s(x)). \quad (4.19)$$

4.2.2 Properties in a SFD distributed 2DEG

Assume that a spin-polarized current is running in a 2DEG that is described by a SFD distribution. We are primarily interested in two quantities, namely the local spin dependent density, $n_s(x)$, and the current density, $J_s(x)$, given by (4.4) and (4.5).

PROPOSITION 4.2.3 *In a SFD distributed 2DEG, the local spin-dependent density is*

$$n_s(x) = n_s^0 + \frac{m}{2\pi\hbar^2}\delta\mu_s(x), \quad (4.20)$$

and there is a local spin-dependent current density

$$J_s(x) = \frac{e\hbar n_s^0}{m}\delta k_s(x), \quad (4.21)$$

in the x-direction.

PROOF. Inserting $f_s(\mathbf{k};\delta k_s(x),\delta\mu_s(x))$ from (4.18) into (4.4), (4.5), gives

$$n_s(x)=\int\frac{d\mathbf{k}}{(2\pi)^2}[f_s^0(k)+\frac{\partial f_s^0}{\partial\varepsilon}(\hbar v_x\delta k_s-\delta\mu_s)]=n_s^0-\delta\mu_s(x)\int\frac{d\mathbf{k}}{(2\pi)^2}\frac{\partial f_s^0}{\partial\varepsilon}=n_s^0+\frac{m}{2\pi\hbar^2}\delta\mu_s(x),$$

proving (4.20). Remembering that f_s^0 and $\partial f_s^0/\partial\varepsilon$ are even functions of $\mathbf{k}$, and using partial integration, we have

$$J_s(x)=\int\frac{d\mathbf{k}}{(2\pi)^2}(-ev_x)[f_s^0(k)+\frac{\partial f_s^0}{\partial\varepsilon}(\hbar v_x\delta k_s-\delta\mu_s)]=-\frac{e\hbar}{m}\delta k_s(x)\int\frac{d\mathbf{k}}{(2\pi)^2}k_x\frac{\partial f_s^0}{\partial k_x}=\frac{e\hbar n_s^0}{m}\delta k_s(x),$$

proving (4.21).

According to (4.3), the density (4.20) can be written as

$$n_s(x)=\frac{m}{2\pi\hbar^2}(\mu^0+\delta\mu_s(x)-\varepsilon_s^0), \tag{4.22}$$

which leads to the following definition.

DEFINITION 3 *In a SFD distributed 2DEG, the local spin-dependent chemical potential, $\mu_s(x)$, is defined as*

$$\mu_s(x)=\mu^0+\delta\mu_s(x). \tag{4.23}$$

Combining (4.22) and (4.23) gives corollary 4.2.4.

COROLLARY 4.2.4
The local spin-dependent electron density in a SFD distributed 2DEG is

$$n_s(x)=\frac{m}{2\pi\hbar^2}(\mu_s(x)-\varepsilon_s^0). \tag{4.24}$$

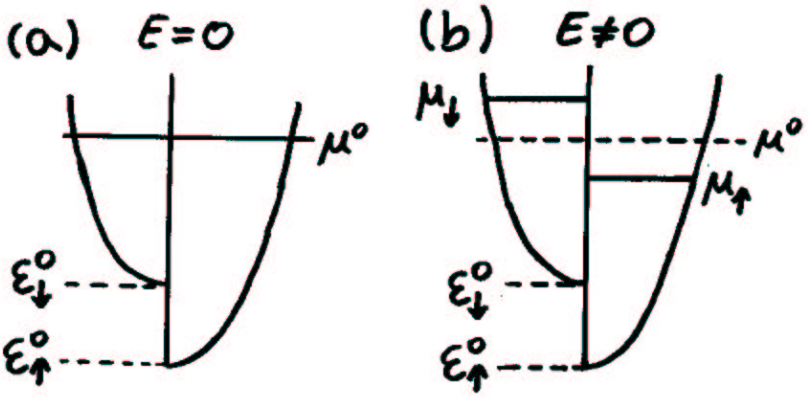

Figure 4.4: (a) Equilibrium distribution when $E=0$. (b) Assumed SFD distribution when $E\neq 0$.

Figure 4.4 sketch the dispersion relations in a 2DEG before and after an electrical field has changed the distribution. If the system is non-magnetic then $\varepsilon_\uparrow^0=\varepsilon_\downarrow^0$, but in general they may differ. Let us assume that, after the field is applied and the transient effects have died out, a current is running through the system. The current depend, among other things, on the polarization of the source and drain and can be spin-polarized in both a non-magnetic and a ferromagnetic 2DEG. Besides having $J_\uparrow(x)\neq J_\downarrow(x)$, the gradients may differ, i.e.

$\partial_x J_\uparrow \neq \partial_x J_\downarrow$, in some parts of space. In such regions the spin-density will change, but this is compensated by spin-flip processes trying to restore the equilibrium spin-density as discussed in section 3.2.1. The relative strength of these two effects determine $\delta\mu_s(x)$ and thereby $\mu_s(x)$. Often the spin-flip rate is relatively small and it is not surprising that $\mu_\uparrow(x) \neq \mu_\downarrow(x)$ in many systems.

4.2.3 The linearized Boltzmann equation in a SFD distributed 2DEG

The collision integrals in the linearized Boltzmann equation can be evaluated when f_s is a SFD distribution, and the results are summarized in the following definition and proposition.

DEFINITION 4 *For an isotropic 2DEG, we define the spin dependent Fermi wave number*

$$k_{Fs} = \sqrt{\frac{2m(\mu_0 - \varepsilon_s^0)}{\hbar^2}}, \tag{4.25}$$

and the following collision rates

$$\frac{1}{\tau_{tr,s}^0} = \int \frac{d\mathbf{k}'}{(2\pi)^2} w_s^0(\mathbf{k},\mathbf{k}')(1-\cos\theta_{\mathbf{k}\cdot\mathbf{k}'})\delta(\varepsilon_{ks}-\varepsilon_{k's}), \tag{4.26}$$

$$\frac{1}{\tau_{sf}} = \int \frac{d\mathbf{k}'}{(2\pi)^2} w_{sf}(\mathbf{k},\mathbf{k}')\delta(\varepsilon_{ks}-\varepsilon_{k'-s}), \tag{4.27}$$

$$\frac{1}{\tau_{tr,s}^{sf}} = \int \frac{d\mathbf{k}'}{(2\pi)^2} w_{sf}(\mathbf{k},\mathbf{k}')(1-\frac{k_{F-s}}{k_{Fs}}\cos\theta_{\mathbf{k}\cdot\mathbf{k}'})\delta(\varepsilon_{ks}-\varepsilon_{k'-s}), \tag{4.28}$$

$$\frac{1}{\tau_{sf,s}} = \frac{k_{F-s}}{k_{Fs}} \int \frac{d\mathbf{k}'}{(2\pi)^2} w_{sf}(\mathbf{k},\mathbf{k}')\cos\theta_{\mathbf{k}\cdot\mathbf{k}'}\delta(\varepsilon_{ks}-\varepsilon_{k'-s}), \tag{4.29}$$

$$\frac{1}{\tau_{tr,s}} = \frac{1}{\tau_{tr,s}^0} + \frac{1}{\tau_{tr,s}^{sf}}, \tag{4.30}$$

where $\theta_{\mathbf{k}\cdot\mathbf{k}'}$ is the angle between $\mathbf{k}$ and $\mathbf{k}'$.

PROPOSITION 4.2.5 *Let $f_s(\mathbf{k}) = f_s(\mathbf{k};\delta k_s,\delta\mu_s)$. Then the linearized collision integrals are given by*

$$H_0[\Psi_s](\mathbf{k}) = -\frac{\partial f_s^0(k)}{\partial\varepsilon}\frac{\hbar v_x \delta k_s}{\tau_{tr,s}^0}, \tag{4.31}$$

$$H_{sf}[\Psi_s,\Psi_{-s}](\mathbf{k}) = \frac{\partial f_s^0(k)}{\partial\varepsilon}\left[\frac{\delta\mu_s-\delta\mu_{-s}}{\tau_{sf}} - \frac{\hbar v_x\delta k_s}{\tau_{tr,s}^{sf}} - \frac{\hbar v_x(\delta k_s-\delta k_{-s})}{\tau_{sf,s}}\right], \tag{4.32}$$

$$H_{ee}[\Psi_s,\Psi_{s'}](\mathbf{k}) = -\frac{\beta\hbar^2(\delta k_s-\delta k_{s'})}{m}\int\frac{d\mathbf{k}'}{(2\pi)^2}\int\frac{d\mathbf{q}}{(2\pi)^2} w(q) q_x \Delta_{ss'}(\mathbf{k},\mathbf{k}',\mathbf{k}+\mathbf{q},\mathbf{k}'-\mathbf{q}). \tag{4.33}$$

PROOF. It is straightforward to find (4.31) and (4.33) by inserting (4.19) into (4.12) and (4.14). Writing the angle between $\mathbf{k}$ and the x-axis as $\theta_{\mathbf{k}}$, and using (4.19) and (4.13) we have

$$H_{sf}[\Psi_s,\Psi_{-s}](\mathbf{k}) = \frac{\partial f_s^0(k)}{\partial\varepsilon}\left[\frac{\delta\mu_s-\delta\mu_{-s}}{\tau_{sf}}+I\right],$$

where

$$\begin{aligned} I &= \int \frac{d\mathbf{k}'}{(2\pi)^2} w_{sf}(\mathbf{k},\mathbf{k}')(-\hbar v_{Fs}\cos\theta_{\mathbf{k}}\delta k_s + \hbar v_{F-s}\cos\theta_{\mathbf{k}'}\delta k_{-s})\delta(\varepsilon_{ks}-\varepsilon_{k'-s}) \\ &= -\hbar v_{Fs}\cos\theta_{\mathbf{k}}\int\frac{d\mathbf{k}'}{(2\pi)^2}w_{sf}(\mathbf{k},\mathbf{k}')\big[\delta k_s - \frac{k_{F-s}}{k_{Fs}}(\cos\theta_{\mathbf{k}\cdot\mathbf{k}'}+\tan\theta_{\mathbf{k}}\sin\theta_{\mathbf{k}\cdot\mathbf{k}'})\delta k_{-s}\big]\delta(\varepsilon_{ks}-\varepsilon_{k'-s}) \\ &= -\hbar v_{Fs}\cos\theta_{\mathbf{k}}\left[\frac{\delta k_s}{\tau^{sf}_{tr,s}}+\frac{\delta k_s-\delta k_{-s}}{\tau_{sf,s}}\right]. \end{aligned}$$

Remembering that $v_x = v_{Fs}\cos\theta_{\mathbf{k}}$ when I is multiplied with $\partial_\varepsilon f_s^0$, proves (4.32). We have used that $\cos\theta_{\mathbf{k}'} = \cos(\theta_{\mathbf{k}\cdot\mathbf{k}'}+\theta_{\mathbf{k}}) = \cos\theta_{\mathbf{k}\cdot\mathbf{k}'}\cos\theta_{\mathbf{k}}+\sin\theta_{\mathbf{k}\cdot\mathbf{k}'}\sin\theta_{\mathbf{k}}$, and that the integral over $\sin\theta_{\mathbf{k}\cdot\mathbf{k}'}$ vanish. This is because the scattering probability, $w_{sf}(\mathbf{k},\mathbf{k}')$, in an isotropic system is a function of $\cos\theta_{\mathbf{k}\cdot\mathbf{k}'}$ due to symmetry reasons.

The following definition defines a quantity that will appear in future calculations.

DEFINITION 5 *In a SFD distributed 2DEG the local spin-dependent electrochemical potential, $\bar\mu_s(x)$, is defined as*

$$\bar\mu_s(x) = \mu_s(x) - e\phi(x), \tag{4.34}$$

where $\phi(x)$ is the effective electrical potential and $\mu(x)$ is the local chemical potential.

From (4.33) it is obvious that $\delta k_s = \delta k_{s'} \Rightarrow H_{ee}[\Psi_s,\Psi_{s'}] = 0$, and as a trivial consequence

$$H_{ee}[\Psi_s,\Psi_s] = 0. \tag{4.35}$$

So, the steady state linearized Boltzmann equation reads

$$v_x\frac{\partial f_s}{\partial x} - \frac{eE}{\hbar}\frac{\partial f_s^0}{\partial k_x} = \frac{\partial f_s^0}{\partial\varepsilon}\left[\frac{\delta\mu_s-\delta\mu_{-s}}{\tau_{sf}} - \frac{\hbar v_x\delta k_s}{\tau_{tr,s}} - \frac{\hbar v_x(\delta k_s-\delta k_{-s})}{\tau_{sf,s}}\right] + H_{ee}[\Psi_s,\Psi_{-s}](\mathbf{k},x), \tag{4.36}$$

where the transport time, $\tau^{-1}_{tr,s}$, is defined in (4.30). Using (4.18) and

$$\frac{\partial f_s^0}{\partial\varepsilon} = \frac{1}{\hbar v_x}\frac{\partial f_s^0}{\partial k_x}, \tag{4.37}$$

we can write

$$v_x\frac{\partial f_s}{\partial x} - \frac{eE}{\hbar}\frac{\partial f_s^0}{\partial k_x} = \frac{\partial f_s^0}{\partial k_x}\left[v_x\frac{\partial(\delta k_s)}{\partial x} - \frac{1}{\hbar}\big(\frac{\partial\mu_s}{\partial x}+e\frac{\partial\phi}{\partial x}\big)\right] = \frac{\partial f_s^0}{\partial k_x}\left[v_x\frac{\partial(\delta k_s)}{\partial x} - \frac{1}{\hbar}\frac{\partial\bar\mu_s}{\partial x}\right]. \tag{4.38}$$

Inserting $\delta\mu_s-\delta\mu_{-s} = \bar\mu_s-\bar\mu_{-s}$ in (4.36), and using (4.38), proves proposition 4.2.6.

PROPOSITION 4.2.6 *In a SFD distributed 2DEG, the low temperature, linearized, steady state Boltzmann equation is*

$$\frac{\partial f_s^0}{\partial k_x}\left[v_x\frac{\partial(\delta k_s)}{\partial x} - \frac{1}{\hbar}\frac{\partial\bar\mu_s}{\partial x}\right] = \frac{\partial f_s^0}{\partial\varepsilon}\left[\frac{\bar\mu_s-\bar\mu_{-s}}{\tau_{sf}} - \frac{\hbar v_x\delta k_s}{\tau_{tr,s}} - \frac{\hbar v_x(\delta k_s-\delta k_{-s})}{\tau_{sf,s}}\right] + H_{ee}[\Psi_s,\Psi_{-s}](\mathbf{k},x). \tag{4.39}$$

The electrochemical potential (4.34) appearing in (4.38) is one of the essential transport quantities we shall consider in the remaining thesis.

4.2.4 Ordinary impurity scattering

Let us show that the SFD distribution is an exact solution to the linearized Boltzmann equation for a non-magnetic 2DEG with $n_\uparrow^0 = n_\downarrow^0$ and an unpolarized current, $J_\uparrow = J_\downarrow$.

The linearized Boltzmann equation is given by (4.36), and we guess on a SFD distribution $f_\uparrow(\mathbf{k}) = f_\downarrow(\mathbf{k}) = f(\mathbf{k}; \delta k, 0)$, since this satisfies the conditions, $J_\uparrow = J_\downarrow = J/2$ and $n_\uparrow = n_\downarrow = n^0/2$. Inserting $f_s = f(\mathbf{k}; \delta k, 0)$ and using $\partial_x f_s = 0$, (4.36) reduces to

$$-\frac{eE}{\hbar}\frac{\partial f_s^0(k)}{\partial k_x} = -\frac{\partial f_s^0(k)}{\partial k_x}\frac{\delta k}{\tau_{tr,s}}. \tag{4.40}$$

From (4.40) and (4.21), we find

$$\delta k = \frac{e\tau_{tr,s}}{\hbar}E \Rightarrow J = 2\frac{e\hbar n_s^0}{m}\delta k = \frac{n^0 e^2 \tau_{tr,s}}{m}E = \sigma E, \tag{4.41}$$

and recognize σ as the Drude conductivity.

So, the solution to the Boltzmann equation with solely elastic impurity scattering terms is a SFD distribution, with a deviation that is found by comparing (4.41) with (4.19) to be

$$\Psi_s(\mathbf{k}) = -\beta\hbar v_x \delta k = -\beta\tau_{tr,s} e v_x E. \tag{4.42}$$

4.3 Coulomb drag in DQW, revisited

In section 3.1.2 it was stated that the drag rate, τ_D^{-1}, measured in Gramilla's experiment can be calculated using two coupled linearized Boltzmann equations. The result was claimed to be

$$\frac{1}{\tau_D} = \frac{\beta\hbar^2}{2\pi^2 n_2 m_1}\int_0^\infty dq \int_0^\infty d\omega\, q^3 |e\phi(q)|^2 \frac{Im\chi_1(q,\omega) Im\chi_2(q,\omega)}{\sinh^2(\beta\hbar\omega/2)}. \tag{4.43}$$

In this section we will show this, taking an approach similar to the one used by Jauho and Smith [16].

4.3.1 Mathematical tricks

In order to calculate the drag rate we first need to prove two propositions. To that end the following trivial lemma is used.

LEMMA 4.3.1 *Dirac's delta function satisfies that*

$$\delta(\varepsilon_{\mathbf{k}} + \varepsilon_{\mathbf{k}'} - \varepsilon_{\mathbf{k}+\mathbf{q}} - \varepsilon_{\mathbf{k}'-\mathbf{q}}) = \hbar\int_{-\infty}^{\infty} d\omega\, \delta(\varepsilon_{\mathbf{k}} - \varepsilon_{\mathbf{k}+\mathbf{q}} - \hbar\omega)\delta(\varepsilon_{\mathbf{k}'} - \varepsilon_{\mathbf{k}'-\mathbf{q}} + \hbar\omega). \tag{4.44}$$

The Fermi-Dirac distribution satisfies that

$$f^0(\varepsilon)(1 - f^0(\varepsilon + \hbar\omega)) = \frac{f^0(\varepsilon) - f^0(\varepsilon + \hbar\omega)}{1 - e^{-\beta\hbar\omega}}. \tag{4.45}$$

The function Δ_{12} satisfies

$$\Delta_{12}(\mathbf{k}_1, \mathbf{k}_2; \mathbf{k}_1 + \mathbf{q}, \mathbf{k}_2 - \mathbf{q}) = \Delta_{12}(\mathbf{k}_1 + \mathbf{q}, \mathbf{k}_2 - \mathbf{q}; \mathbf{k}_1, \mathbf{k}_2). \tag{4.46}$$

PROOF. The relations (4.44) and (4.45) are trivial and (4.46) follows immediately from use of (2.63).

Now it is straightforward to show the two required propositions, proposition 4.3.2 and proposition 4.3.3.

PROPOSITION 4.3.2 *Let $w(\mathbf{q}) = w(q)$ be an arbitrary isotropic function. Then*

$$\begin{aligned}&\int\frac{d\mathbf{k}}{(2\pi)^2}\int\frac{d\mathbf{k}'}{(2\pi)^2}\int\frac{d\mathbf{q}}{(2\pi)^2}\,w(q)k_xq_x\Delta_{12}(\mathbf{k},\mathbf{k}';\mathbf{k}+\mathbf{q},\mathbf{k}'-\mathbf{q}) = \\ &-\frac{1}{4}\int\frac{d\mathbf{k}}{(2\pi)^2}\int\frac{d\mathbf{k}'}{(2\pi)^2}\int\frac{d\mathbf{q}}{(2\pi)^2}\,w(q)q^2\Delta_{12}(\mathbf{k},\mathbf{k}';\mathbf{k}+\mathbf{q},\mathbf{k}'-\mathbf{q}).\end{aligned} \tag{4.47}$$

PROOF. Let

$$I = \int\frac{d\mathbf{k}}{(2\pi)^2}\int\frac{d\mathbf{k}'}{(2\pi)^2}\int\frac{d\mathbf{q}}{(2\pi)^2}\,w(q)k_xq_x\Delta_{12}(\mathbf{k},\mathbf{k}';\mathbf{k}+\mathbf{q},\mathbf{k}'-\mathbf{q}).$$

I can also be written

$$\begin{aligned}I &= \int\frac{d\mathbf{q}}{(2\pi)^2}\int\frac{d(\mathbf{k}-\mathbf{q})}{(2\pi)^2}\int\frac{d(\mathbf{k}'+\mathbf{q})}{(2\pi)^2}\,w(q)(k_x-q_x)q_x\Delta_{12}(\mathbf{k}-\mathbf{q},\mathbf{k}'+\mathbf{q};\mathbf{k},\mathbf{k}') \\ &= -\int\frac{d\mathbf{q}}{(2\pi)^2}\int\frac{d(\mathbf{k}+\mathbf{q})}{(2\pi)^2}\int\frac{d(\mathbf{k}'-\mathbf{q})}{(2\pi)^2}\,w(q)(k_x+q_x)q_x\Delta_{12}(\mathbf{k},\mathbf{k}';\mathbf{k}+\mathbf{q},\mathbf{k}'-\mathbf{q}) \\ &= -I-\int\frac{d\mathbf{q}}{(2\pi)^2}\int\frac{d\mathbf{k}}{(2\pi)^2}\int\frac{d\mathbf{k}'}{(2\pi)^2}\,w(q)q_x^2\Delta_{12}(\mathbf{k},\mathbf{k}';\mathbf{k}+\mathbf{q},\mathbf{k}'-\mathbf{q}),\end{aligned}$$

when changing variable $\mathbf{q}\to-\mathbf{q}$, using $w(q)=w(-q)$ and (4.46). The proof is completed by noting that, in an isotropic two dimensional system, integrating $q^2=q_x^2+q_y^2$ is the same as integrating $2q_x^2$.

PROPOSITION 4.3.3 *The function Δ_{12} satisfies*

$$\int\frac{d\mathbf{k}}{(2\pi)^2}\int\frac{d\mathbf{k}'}{(2\pi)^2}\,\Delta_{12}(\mathbf{k},\mathbf{k}';\mathbf{k}+\mathbf{q},\mathbf{k}'-\mathbf{q}) = \frac{\hbar}{2\pi^2}\int_0^\infty d\omega\,\frac{Im\chi_1(q,\omega)Im\chi_2(q,\omega)}{\sinh^2(\beta\hbar\omega/2)}. \tag{4.48}$$

PROOF. First we note that

$$\mathrm{Im}\chi(q,\omega) = \lim_{\eta\to0_+}\int\frac{d\mathbf{k}}{(2\pi)^2}\frac{f^0(\mathbf{k}+\mathbf{q})-f^0(\mathbf{k})}{\varepsilon_{\mathbf{k}}-\varepsilon_{\mathbf{k}+\mathbf{q}}+\hbar\omega-i\eta} = -\pi\int\frac{d\mathbf{k}}{(2\pi)^2}\left(f^0(\mathbf{k}+\mathbf{q})-f^0(\mathbf{k})\right)\delta(\varepsilon_{\mathbf{k}}-\varepsilon_{\mathbf{k}+\mathbf{q}}+\hbar\omega). \tag{4.49}$$

Using (4.44), (4.45), (4.49) and $\chi(q,\omega)=-\chi(q,-\omega)$, we find that

$$\begin{aligned}&\int\frac{d\mathbf{k}}{(2\pi)^2}\int\frac{d\mathbf{k}'}{(2\pi)^2}\,f_1^0(\mathbf{k})f_2^0(\mathbf{k}')\big(1-f_1^0(\mathbf{k}+\mathbf{q})\big)\big(1-f_2^0(\mathbf{k}'-\mathbf{q})\big)\delta(\varepsilon_{\mathbf{k}}+\varepsilon_{\mathbf{k}'}-\varepsilon_{\mathbf{k}+\mathbf{q}}-\varepsilon_{\mathbf{k}'-\mathbf{q}}) = \\ &\hbar\int_{-\infty}^\infty d\omega\int\frac{d\mathbf{k}}{(2\pi)^2}\int\frac{d\mathbf{k}'}{(2\pi)^2}\,\frac{f_1^0(\mathbf{k})-f_1^0(\mathbf{k}+\mathbf{q})}{1-e^{\beta\hbar\omega}}\frac{f_2^0(\mathbf{k}')-f_2^0(\mathbf{k}'-\mathbf{q})}{1-e^{-\beta\hbar\omega}}\,\delta(\varepsilon_{\mathbf{k}}-\varepsilon_{\mathbf{k}+\mathbf{q}}-\hbar\omega)\delta(\varepsilon_{\mathbf{k}'}-\varepsilon_{\mathbf{k}'-\mathbf{q}}+\hbar\omega) \\ &= -\frac{\hbar}{4\pi^2}\int_{-\infty}^\infty d\omega\,\frac{\mathrm{Im}\chi_1(q,-\omega)\mathrm{Im}\chi_2(q,\omega)}{\sinh^2(\beta\hbar\omega/2)} = \frac{\hbar}{2\pi^2}\int_0^\infty d\omega\,\frac{\mathrm{Im}\chi_1(q,\omega)\mathrm{Im}\chi_2(q,\omega)}{\sinh^2(\beta\hbar\omega/2)},\end{aligned}$$

which concludes the proof.

4.3.2 The drag rate

When electron tunnelling between the two layers is negligible, the coupled linearized Boltzmann equations read

$$-\frac{eE_1}{\hbar}\frac{\partial f_1^0(k_1)}{\partial k_{1x}} = H_0[\Psi_1](\mathbf{k}_1) + H_{ee}[\Psi_1,\Psi_2](\mathbf{k}_1), \tag{4.50}$$

$$-\frac{eE_2}{\hbar}\frac{\partial f_2^0(k_2)}{\partial k_{2x}} = H_0[\Psi_2](\mathbf{k}_2) + H_{ee}[\Psi_2,\Psi_1](\mathbf{k}_2), \tag{4.51}$$

where H_0 is the elastic impurity- and H_{ee} the interwell electron-electron collision integral. As already mentioned we only take impurity and interlayer Coulomb collision integrals into account, partly for simplicity, but also because phonon and other scattering mechanisms are considered to be negligible at low temperatures. This is not completely true, as Gramilla's experiment showed (section 3.1), and the drag rate calculated here will be approximately a factor of 2 too small.

Since the layers are spatially separated, the momentum loss in layer 1 is clearly dominated by impurity scattering and H_{ee} can be neglected in (4.50). In layer 2, however, no current is running and it is a reasonable assumption[1] that $f_2 = f_2^0$, i.e. the deviation $\Psi_2 = 0$. This in turn means that $H_0[\Psi_2] = 0$ and the Boltzmann equations become

$$-\frac{eE_1}{\hbar}\frac{\partial f_1^0(k_1)}{\partial k_{1x}} = H_0[\Psi_1](\mathbf{k}_1), \tag{4.52}$$

$$-\frac{eE_2}{\hbar}\frac{\partial f_2^0(k_2)}{\partial k_{2x}} = H_{ee}[0,\Psi_1](\mathbf{k}_2). \tag{4.53}$$

According to (4.42), the solution to (4.52) is a SFD distribution with deviation

$$\Psi_1(\mathbf{k}_1) = -\beta\tau_1 e v_{1x} E_1, \tag{4.54}$$

where τ_1^{-1} is the impurity scattering rate in layer 1. At low temperatures τ_1 is taken to be momentum independent. Inserting Ψ_1 into the linearized electron-electron collision integral (4.14) and remembering to sum over the two possible spin directions s_1, equation (4.53) can be written

$$-\frac{eE_2}{\hbar}\frac{\partial f_2^0(k_2)}{\partial k_{2x}} = \frac{\beta\tau_1 e\hbar E_1}{m_1}\sum_{s_1}\int\frac{d\mathbf{k}_1}{(2\pi)^2}\int\frac{d\mathbf{q}}{(2\pi)^2}w(q)q_x\Delta_{21}(\mathbf{k}_2,\mathbf{k}_1,\mathbf{k}_2+\mathbf{q},\mathbf{k}_1-\mathbf{q}). \tag{4.55}$$

Performing the operation $\sum_{s_2}\int\frac{d\mathbf{k}_2}{(2\pi)^2}k_{2x}$ on both sides of (4.55) and using (4.47) and (4.48), we get

$$\frac{en_2E_2}{\hbar} = -\frac{\beta\tau_1 e\hbar^2 E_1}{8\pi^2 m_1}\sum_{s_1s_2}\int\frac{d\mathbf{q}}{(2\pi)^2}\int_0^\infty d\omega w(q)q^2\frac{Im\chi_1(q,\omega)Im\chi_2(q,\omega)}{\sinh^2(\beta\hbar\omega/2)}. \tag{4.56}$$

According to the definition (3.1) it is seen that

$$\frac{m_1}{n_1e^2\tau_D} = \left|\frac{E_1}{J_2}\right| = \left|\frac{E_2}{\sigma_1 E_1}\right| = \left|\frac{m_1E_2}{n_1e^2\tau_1E_1}\right|,$$

which, together with (4.56), gives

$$\frac{1}{\tau_D} = \frac{1}{\tau_1}\left|\frac{E_2}{E_1}\right| = \frac{\beta\hbar^3}{8\pi^2 n_2 m_1}\sum_{s_1s_2}\int\frac{d\mathbf{q}}{(2\pi)^2}\int_0^\infty d\omega w(q)q^2\frac{Im\chi_1(q,\omega)Im\chi_2(q,\omega)}{\sinh^2(\beta\hbar\omega/2)}. \tag{4.57}$$

[1]The assumption is more accurately that $\Psi_2 \ll \Psi_1$ since Ψ_2 is "driven" by Ψ_1 via the weak drag force, and that $H_0 = 0$ in layer 2 since no current is running.

Introducing polar coordinates, performing the spin summation and using the Golden rule scattering rate (2.55), we find

$$\sum_{s_1 s_2} \int \frac{d\mathbf{q}}{(2\pi)^2} w(q) \to 4 \frac{1}{2\pi} \int_0^\infty dq q \frac{2\pi}{\hbar} |e\phi(q)|^2,$$

and it is a simple matter to transform (4.57) into the drag rate, τ_D^{-1}, given by (4.43).

4.4 Spin drag without spin-flip processes for $T \ll T_F$

We want to show that a SFD distribution, at sufficiently low temperatures $T \ll T_F$, is an exact solution to the linearized Boltzmann equation

$$v_x \frac{\partial f_s}{\partial x} - \frac{eE}{\hbar} \frac{\partial f_s^0}{\partial k_x} = H_0[f_s] + H_{ee}[f_s, f_s] + H_{ee}[f_s, f_{-s}], \tag{4.58}$$

where electron-electron interactions are included, but where spin-flip processes are not. Since the system is isotropic, the deviation, ψ_s, has cylindrical symmetry and can be written

$$\psi_s(\mathbf{k}, x) = \psi_s(k, \cos\theta, x). \tag{4.59}$$

Here θ as usual is the angle between the x-axis and $\mathbf{k}$.

The first step in proving that a SFD distribution is an exact solution to (4.58), is showing that the deviation need only be evaluated in the vicinity of the Fermi circle, meaning that (4.59) can be written as

$$\psi_s(k, \cos\theta, x) \approx \psi_s(k_{Fs}, \cos\theta, x) \equiv \psi_s(\cos\theta, x). \tag{4.60}$$

This is obviously the case for all the terms in (4.58), except for the H_{ee} collision integrals. This is because the remaining terms are linear in the distribution f_s, and therefore (4.6) combined with (4.7) gives that

$$f_s(k, \cos\theta) = f_s^0(k) - \frac{1}{\beta} \frac{\partial f_s^0}{\partial \varepsilon} \psi_s(k_{Fs}, \cos\theta), \tag{4.61}$$

can immediately be used. In H_{ee} the situation is more complicated since these collision integrals are not linear in the distribution f_s. Using (4.11), (4.14) and lemma 4.3.1, we write (omitting the x-dependence for convenience)

$$\begin{aligned} H_{ee}[f_s, f_{s'}](\mathbf{k}) &= -\int \frac{d\mathbf{k}'}{(2\pi)^2} \int \frac{d\mathbf{q}}{(2\pi)^2} w(q) \Delta_{ss'}(\mathbf{k}, \mathbf{k}', \mathbf{k}+\mathbf{q}, \mathbf{k}'-\mathbf{q}) [\psi_s(\mathbf{k}) + \psi_{s'}(\mathbf{k}') - \psi_s(\mathbf{k}+\mathbf{q}) - \psi_{s'}(\mathbf{k}'-\mathbf{q})] \\ &= -\hbar \int_{-\infty}^{\infty} d\omega \int \frac{d\mathbf{k}'}{(2\pi)^2} \int \frac{d\mathbf{q}}{(2\pi)^2} w(q) \frac{Im\chi_s(\mathbf{k}, \mathbf{q}; \omega) Im\chi_{s'}(\mathbf{k}', \mathbf{q}; \omega)}{\sinh^2(\beta\hbar\omega)} [\psi_s(\mathbf{k}) + \psi_{s'}(\mathbf{k}') - \psi_s(\mathbf{k}+\mathbf{q}) - \psi_{s'}(\mathbf{k}'-\mathbf{q})], \end{aligned} \tag{4.62}$$

where we have defined

$$Im\chi_s(\mathbf{k}, \mathbf{q}; \omega) = (f_s^0(\mathbf{k}+\mathbf{q}) - f_s^0(\mathbf{k})) \delta(\varepsilon_{\mathbf{k}+\mathbf{q}s} - \varepsilon_{\mathbf{k}s} - \hbar\omega). \tag{4.63}$$

At the low temperatures were are dealing with, the function $\sinh^{-2}(\beta\hbar\omega/2)$ is sharply peaked around zero, so the ω-integral is restricted to small ω of order $k_B T$. Using this in the δ-function it is seen that $\varepsilon_{\mathbf{k}+\mathbf{q}s}$ and $\varepsilon_{\mathbf{k}s}$ deviate at most by an amount $k_B T$ from each other. At low temperatures $Im\chi_s(\mathbf{k}, \mathbf{q}; \omega)$ can therefore be expanded as

$$Im\chi_s(\mathbf{k},\mathbf{q};\omega) = \hbar\omega\left(-\frac{f^0(\varepsilon_{ks}-f^0(\varepsilon_{ks}+\hbar\omega)}{\hbar\omega}\right)\delta(\varepsilon_{\mathbf{k}+\mathbf{q}s}-\varepsilon_{\mathbf{k}s}-\hbar\omega) \approx \hbar\omega\left(-\frac{\partial f_s^0}{\partial\varepsilon_{ks}}\right)\delta(\varepsilon_{\mathbf{k}+\mathbf{q}s}-\varepsilon_{\mathbf{k}s}-\hbar\omega). \tag{4.64}$$

According to (4.7) it is obvious that ε_{ks} and therefore also $\varepsilon_{\mathbf{k}+\mathbf{q}s}$ in (4.64) lie within k_BT from the Fermi level. The same consideration holds for $\varepsilon_{k's}$ and $\varepsilon_{\mathbf{k}'-\mathbf{q}s}$, so to leading order in k_BT/ε_{Fs} we can neglect the k dependance of ψ_s so that (4.60) hold.

The next step is to expand the deviation in harmonics of the angle θ

$$\psi_s(x,\cos\theta) = \sum_{n=0}^{\infty} g_s^{(n)}(x)\cos(n\theta). \tag{4.65}$$

Let us insert (4.65) into the Boltzmann equation (4.58). On the left hand side (LHS), we have

$$LHS = -v_x\frac{\partial f_s^0}{\partial\varepsilon}\left(\frac{1}{\beta}\frac{\partial\psi_s}{\partial x}-eE\right) = v_{Fs}\cos\theta\frac{\partial f_s^0}{\partial\varepsilon}\left(\frac{1}{\beta}\sum_{n=0}^{\infty}\frac{\partial g_s^{(n)}}{\partial x}\cos(n\theta)-eE\right). \tag{4.66}$$

On the right hand side of (4.58) we have three collision integrals. Defining $\theta_{\mathbf{k}\cdot\mathbf{k}'}$ as the angle between $\mathbf{k}$ and $\mathbf{k}'$ and θ' between $\mathbf{k}'$ and the x-axis, so that $\theta' = \theta + \theta_{\mathbf{k}\cdot\mathbf{k}'}$, using the trigonometric formula

$$\cos(n\theta') = \cos(n\theta+n\theta_{\mathbf{k}\cdot\mathbf{k}'}) = \cos(n\theta)\cos(n\theta_{\mathbf{k}\cdot\mathbf{k}'}) - \sin(n\theta)\sin(n\theta_{\mathbf{k}\cdot\mathbf{k}'}), \tag{4.67}$$

and remembering that $w_s^0(\mathbf{k},\mathbf{k}')$ has the same symmetry as $\cos\theta$ so the integration over $\sin\theta_{\mathbf{k}\cdot\mathbf{k}'}$ vanishes, we write the impurity collision integral, H_0, as

$$H_0[f_s] = -\frac{\partial f_s^0}{\partial\varepsilon}\sum_{n=1}^{\infty}\frac{g_s^{(n)}\cos(n\theta)}{\beta\tau_{tr,s}^{(n)}}. \tag{4.68}$$

Here

$$\frac{1}{\tau_{tr,s}^{(n)}} = \int\frac{d\mathbf{k}'}{(2\pi)^2}w_s^0(\mathbf{k},\mathbf{k}')[1-\cos(n\theta_{\mathbf{k}\cdot\mathbf{k}'})]\delta(\varepsilon_{ks}-\varepsilon_{k's}). \tag{4.69}$$

When (4.65) is inserted into the two remaining collision integrals corresponding to electron-electron scattering the different n-terms do not couple. We will not prove this result here, but refer the interested reader to [15] where it is stated that

$$H_{ee}[f_s,f_{s'}](x,\cos\theta) = \sum_{n=1}^{\infty}\cos(n\theta)\left(g_s^{(n)}J^{(n)}+g_{s'}^{(n)}I^{(n)}\right), \tag{4.70}$$

where $J^{(n)}$ refer to the first and third terms in (4.62), and $I^{(n)}$ to the second and fourth terms. The $n=0$ term in (4.70) vanish which is seen in (4.62) where the constant terms $g_s^{(0)}$ and $g_{-s}^{(0)}$ cancel each other. All in all, defining

$$\eta_s = -\frac{\partial f_s^0}{\partial\varepsilon}, \tag{4.71}$$

using (4.66), (4.68), (4.70) and $2\cos\theta\cos(n\theta) = \cos(n-1)\theta+\cos(n+1)\theta$, we find that the Boltzmann equation can be written as

$$\begin{aligned} v_{Fs}\left(\frac{\eta_s}{2\beta}\sum_{n=0}^{\infty}\frac{\partial g_s^{(n)}}{\partial x}(\cos(n-1)\theta+\cos(n+1)\theta)-eE\cos\theta\right) &= \sum_{n=1}^{\infty}\cos(n\theta) \\ &\times\left[g_s^{(n)}\left(\frac{\eta_s}{\beta\tau_{tr,s}^{(n)}}+2J^{(n)}+I^{(n)}\right)+g_{-s}^{(n)}I^{(n)}\right]. \end{aligned} \tag{4.72}$$

Multiplying (4.72) with $\cos(m\theta)$ and integrating over θ while using

$$\int_0^{2\pi} d\theta \cos(m\theta)\cos(n\theta) = \pi\delta_{m,n}(\delta_{m,0}+1), \tag{4.73}$$

gives the following set of equations:

$$m=0: \quad \frac{\partial g_s^{(1)}}{\partial x} = 0, \tag{4.74}$$

$$m=1: \quad \frac{\eta_s v_{Fs}}{2\beta}\left(\frac{\partial g_s^{(2)}}{\partial x}+\frac{\partial g_s^{(0)}}{\partial x}\right) - v_{Fs}eE = g_s^{(1)}\left(\frac{\eta_s}{\beta\tau_{tr,s}^{(1)}}+2J^{(1)}+I^{(1)}\right)+g_{-s}^{(1)}I^{(1)}, \tag{4.75}$$

$$m\geq 2: \quad \frac{\eta_s v_{Fs}}{2\beta}\left(\frac{\partial g_s^{(m+1)}}{\partial x}+\frac{\partial g_s^{(m-1)}}{\partial x}\right) = g_s^{(m)}\left(\frac{\eta_s}{\beta\tau_{tr,s}^{(m)}}+2J^{(m)}+I^{(m)}\right)+g_{-s}^{(m)}I^{(m)}. \tag{4.76}$$

We see that a solution to these equations appear when $g_s^{(m)}=0$ for $m\geq 2$. This is because, when $\partial_x g_s^{(1)}=0$ is inserted in (4.76) for $m=2$, the equations for $m\geq 2$ decouples from (4.74) and (4.75). Equation (4.74) expresses the current conservation of each spin component. If spin-flip scattering is included in the Bolztmann equation, then $\partial_x g_s^{(1)}\neq 0$, which means that the equations couple and $g_s^{(m)}=0$ for $m\geq 2$ is no longer a solution.

Finally we note, by comparing with (4.18), that setting $g_s^{(m)}=0$ for $m\geq 2$ corresponds to a SFD distribution $f_s(\mathbf{k};\delta k_s,\delta\mu_s)$, where

$$g_s^{(0)} = \beta\delta\mu_s, \quad g_s^{(1)} = -\hbar v_{Fs}\delta k_s. \tag{4.77}$$

Therefore (4.58) has an exact solution that is SFD distributed.

4.5 Transport equations and spin drag in spin-polarized transport

Consider a 2DEG in which a spin-polarized current is running. This constitutes a two-component system analogous to the DQW, the components now being the spin $\uparrow$ and $\downarrow$ electrons. These are not spatially separated, and as a consequence spin drag effects may be significantly larger than drag effects in DQW systems. A simple calculation (section 4.7 and 4.8.1) shows that spin drag resistivity is appreciable, even compared to the impurity resistivity, and hence is not negligible in spin-polarized transport. Our main objective is to find two macroscopic transport equations in the low temperature linear regime, similar to the transport equations found by Valet an Fert, but now taking spin drag into account.

Previously in this chapter, we have shown that SFD distributions solve the Boltzmann equations for normal impurity scattering (section 4.2.4), and also when spin-flip processes are neglected at either very low temperatures (section 4.4) or when the e-e interaction is weak (section 4.3, generalized to spin drag). At higher temperatures, with general interaction strength and finite spin-flip scattering the SFD distribution is not an exact solution. Nevertheless we assume that it is a good approximation. This we call the SFD ansatz or SFD approximation. In the following we shall find the generalized macroscopic transport equations using the SFD ansatz.

4.5.1 The spin drag rate

Inspired by Jauho and Smith's drag rate calculation (section 4.3), the following proposition hold.

PROPOSITION 4.5.1 *The spin drag rate, $\tau_{D,s}^{-1}$, in a 2DEG with negligible spin flip processes and with a fully spin s polarized current, i.e. $J_s = J$ and $J_{-s}=0$, is*

$$\frac{1}{\tau_{D,s}} = \frac{\beta\hbar^2}{8\pi^2 n^0_{-s} m}\int_0^\infty dq \int_0^\infty d\omega\, q^3 |e\phi(q)|^2 \frac{Im\chi_\uparrow(q,\omega) Im\chi_\downarrow(q,\omega)}{\sinh^2(\beta\hbar\omega/2)}. \tag{4.78}$$

PROOF. All the calculations go as in the DQW calculation, except for the spin summation in (4.56), which now gives a factor 1 instead of a factor 4. So taking (4.43), replacing index $1 \leftrightarrow s$, $2 \leftrightarrow -s$ and dividing with 4 gives (4.78).

The spin rate (4.78) appears in the transport equations through the electron-electron collision integral, H_{ee}. The connection between the two is clearly stated in proposition 4.5.2.

PROPOSITION 4.5.2 *For a SFD distributed 2DEG the electron-electron collision integral fulfils*

$$\int \frac{d\mathbf{k}}{(2\pi)^2} H_{ee}[\Psi_s, \Psi_{-s}](\mathbf{k}, x) = 0, \tag{4.79}$$

$$\int \frac{d\mathbf{k}}{(2\pi)^2} k_x H_{ee}[\Psi_s, \Psi_{-s}](\mathbf{k}, x) = \frac{n^0_{-s}}{\tau_{D,s}}\big(\delta k_s(x) - \delta k_{-s}(x)\big). \tag{4.80}$$

PROOF. First we prove (4.79). Using (4.33) and (4.48) we have that

$$\begin{aligned}\int \frac{d\mathbf{k}}{(2\pi)^2} H_{ee}[\Psi_s, \Psi_{-s}](\mathbf{k}, x) &= -\frac{\beta\hbar^2(\delta k_s - \delta k_{-s})}{m}\int \frac{d\mathbf{k}}{(2\pi)^2}\int \frac{d\mathbf{k}'}{(2\pi)^2}\int \frac{d\mathbf{q}}{(2\pi)^2} w(q) q_x \Delta_{s-s}(\mathbf{k}, \mathbf{k}', \mathbf{k}+\mathbf{q}, \mathbf{k}'-\mathbf{q}) \\ &= -\frac{\beta\hbar^3(\delta k_s - \delta k_{-s})}{2\pi^2 m}\int_0^\infty d\omega \int \frac{d\mathbf{q}}{(2\pi)^2} w(q) q_x \frac{Im\chi_\uparrow(q,\omega) Im\chi_\downarrow(q,\omega)}{\sinh^2(\beta\hbar\omega/2)} = 0,\end{aligned}$$

since $w(q)$ and $\chi_s(q,\omega)$ are even functions and q_x is an odd function of $\mathbf{q}$.
When proving (4.80) we use (4.33), (4.47) and (4.48) to find

$$\begin{aligned}I = \int \frac{d\mathbf{k}}{(2\pi)^2} k_x H_{ee}[\Psi_s, \Psi_{-s}](\mathbf{k}, x) &= \frac{\beta\hbar^2(\delta k_s - \delta k_{-s})}{4m}\int \frac{d\mathbf{k}}{(2\pi)^2}\int \frac{d\mathbf{k}'}{(2\pi)^2}\int \frac{d\mathbf{q}}{(2\pi)^2} w(q) q^2 \Delta_{s-s}(\mathbf{k}, \mathbf{k}', \mathbf{k}+\mathbf{q}, \mathbf{k}'-\mathbf{q}) \\ &= \frac{\beta\hbar^3(\delta k_s - \delta k_{-s})}{8\pi^2 m}\int_0^\infty d\omega \int \frac{d\mathbf{q}}{(2\pi)^2} w(q) q^2 \frac{Im\chi_\uparrow(q,\omega) Im\chi_\downarrow(q,\omega)}{\sinh^2(\beta\hbar\omega/2)}.\end{aligned}$$

Remembering that $w(q) = (2\pi/\hbar)|e\phi(q)|^2$, so that

$$\int \frac{d\mathbf{q}}{(2\pi)^2} w(q) \to \frac{1}{2\pi}\int_0^\infty dq q \frac{2\pi}{\hbar}|e\phi(q)|^2,$$

and introducing (4.78), we find that

$$I = \frac{\beta\hbar^2(\delta k_s - \delta k_{-s})}{8\pi^2 m}\int_0^\infty dq \int_0^\infty d\omega\, q^3 |e\phi(q)|^2 \frac{Im\chi_\uparrow(q,\omega) Im\chi_\downarrow(q,\omega)}{\sinh^2(\beta\hbar\omega/2)} = \frac{n^0_{-s}}{\tau_{D,s}}\big(\delta k_s - \delta k_{-s}\big),$$

which proves (4.80).

4.5.2 The macroscopic transport equations

For a SFD distributed 2DEG, the Boltzmann equation is in (4.39) given as

$$\frac{\partial f^0_s}{\partial k_x}\left[v_x \frac{\partial(\delta k_s)}{\partial x} - \frac{1}{\hbar}\frac{\partial \bar{\mu}_s}{\partial x}\right] = \frac{\partial f^0_s(k)}{\partial \varepsilon}\left[\frac{\bar{\mu}_s - \bar{\mu}_{-s}}{\tau_{sf}} - \frac{\hbar v_x \delta k_s}{\tau_{tr,s}} - \frac{\hbar v_x(\delta k_s - \delta k_{-s})}{\tau_{sf,s}}\right] + H_{ee}[\Psi_s, \Psi_{-s}](\mathbf{k}, x). \tag{4.81}$$

Two transport equations can be extracted from this Boltzmann equation. We first introduce some definitions.

DEFINITION 6 *The following spin-independent conductivity is defined*

$$\sigma_D = \frac{n_s^0 e^2 \tau_{D,s}}{m}, \tag{4.82}$$

and also the following spin-dependent quantities

$$\sigma_{tr,s} = \frac{n_s^0 e^2 \tau_{tr,s}}{m}, \tag{4.83}$$

$$\sigma_{sf,s} = \frac{n_s^0 e^2 \tau_{sf,s}}{m}, \tag{4.84}$$

$$\alpha_s = \frac{n_s^0}{n_{-s}^0}. \tag{4.85}$$

Now we can prove proposition 4.5.3, giving the two generalized transport equations.

PROPOSITION 4.5.3 *In the SFD-approximation the following two transport equations hold*

$$\textit{Steady state continuity equation :} \qquad \frac{\partial J_s}{\partial x} = \frac{me}{2\pi\hbar^2}\frac{\bar{\mu}_s - \bar{\mu}_{-s}}{\tau_{sf}}, \tag{4.86}$$

$$\textit{Generalized Ohm's law :} \qquad \frac{\partial \bar{\mu}_s}{\partial x} = \frac{e}{\sigma_{tr,s}} J_s + \left(\frac{e}{\sigma_{sf,s}} + \frac{e}{\alpha_s \sigma_D}\right)\left(J_s - \alpha_s J_{-s}\right). \tag{4.87}$$

PROOF. Let LHS be the left hand side and RHS the right hand side of (4.81). Performing the operation $\int \frac{d\mathbf{k}}{(2\pi)^2}$ and using (4.79) gives

$$\int \frac{d\mathbf{k}}{(2\pi)^2} LHS = \frac{\hbar}{m}\frac{\partial(\delta k_s)}{\partial x}\int \frac{d\mathbf{k}}{(2\pi)^2} k_x \frac{\partial f_s^0}{\partial k_x} = -\frac{\hbar n_s^0}{m}\frac{\partial(\delta k_s)}{\partial x}, \tag{4.88}$$

$$\int \frac{d\mathbf{k}}{(2\pi)^2} RHS = \frac{\bar{\mu}_s - \bar{\mu}_{-s}}{\tau_{sf}}\int \frac{d\mathbf{k}}{(2\pi)^2}\frac{\partial f_s^0}{\partial \varepsilon} = -\frac{m}{2\pi\hbar^2}\frac{\bar{\mu}_s - \bar{\mu}_{-s}}{\tau_{sf}}. \tag{4.89}$$

Setting (4.88)=(4.89) and introducing J_s by (4.21), results in the first transport equation

$$\frac{\partial J_s}{\partial x} = \frac{me}{2\pi\hbar^2}\frac{\bar{\mu}_s - \bar{\mu}_{-s}}{\tau_{sf}}.$$

Obtaining the second transport equation requires a bit more work. Performing the operation $\int \frac{d\mathbf{k}}{(2\pi)^2} k_x$ and using (4.80) gives

$$\int \frac{d\mathbf{k}}{(2\pi)^2} k_x LHS = -\frac{1}{\hbar}\frac{\partial \bar{\mu}_s}{\partial x}\int \frac{d\mathbf{k}}{(2\pi)^2} k_x \frac{\partial f_s^0}{\partial k_x} = \frac{n_s^0}{\hbar}\frac{\partial \bar{\mu}_s}{\partial x}, \tag{4.90}$$

$$\int \frac{d\mathbf{k}}{(2\pi)^2} k_x RHS = \frac{n_s^0}{\tau_{tr,s}}\delta k_s + \left(\frac{n_s^0}{\tau_{sf}} + \frac{n_{-s}^0}{\tau_{D,s}}\right)(\delta k_s - \delta k_{-s}). \tag{4.91}$$

Setting (4.90)=(4.91), introducing the relative spin density, $\alpha_s = n_s^0/n_{-s}^0$, and once again (4.21), gives

$$\frac{n_s^0}{\hbar}\frac{\partial \bar{\mu}_s}{\partial x} = \frac{m}{e\hbar\tau_{tr,s}}J_s + \frac{m}{e\hbar}\left(\frac{n_s^0}{\tau_{sf}} + \frac{n_{-s}^0}{\tau_{D,s}}\right)\left(\frac{J_s}{n_s^0} - \frac{J_{-s}}{n_{-s}^0}\right) = \frac{m}{e\hbar\tau_{tr,s}}J_s + \frac{m}{e\hbar}\left(\frac{1}{\tau_{sf,s}} + \frac{1}{\alpha_s\tau_{D,s}}\right)\left(J_s - \alpha_s J_{-s}\right). \tag{4.92}$$

This is essentially the second transport equation, and using (4.82)-(4.85) it is easy to rewrite (4.92) to the form given in (4.87).

In analogue with the discussion in section 3.2.1, we see that (4.86) is a steady state continuity equation where the spin flip processes are added as drain or source terms. The equation has the same formal structure as (3.10) found by Valet and Fert.

The generalized Ohm's law given in (4.87) is not identical to Valet and Fert's equation (3.11). The major difference between the two is the explicit appearance of the term

$$\left(\frac{e}{\sigma_{sf,s}} + \frac{e}{\alpha_s\sigma_D}\right)\left(J_s - \alpha_s J_{-s}\right), \tag{4.93}$$

lacking in (3.11). It's physical origin can be understood by writing (4.93) as

$$n_s^0\left(\frac{e}{\sigma_{sf,s}} + \frac{e}{\alpha_s\sigma_D}\right)\left(\frac{J_s}{n_s^0} - \frac{J_{-s}}{n_{-s}^0}\right). \tag{4.94}$$

The last parenthesis in (4.94) shows that an additional resistance arises when the average momentum, J_s/n_s^0, per spin s electron is larger the the average momentum, J_{-s}/n_{-s}^0, per spin $-s$ electron. This additional resistance furthermore depends on processes that transfer momentum between the two spin directions. Such processes are responsible for the two terms in the second parenthesis.

The first term, $\sigma_{sf,s}$, describe that spin-flip processes may transfer momentum between the spin components. Consider a process where an electron with momentum $\mathbf{k}$ and spin s is scattered on a magnetic impurity or such, ending up with momentum $\mathbf{k}'$ and spin $-s$. The probability for such a process is given by $w_{sf}(\mathbf{k},\mathbf{k}')$. If for instance $w_{sf}(\mathbf{k},\mathbf{k}')$ favours forward scattering, i.e. scattering in the $\mathbf{k}$ direction, then a net momentum can be transferred between the spin current components. If the spin-flip process does not favor any particular $\mathbf{k}'$ direction, the net momentum transfer is zero. This is known as s-wave scattering and can be expressed by saying that the scattering processes has no memory of the state of incoming electrons. These considerations are confirmed mathematically in (4.29) where it seen that $(\tau_{sf,s})^{-1} = 0$ if $w_{sf}(\mathbf{k},\mathbf{k}')$ is isotropic. When Valet and Fert derived the transport equations they were interested in the "big picture" and neglected all but s-wave spin-flip scattering. Therefore this term is missing in (3.11).

The second term, σ_D, is caused by spin drag, i.e. processes where electrons scatter on electrons with opposite spin and exchange momentum. This term eluded Valet and Fert because they did not consider electron-electron scattering.

4.5.3 The generalized diffusion and Laplace equation

In order to calculate the spin polarized transport properties through magnetic multilayers, Valet and Fert derived the two second order equations (3.16) and (3.17). Here we wish to find the equivalent second order equations corresponding to the general case with spin-drag and anisotropic spin-flip scattering.

First we prove the following proposition.

PROPOSITION 4.5.4 *Suppose that $\bar{\mu}_s$ and J_s fulfills the transport equations given in proposition 4.5.3, and D_s is an arbitrary constant. Then*

$$\frac{\partial^2}{\partial x^2}\left(D_s\bar{\mu}_s + D_{-s}\bar{\mu}_{-s}\right) = \frac{m}{2\pi\hbar^2}\frac{e^2}{\tau_{sf}}\left(\frac{D_s}{\sigma_s} - \frac{D_{-s}}{\sigma_{-s}}\right)(\bar{\mu}_s - \bar{\mu}_{-s}), \tag{4.95}$$

where

$$\frac{1}{\sigma_s} = \frac{1}{\sigma_{tr,s}} + \frac{1+\alpha_s}{\sigma_{sf,s}} + \frac{1+\alpha_{-s}}{\sigma_D}. \tag{4.96}$$

PROOF. We write (4.87) as

$$\frac{\partial \bar{\mu}_s}{\partial x} = e\rho_s^{\shortparallel} J_s - e\rho_s^{\perp} J_{-s}, \tag{4.97}$$

where the 'direct resistivity', $\rho_s^{\shortparallel}$, and the 'transresistivity', $\rho_s^{\perp}$, are given by

$$\rho_s^{\shortparallel} = \frac{1}{\sigma_{tr,s}} + \frac{1}{\sigma_{sf,s}} + \frac{1}{\alpha_s \sigma_D}, \tag{4.98}$$

$$\rho_s^{\perp} = \frac{\alpha_s}{\sigma_{sf,s}} + \frac{1}{\sigma_D}. \tag{4.99}$$

Taking the derivative of (4.97) and using (4.86) gives

$$\frac{\partial^2 \bar{\mu}_s}{\partial x^2} = e\rho_s^{\shortparallel} \frac{\partial J_s}{\partial x} - e\rho_s^{\perp} \frac{\partial J_{-s}}{\partial x} = \frac{m}{2\pi\hbar^2} \frac{e^2}{\tau_{sf}} \left(\rho_s^{\shortparallel} + \rho_s^{\perp}\right) \left(\bar{\mu}_s - \bar{\mu}_{-s}\right). \tag{4.100}$$

Armed with (4.100) it is now trivial to show (4.95), where $(\sigma_s)^{-1} = \rho_s^{\shortparallel} + \rho_s^{\perp}$ (which is easily seen to be equivalent with (4.96)).

We proceed by defining a couple of useful quantities.

DEFINITION 7 *We define the effective conductivity, σ, by*

$$\frac{1}{\sigma} = \frac{1}{\sigma_s} + \frac{1}{\sigma_{-s}}, \tag{4.101}$$

and the effective spin-flip length, l_{sf}, by

$$\frac{1}{l_{sf}^2} = \frac{m}{2\pi\hbar^2} \frac{e^2}{\sigma\tau_{sf}}. \tag{4.102}$$

Here σ_s is the conductivity introduced by (4.96) and τ_{sf} the relaxation time defined in (4.27).

Using proposition 4.5.4 it is easy to find the generalized second order equations equivalent to (3.16) and (3.17).

COROLLARY 4.5.5
If $\bar{\mu}_s$ and J_s fulfil the transport equations given in proposition 4.5.3, then

$$\textit{Diffusion equation :} \qquad \frac{\partial^2}{\partial x^2}(\bar{\mu}_s - \bar{\mu}_{-s}) = \frac{\bar{\mu}_s - \bar{\mu}_{-s}}{l_{sf}^2}, \tag{4.103}$$

$$\textit{Generalized Laplace equation :} \qquad \frac{\partial^2}{\partial x^2}(\sigma_s \bar{\mu}_s + \sigma_{-s}\bar{\mu}_{-s}) = 0. \tag{4.104}$$

PROOF. Both equations follow immediately from (4.95). Inserting $D_s = 1$ and $D_{-s} = -1$ gives (4.103), and inserting $D_s = \sigma_s$ and $D_{-s} = \sigma_{-s}$ gives (4.104).

We can use (4.103) and (4.104) to find the spin polarized transport through magnetic multilayers in a manner similar to the one described in section 3.2.2. Solving the two equations shows that the characteristic

Transport equations for a 2DEG including spin drag

Steady state continuity equation :
$$\frac{\partial J_s}{\partial x} = \frac{me}{2\pi\hbar^2}\frac{\bar{\mu}_s - \bar{\mu}_{-s}}{\tau_{sf}},$$

Generalized Ohm's law :
$$\frac{\partial \bar{\mu}_s}{\partial x} = \frac{e}{\sigma_{tr,s}}J_s + \left(\frac{e}{\sigma_{sf,s}} + \frac{e}{\alpha_s\sigma_D}\right)\left(J_s - \alpha_s J_{-s}\right),$$

Diffusion equation :
$$\frac{\partial^2}{\partial x^2}(\bar{\mu}_s - \bar{\mu}_{-s}) = \frac{\bar{\mu}_s - \bar{\mu}_{-s}}{l_{sf}^2},$$

Generalized Laplace equation :
$$\frac{\partial^2}{\partial x^2}(\sigma_s\bar{\mu}_s + \sigma_{-s}\bar{\mu}_{-s}) = 0.$$

The relative equilibrium spin density, α_s :
$$\alpha_s = \frac{n_s^0}{n_{-s}^0}$$

The spin dependent constant σ_s is given by :
$$\frac{1}{\sigma_s} = \frac{1}{\sigma_{tr,s}} + \frac{1+\alpha_s}{\sigma_{sf,s}} + \frac{1+\alpha_{-s}}{\sigma_D}$$

The effective conductivity σ is given by :
$$\frac{1}{\sigma} = \frac{1}{\sigma_s} + \frac{1}{\sigma_{-s}}$$

The spin flip length l_{sf} is given by :
$$\frac{1}{l_{sf}^2} = \frac{m}{2\pi\hbar^2}\frac{e^2}{\sigma\tau_{sf}}$$

Event	**Related rate**	**Related resistivity**
Spin flip event	$\frac{1}{\tau_{sf}}$	
Momentum loss of spin current component, J_s, due to spin conserving elastic collisions between an electron with spin s and an impurity	$\frac{1}{\tau_{tr,s}^0}$	
Momentum loss of the total current, $J = J_s + J_{-s}$, due to spin flip event $s \to -s$	$\frac{1}{\tau_{tr,s}^{sf}}$	
Momentum loss of the total current, $J = J_s + J_{-s}$, due to scattering processes where the initial electron has spin s	$\frac{1}{\tau_{tr,s}} = \frac{1}{\tau_{tr,s}^0} + \frac{1}{\tau_{tr,s}^{sf}}$	$\frac{1}{\sigma_{tr,s}}$
Momentum transfer from $J_s \to J_{-s}$ due to spin flip event $s \to -s$	$\frac{1}{\tau_{sf,s}}$	$\frac{1}{\sigma_{sf,s}}$
Momentum transfer from $J_s \to J_{-s}$, due to electron-electron interaction	$\frac{1}{\tau_{D,s}}$	$\frac{1}{\sigma_D}$

Table 4.1: Transport equations in the SFD approximation for a 2DEG, and the physical origin of various constants.

length scale for spin current conversion, in analogy to the discussion in section 3.2.2, is the spin-flip length, l_{sf}, given by (4.102).

In table 4.1 we summarize the results achieved so far. We also list in the table the physical origin of many of the rates and conductivities introduced in the transport equations. They are typically related to various scattering events, and the corresponding scattering times can be divided into three categories.

The first is the ordinary spin flip relaxation time, τ_{sf}. It is simply the "mean" time between two consecutive spin flip processes. The second category are transport relaxation times, $\tau^1_{tr,s}, \tau^s_{tr,sf}, \tau_{tr,s}$, relating to processes that alters the total current. The last type of times, $\tau^s_{sf}, \tau_{D,s}$, describe processes that transfer a net momentum from one spin current component to the other.

4.6 Consequences of spin drag

In the following we investigate some effects of spin drag compared to systems where spin drag can be neglected.

4.6.1 The equations with negligible spin drag

We begin by finding the equations in systems with negligible spin drag . This is done by taking the generalized equations and letting the time between two spin drag "events" $\tau_D \to \infty$, since this express that the time between two consequtive drag "events" is infinity and therefore plays no role.

Definition 8 *We define the spin-dependent conductivity, $\sigma_{s,0}$, by*

$$\frac{1}{\sigma_{s,0}} = \frac{1}{\sigma_{tr,s}} + \frac{1+\alpha_s}{\sigma_{sf,s}}, \tag{4.105}$$

the reduced conductivity, σ_0, by

$$\frac{1}{\sigma_0} = \frac{1}{\sigma_{s,0}} + \frac{1}{\sigma_{-s,0}}, \tag{4.106}$$

and the spin-flip length, $l_{sf,0}$ by

$$\frac{1}{l^2_{sf,0}} = \frac{m}{2\pi\hbar^2}\frac{e^2}{\sigma_0\tau_{sf}}. \tag{4.107}$$

Here τ_{sf} is the relaxation time defined in (4.27).

Inserted $\tau_D \to \infty$ in (4.86), (4.87), (4.103) and (4.104) easily gives the relevant equations, listed in the following corollary.

Corollary 4.6.1
In the SFD approximation, the following equations hold in a 2DEG with negligible spin drag

$$\textit{Steady state continuity equation :} \qquad \frac{\partial J_s}{\partial x} = \frac{me}{2\pi\hbar^2}\frac{\bar{\mu}_s - \bar{\mu}_{-s}}{\tau_{sf}}, \tag{4.108}$$

$$\textit{Generalized Ohm's law :} \qquad \frac{\partial \bar{\mu}_s}{\partial x} = \frac{e}{\sigma_{tr,s}}J_s + \frac{e}{\sigma_{sf,s}}\big(J_s - \alpha_s J_{-s}\big), \tag{4.109}$$

$$\textit{Diffusion equation :} \qquad \frac{\partial^2}{\partial x^2}(\bar{\mu}_s - \bar{\mu}_{-s}) = \frac{\bar{\mu}_s - \bar{\mu}_{-s}}{l^2_{sf,0}}, \tag{4.110}$$

$$\textit{Generalized Laplace equation :} \qquad \frac{\partial^2}{\partial x^2}(\sigma_{s,0}\bar{\mu}_s + \sigma_{-s,0}\bar{\mu}_{-s}) = 0. \tag{4.111}$$

4.6.2 Drag enhanced resistivity

In ordinary electromagnetism the voltage , U_{AB}, between two points, A and B, is defined as

$$U_{AB} = \int_A^B \mathbf{E} \cdot d\mathbf{s}, \tag{4.112}$$

in a system without a time varying magnetic field. Introducing the electrical potential, ϕ, by

$$\mathbf{E} = -\nabla\phi, \tag{4.113}$$

we see that

$$U_{AB} = \int_A^B \mathbf{E} \cdot d\mathbf{s} = -\int_A^B \nabla\phi \cdot d\mathbf{s} = \phi(A) - \phi(B). \tag{4.114}$$

The voltage, U_{AB}, is typically measured by a voltmeter. The voltmeter measures the current, I_V, through a large and known resistance, R_V, and uses Ohm's law

$$U_{AB} = R_V I_V, \tag{4.115}$$

to find U_{AB} (figure 4.5a). If we know the current, I, through the component, Ω, the resistance, R, of Ω is given by

$$RI = U_{AB} = \int_A^B \mathbf{E} \cdot d\mathbf{s}. \tag{4.116}$$

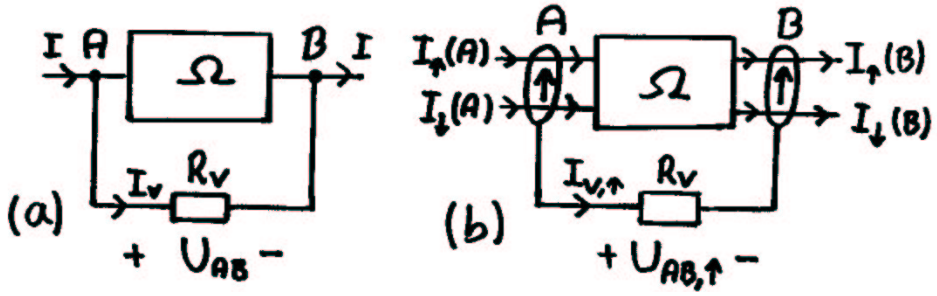

Figure 4.5: (a) Normal voltmeter measurement of the voltage U_{AB}. (b) Voltmeter measurement of $U_{AB,\uparrow}$ in spin polarized transport.

It is important to know that the voltmeter measures the current running through a well-known resistance. Hence the voltmeter measures the total effect of all the current driving processes, and not just the electrical potential. Consider for instance the spin polarized transport experiment sketched in figure 4.5b, and suppose that the contacts connecting the voltmeter and the system are constructed in such a way that only spin $\uparrow$ electrons are allowed to pass. This can for instance be done by choosing a ferromagnetic material as contacts. The measured voltage will reflect the total spin $\uparrow$ current driving processes. The spin $\uparrow$ current is driven by the electrical potential, ϕ, but, as we have seen, also contains a diffusion contribution due to a possible non-zero spin $\uparrow$ density gradient. In this case, the readout, $U_{AB,\uparrow}$, on the voltmeter is a sum of the two contributions. In general $U_{AB,s}$ can be written

$$U_{AB,s} = \int_A^B (\frac{1}{e}\nabla\mu_s - \nabla\phi) \cdot d\mathbf{s} = \frac{1}{e}\int_A^B \nabla\bar{\mu}_s \cdot d\mathbf{s} = \int_A^B \mathbf{E}_s \cdot d\mathbf{s}, \tag{4.117}$$

where $U_{AB,s}$ is the measured voltage when only spin s electrons are allowed to pass through the voltmeter contacts. Here $\bar{\mu}_s$ is the electrochemical potential given by (4.34) and we have introduced an effective "pseudo-electrical" field

$$\mathbf{E}_s = \frac{1}{e}\nabla\bar{\mu}_s. \tag{4.118}$$

Let us consider the system sketched in figure 4.6a, where the source and drain only allows spin ↑ electrons to pass. When the dimensions of the system fulfil that $l_{diff} < |AB| < l_{sf}$, where l_{diff} is the minimum width of a 2DEG in the diffusive regime and l_{sf} is the spin flip length given by (4.102), we can safely assume that the current, $\mathbf{J} = J\mathbf{e}_x$ is totally spin polarized throughout the 2DEG. Choosing the x-direction in the direction of the current, this means that

$$J_s(x) = J, \quad J_{-s}(x) = 0, \tag{4.119}$$

in the 2DEG. We shall not be concerned about the feasibility of the setup, but in the following assume that in principle it can be constructed.

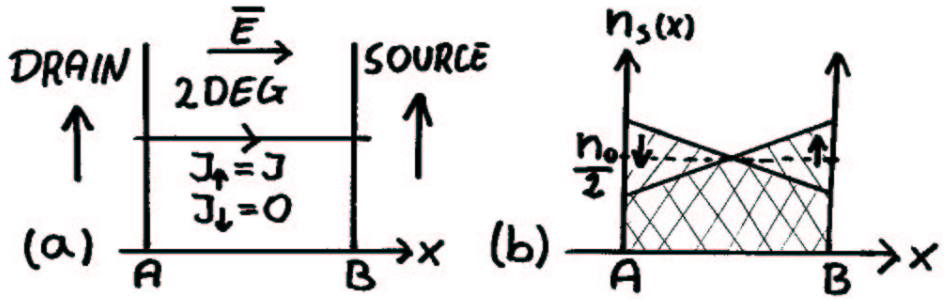

Figure 4.6: (a) An experiment where the current is composed of purely spin ↑ electrons throughout the 2DEG. (b) The spin density has a gradient throughout the 2DEG. This is needed to oppose the electrical force that otherwise would drive a spin ↓ current.

Using (4.97) we write the effective field, E_s, as

$$E_\uparrow(x) = \frac{1}{e}\frac{\partial\bar{\mu}_\uparrow}{\partial x} = \rho^{\shortparallel}_{\downarrow} J, \quad E_\downarrow(x) = -\rho^{\perp}_{\downarrow} J, \tag{4.120}$$

where the direct- and transresistivity are given by (4.98) and (4.99). Without spin drag ($\sigma_D \to \infty$) we find that

$$E_\uparrow(x) = \frac{1}{e}\frac{\partial\bar{\mu}_\uparrow}{\partial x} = \rho^{\shortparallel}_{\uparrow,0} J, \quad E_\downarrow(x) = -\rho^{\perp}_{\downarrow,0} J, \tag{4.121}$$

where

$$\rho^{\shortparallel}_{s,0} = \frac{1}{\sigma_{tr,s}} + \frac{1}{\sigma_{sf,s}} \equiv \frac{1}{\sigma^{\shortparallel}_{s,0}}, \quad \rho^{\perp}_{s,0} = \frac{\alpha_s}{\sigma_{sf,s}} \equiv \frac{1}{\sigma^{\perp}_{s,0}}. \tag{4.122}$$

Using (4.98), (4.99), (4.121) and (4.122) we can write the drag enhanced resistivities as

$$\rho^{\shortparallel}_s = \rho^{\shortparallel}_{s,0}\left(1 + \frac{\sigma^{\shortparallel}_{s,0}}{\sigma_D}\right), \tag{4.123}$$

$$\rho^{\perp}_s = \rho^{\perp}_{s,0}\left(1 + \frac{\sigma^{\perp}_{s,0}}{\sigma_D}\right). \tag{4.124}$$

When we consider spin drag in a 2DEG, σ_D is often comparable to $\sigma^{\shortparallel}_{s,0}$, and the drag enhancement of the resistivity cannot be neglected. As usual, the Valet and Fert expressions are found by letting $\sigma_D \to \infty$ and $\sigma_{sf,s} \to \infty$.

The spin density, $n_s(x)$, must have a non-zero gradient throughout the 2DEG in order for $J_\downarrow$ to be zero. This gradient provides a diffusion contribution to $J_\downarrow$ that exactly cancels the contribution from the electrical potential. This is sketched in figure 4.6b for a 2DEG with equilibrium densities $n_\uparrow^0 = n_\downarrow^0 = n^0/2$.

4.6.3 Drag decreased spin flip length

Another consequence of spin drag is that the spin flip length, l_{sf}, is shorter in a system with large drag than in one with small. This is understandable since the drag will "slow down" the electrons so they spend an increasing time in the vicinity of the magnetic ions that cause the spin flip, thus enhancing the process probability. Comparing (4.102) and (4.107) we immediately find l_{sf} in the presence of spin drag compared to $l_{sf,0}$.

PROPOSITION 4.6.2 *The generalized spin flip length, l_{sf}, can be written as*

$$l_{sf} = \frac{l_{sf,0}}{\sqrt{1 + \dfrac{(2+\alpha_s+\alpha_{-s})\sigma_0}{\sigma_D}}}, \tag{4.125}$$

where $l_{sf,0}$ is the spin flip length given by (4.107).

PROOF. Comparing (4.96) and (4.105) it is obvious that

$$\frac{1}{\sigma_s} = \frac{1}{\sigma_{s,0}} + \frac{1+\alpha_{-s}}{\sigma_D}.$$

Now we see from (4.101) and (4.106), that

$$\frac{1}{\sigma} = \frac{1}{\sigma_0} + \frac{2+\alpha_s+\alpha_{-s}}{\sigma_D},$$

which used in (4.102) gives (4.125).

Needless to say, the Valet and Fert spin flip length is found in the usual manner ($\sigma_D \to \infty$ and $\sigma_{sf,s} \to \infty$).

4.7 Evaluating the spin drag rate in a 2DEG

It is time to show that the low temperature spin drag rate, $\tau_{D,s}^{-1}$, in many realistic 2DEG, created for instance in GaAs/AlGaAs heterostructures, will be comparable to the impurity scattering time, τ_0^{-1}.

We consider an nonmagnetic 2DEG, where $n_\uparrow^0 = n_\downarrow^0 = n^0/2$. The spin drag rate is given by (4.78), which we write as

$$\frac{1}{\tau_{D,s}} = \frac{\beta\hbar^2}{8\pi^2 n_{-s}^0 m} I = \frac{\beta\hbar^2}{4\pi^2 n^0 m} I, \tag{4.126}$$

where

$$I = \int_0^\infty dq \int_0^\infty d\omega q^3 |e\phi(q)|^2 \frac{\mathrm{Im}\chi_\uparrow(q,\omega)\mathrm{Im}\chi_\downarrow(q,\omega)}{\sinh^2(\beta\hbar\omega/2)}. \tag{4.127}$$

For our purpose, and at sufficiently low temperatures, it is a reasonable approximation to use the zero-temperature, low-frequency susceptibility (valid for $q \ll 2k_F$)

$$\mathrm{Im}\chi_s(q,\omega) = \frac{m^2\omega}{2\pi\hbar^3 q k_F}, \tag{4.128}$$

given by (2.188). We furthermore introduce the screened Thomas-Fermi potential (2.103), so that

$$|e\phi(q)| = \frac{e^2}{2\varepsilon_0\varepsilon_b(q+q_{TF})}. \tag{4.129}$$

Here the two-dimensional Thomas-Fermi wave vector, q_{TF}, is given by (2.102). Using (4.128) and (4.129), we write (4.127) as

$$I = \left(\frac{m^2e^2}{4\pi\hbar^3k_F\varepsilon_0\varepsilon_b}\right)^2 \int_0^\infty dq \frac{q^3}{(q+q_{TF})^2}\frac{1}{q^2}\int_0^\infty d\omega \frac{\omega^2}{\sinh^2(\beta\hbar\omega/2)} = \left(\frac{m}{\gamma\hbar}\right)^2 I_1 I_2, \tag{4.130}$$

where

$$\gamma = \frac{2k_F}{q_{TF}}, \quad I_1 = \int_0^\infty dq \frac{q}{(q+q_{TF})^2}, \quad I_2 = \int_0^\infty d\omega \frac{\omega^2}{\sinh^2(\beta\hbar\omega/2)}.$$

The integral I_1 is not convergent, but since $Im\chi \approx 0$ for momentum exchanges larger than $2k_F$, we introduce a cut-off frequency of $2k_F$ and find

$$I_1 = \int_0^{2k_F} dq \frac{q}{(q+q_{TF})^2} = \left[\frac{q_{TF}}{q+q_{TF}} + \ln(q+q_{TF})\right]_0^{2k_F} = \frac{(1+\gamma)\ln(1+\gamma)-\gamma}{1+\gamma}.$$

Using the formula

$$\int_0^\infty dx \frac{x^p}{4\sinh^2(x/2)} = p!\zeta(p),$$

where ζ is Riemann's zeta-function, we find that

$$I_2 = \left(\frac{1}{\beta\hbar}\right)^3 \int_0^\infty dx \frac{x^2}{\sinh(x/2)} = 8\zeta(2)\left(\frac{1}{\beta\hbar}\right)^3.$$

All in all, defining

$$\tau_F = \frac{\hbar}{\varepsilon_F}, \quad \Gamma = \frac{(1+\gamma)\ln(1+\gamma)-\gamma}{(1+\gamma)\gamma^2},$$

using $\zeta(2) = \pi^2/6$, and remembering that

$$n^0 = \frac{m\varepsilon_F}{\pi\hbar^2},$$

we write the spin drag rate (4.126) as

$$\frac{1}{\tau_D, s} = \frac{m\Gamma}{3n^0\hbar^3}(k_BT)^2 = \frac{\pi\varepsilon_F\Gamma}{3\hbar}\left(\frac{k_BT}{\varepsilon_F}\right)^2 = \frac{\pi\Gamma}{3\tau_F}\left(\frac{T}{T_F}\right)^2. \tag{4.131}$$

Typical numbers for GaAs are $\varepsilon_b \simeq 13$, $m \simeq 0.07m_e$, $\tau_0 \simeq 38$ ps and $\varepsilon_F \simeq 10$ meV resulting in $\tau_F \simeq 6.3\cdot10^{-14}$ s, $k_F = 1.4\cdot10^8$ m^{-1}, and $q_{TF} = 2.2\cdot10^8$ m^{-1}. This gives the values $\gamma = 1.27$ and $\Gamma = 0.16$, which inserted in (4.131) gives

$$\frac{1}{\tau_D, s} \simeq 2.7\cdot10^{12}s^{-1}\left(\frac{T}{T_F}\right)^2. \tag{4.132}$$

Comparing (4.132) with

$$\frac{1}{\tau_0} \simeq 2.6\cdot10^{10}s^{-1}, \tag{4.133}$$

we see that even at temperatures considerably under the Fermi temperature ($T_F \sim 110$ K in a AlGaAs/GaAs 2DEG with $\varepsilon_F \sim 10$ meV) the spin drag rate is comparable to the impurity scattering rate. This stand in contrast to the ordinary DQW coulomb drag, where Gramilla's experiment showed that $\tau_D^{-1} \sim 10^7$ s^{-1} at

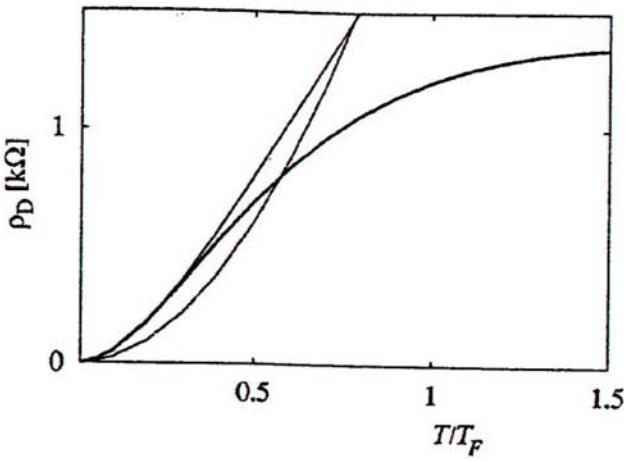

Figure 4.7: [10] The two-dimensional spin drag resistivity as a function of the temperature. The full line is a numerical integration for a two dimensional quantum well of thickness 10 nm and electron density $2 \cdot 10^{15}$ m^{-2} using a finite T expression for $\chi(q,\omega)$. The left thin line is a numerical calculation, but using the zero temperature susceptibility. The rightmost thin line is the resistivity corresponding to the drag rate given by (4.131).

temperatures around 5 K (figure 3.3a), and where the corresponding resistivity in the driving layer therefore is virtual non-detectable.

In [10] we have calculated the drag resistance numerically in different approximations (figure 4.7). Even though the temperature dependence varies, the order of magnitude does not, and shows once again that the 2DEG drag resistance is comparable to the ordinary impurity resistance in typical GaAlAs/AlAs heterostructures.

4.8 The spin drag rate in a 3DEG

It is easy to generalize the calculation of the 2DEG spin drag rate to a 3DEG.

PROPOSITION 4.8.1 *The spin drag rate, $\tau_{D,s}^{-1}$, in a 3DEG with negligible spin flip processes and with a fully spin s polarized current, i.e. $J_s = J$ and $J_{-s} = 0$, is*

$$\frac{1}{\tau_{D,s}} = \frac{\beta\hbar^2}{12\pi^3 n_{-s}^0 m} \int_0^\infty dq \int_0^\infty d\omega\, q^4 |e\phi(q)|^2 \frac{Im\chi_\uparrow(q,\omega) Im\chi_\downarrow(q,\omega)}{\sinh^2(\beta\hbar\omega/2)}. \tag{4.134}$$

PROOF. The calculations differ from the two dimensional calculation only slightly. We replace two dimensional polar coordinates with three dimensional spherical coordinates, i.e.

$$\int \frac{d\mathbf{k}}{(2\pi)^2} = \frac{1}{2\pi}\int dk k \rightarrow \int \frac{d\mathbf{k}}{(2\pi)^3} = \frac{1}{2\pi^2}\int dk k^2, \tag{4.135}$$

and note that the three dimensional version of (4.47) reads

$$\begin{aligned}\int\frac{d\mathbf{k}}{(2\pi)^3}\int\frac{d\mathbf{k}'}{(2\pi)^2}\int\frac{d\mathbf{q}}{(2\pi)^3}\, w(q)k_x q_x \Delta_{12}(\mathbf{k},\mathbf{k}';\mathbf{k}+\mathbf{q},\mathbf{k}'-\mathbf{q}) = \\ -\frac{1}{6}\int\frac{d\mathbf{k}}{(2\pi)^3}\int\frac{d\mathbf{k}'}{(2\pi)^2}\int\frac{d\mathbf{q}}{(2\pi)^3}\, w(q)q^2 \Delta_{12}(\mathbf{k},\mathbf{k}';\mathbf{k}+\mathbf{q},\mathbf{k}'-\mathbf{q}),\end{aligned} \tag{4.136}$$

since the only difference in the proof of (4.47) is that now $q^2 = q_x^2 + q_y^2 + q_z^2$ instead of $q^2 = q_x^2 + q_y^2$. In three dimensions (4.48) is virtually unchanged, so now

$$\int\frac{d\mathbf{k}}{(2\pi)^3}\int\frac{d\mathbf{k}'}{(2\pi)^3}\,\Delta_{12}(\mathbf{k},\mathbf{k}';\mathbf{k}+\mathbf{q},\mathbf{k}'-\mathbf{q}) = \frac{\hbar}{2\pi^2}\int_0^\infty d\omega\,\frac{Im\chi_1(q,\omega)Im\chi_2(q,\omega)}{\sinh^2(\beta\hbar\omega/2)}. \tag{4.137}$$

(4.135), (4.136) and (4.137) are the only differences between the two dimensional and the three dimensional calculation, and using them makes it trivial to generalize (4.78) to the three dimensional rate given by (4.134).

4.8.1 Evaluating the 3DEG spin drag rate in a metal

Our starting point is (4.134), where the three dimensional Thomas-Fermi expression (2.92) is inserted, giving

$$|e\phi(q)| = \frac{e^2}{\varepsilon_0\varepsilon_b(q^2+k_{TF}^2)}, \tag{4.138}$$

with the three dimensional Thomas-Fermi screening wave number, k_{TF}, given by (2.90). We also use the imaginary part of the low-frequency three dimensional susceptibility

$$Im\chi(q,\omega) = \frac{m^2}{4\pi\hbar^3}\frac{\omega}{q}, \tag{4.139}$$

found in (2.186). Inserting (4.138) and (4.139) into (4.134), gives

$$\frac{1}{\tau_D} = \frac{\beta m^3 e^4}{96\pi^3\hbar^4\varepsilon_0^2\varepsilon_b^2 n} I_q I_\omega, \tag{4.140}$$

where $n = 2n_{-s}$ and

$$I_q = \int_0^\infty dq \frac{q^2}{(q^2+k_{TF}^2)^2} = \frac{\pi}{4k_{TF}}, \tag{4.141}$$

$$I_\omega = \int_0^\infty d\omega \frac{\omega^2}{\sinh^2(\beta\hbar\omega/2)} = \frac{8\pi^2}{6}\left(\frac{2}{\beta\hbar}\right)^3. \tag{4.142}$$

Inserting a electron density like $n \sim 10^{29}$ m^{-3}, typical for many metals, we find that

$$\frac{1}{\tau_D} \sim T^2 \cdot 10^8 s^{-1}K^{-2}. \tag{4.143}$$

Comparing with typical Drude relaxation rates for metals

$$\frac{1}{\tau_0} \sim 10^{14} s^{-1} \tag{4.144}$$

we see that the 3DEG spin drag, although being of less significance than spin drag in a 2DEG, is noticeable at for instance room temperatures.

4.9 The transport equations in a both a 2DEG and a 3DEG

It is easy to generalize the transport equations given in table 4.1 to a 3DEG. Replacing all two dimensional quantities with the corresponding three dimensional quantities it is straightforward to see the the SFD distribution is still written as in (4.18), and the linearized Boltzmann equation still as in (4.39). Also the three dimensional versions of (4.21), (4.79) and (4.80) are left unaltered. Having

$$\int \frac{d\mathbf{k}}{(2\pi)^3} k_x \frac{\partial f_s^0}{\partial k_x} = -n_s^0, \tag{4.145}$$

the only significant difference appears in the following integral

$$\int \frac{d\mathbf{k}}{(2\pi)^3} \frac{\partial f_s^0}{\partial \varepsilon} = \int d\varepsilon d_{3D}(\varepsilon) \frac{\partial f_s^0}{\partial \varepsilon} = -d_{3D}(\varepsilon_{Fs}) = -\frac{m k_{Fs}}{2\pi^2 \hbar^2}, \tag{4.146}$$

where $d_{3D}(\varepsilon)$ is the three dimensional density of states given in table 2.1. Using that

$$d(\varepsilon_{Fs}) = \frac{\partial n_s^0}{\partial \varepsilon}, \tag{4.147}$$

in both two and three dimensions, we immediately find the equations generalized to both a 2DEG and a 3DEG, simply by replacing

$$d_{2D}(\varepsilon_{Fs}) = \frac{m}{2\pi\hbar^2} \to \frac{\partial n_s^0}{\partial \varepsilon}, \tag{4.148}$$

at appropriate places. The two equations (4.86) and (4.86) can be written

$$\text{Steady state continuity equation :} \qquad \frac{\partial J_s}{\partial x} = e \frac{\partial n_s^0}{\partial \varepsilon} \frac{\bar{\mu}_s - \bar{\mu}_{-s}}{\tau_{sf}}, \tag{4.149}$$

$$\text{Generalized Ohm's law :} \qquad \frac{\partial \bar{\mu}_s}{\partial x} = \frac{e}{\sigma_{tr,s}} J_s + \left(\frac{e}{\sigma_{sf,s}} + \frac{e}{\alpha_s \sigma_D} \right) \left(J_s - \alpha_s J_{-s} \right), \tag{4.150}$$

in both the two and three dimensional case. From (4.149) and (4.150) we find

$$\frac{\partial^2 \bar{\mu}_s}{\partial x^2} = e\rho_s^{\shortparallel} \frac{\partial J_s}{\partial x} - e\rho_s^{\perp} \frac{\partial J_s}{\partial x} = \frac{e^2}{\tau_{sf}} \left(\rho_s^{\shortparallel} \frac{\partial n_s^0}{\partial \varepsilon} + \rho_s^{\perp} \frac{\partial n_{-s}^0}{\partial \varepsilon} \right) = \frac{e^2}{\tau_{sf}} \frac{1}{2} \frac{\partial n^0}{\partial \varepsilon} \frac{\bar{\mu}_s - \bar{\mu}_{-s}}{\sigma_s}. \tag{4.151}$$

Here the direct- and transresistivity is given by (4.98) and (4.99), the total density $n^0 = n_s^0 + n_{-s}^0$, and

$$\frac{1}{\sigma_s} = \left(\rho_s^{\shortparallel} \frac{\partial n_s^0}{\partial \varepsilon} + \rho_s^{\perp} \frac{\partial n_{-s}^0}{\partial \varepsilon} \right) \left(\frac{1}{2} \frac{\partial n^0}{\partial \varepsilon} \right)^{-1} = \left(\frac{\frac{\partial n_s^0}{\partial \varepsilon}}{\sigma_{tr,s}} + \frac{\frac{\partial n_s^0}{\partial \varepsilon} + \alpha_s \frac{\partial n_{-s}^0}{\partial \varepsilon}}{\sigma_{sf,s}} + \frac{\frac{\partial n_{-s}^0}{\partial \varepsilon} + \alpha_{-s} \frac{\partial n_s^0}{\partial \varepsilon}}{\sigma_D} \right) \left(\frac{1}{2} \frac{\partial n^0}{\partial \varepsilon} \right)^{-1}. \tag{4.152}$$

Comparing (4.151) with (4.100) we see all the results following from (4.100) can be generalized from the two dimensional case without difficulties. We summarize the results in table 4.2.

Transport equations including spin drag

Steady state continuity equation : $$\frac{\partial J_s}{\partial x} = e\frac{\partial n_s^0}{\partial \varepsilon}\frac{\bar{\mu}_s - \bar{\mu}_{-s}}{\tau_{sf}},$$

Generalized Ohm's law : $$\frac{\partial \bar{\mu}_s}{\partial x} = \frac{e}{\sigma_{tr,s}}J_s + \left(\frac{e}{\sigma_{sf,s}} + \frac{e}{\alpha_s \sigma_D}\right)(J_s - \alpha_s J_{-s}),$$

Diffusion equation : $$\frac{\partial^2}{\partial x^2}(\bar{\mu}_s - \bar{\mu}_{-s}) = \frac{\bar{\mu}_s - \bar{\mu}_{-s}}{l_{sf}^2},$$

Generalized Laplace equation : $$\frac{\partial^2}{\partial x^2}(\sigma_s \bar{\mu}_s + \sigma_{-s}\bar{\mu}_{-s}) = 0.$$

The total density, n^0 : $n^0 = n_s^0 + n_{-s}^0$

The relative equilibrium spin density, α_s : $\alpha_s = \frac{n_s^0}{n_{-s}^0}$

The spin dependent constant σ_s is given by : $$\frac{1}{\sigma_s} = \left(\frac{\frac{\partial n_s^0}{\partial \varepsilon}}{\sigma_{tr,s}} + \frac{\frac{\partial n_s^0}{\partial \varepsilon} + \alpha_s \frac{\partial n_{-s}^0}{\partial \varepsilon}}{\sigma_{sf,s}} + \frac{\frac{\partial n_{-s}^0}{\partial \varepsilon} + \alpha_{-s}\frac{\partial n_s^0}{\partial \varepsilon}}{\sigma_D}\right)\left(\frac{1}{2}\frac{\partial n^0}{\partial \varepsilon}\right)^{-1}$$

The effective conductivity σ is given by : $\frac{1}{\sigma} = \frac{1}{\sigma_s} + \frac{1}{\sigma_{-s}}$

The spin flip length l_{sf} is given by : $\frac{1}{l_{sf}^2} = \frac{1}{2}\frac{\partial n^0}{\partial \varepsilon}\frac{e^2}{\sigma \tau_{sf}}$

The two dimensional density of state : $\frac{\partial n_s^0}{\partial \varepsilon} = \frac{m}{2\pi\hbar^2}$

The three dimensional density of state : $\frac{\partial n_s^0}{\partial \varepsilon} = \frac{m k_{Fs}}{2\pi^2\hbar^2}$

Event	**Related rate**	**Related resistivity**
Spin flip event	$\frac{1}{\tau_{sf}}$	
Momentum loss of spin current component, J_s, due to spin conserving elastic collisions between an electron with spin s and an impurity	$\frac{1}{\tau_{tr,s}^0}$	
Momentum loss of the total current, $J = J_s + J_{-s}$, due to spin flip event $s \to -s$	$\frac{1}{\tau_{tr,s}^{sf}}$	
Momentum loss of the total current, $J = J_s + J_{-s}$, due to scattering processes where the initial electron has spin s	$\frac{1}{\tau_{tr,s}} = \frac{1}{\tau_{tr,s}^0} + \frac{1}{\tau_{tr,s}^{sf}}$	$\frac{1}{\sigma_{tr,s}}$
Momentum transfer from $J_s \to J_{-s}$ due to spin flip event $s \to -s$	$\frac{1}{\tau_{sf,s}}$	$\frac{1}{\sigma_{sf,s}}$
Momentum transfer from $J_s \to J_{-s}$, due to electron-electron interaction	$\frac{1}{\tau_{D,s}}$	$\frac{1}{\sigma_D}$

Table 4.2: Transport equations in the SFD approximation for a 2DEG and a 3DEG, and the physical origin

Chapter 5

Concluding remarks

> A conclusion is the place where you got tired of thinking. *Arthur Bloch*

The transport equations governing spin-polarized transport has to this date described a two-component system where no momentum is transferred between the two spin-current components, $J_\uparrow$ and $J_\downarrow$. In this thesis, we have used the semiclassical Boltzmann equation and the SFD ansatz to include spin-momentum transfer processes into the transport equations, with the results given in table 4.2.

The SFD ansatz assume that a shifted Fermi-Dirac (SFD) distribution, even though it is not an exact solution to the Boltzmann equation, is sufficient to describe the transport properties of a degenerate two- and three dimensional electron gas. In order to justify this assumption, we have showed that the SFD distribution is an exact solution to the Boltzmann equation for many related systems.

There are two processes that transfer momentum between the spin-current components, namely anisotropic spin-inverting elastic collisions between electrons and impurities, and electron-electron interactions between electrons of opposite spin. The spin-flip scattering rate is temperature independent, while the electron-electron scattering rate is temperature dependent. The effect of electron-electron interactions is described by the spin-drag rate, τ_D^{-1}, which we have evaluated for two- and three-dimensional systems. We have found that τ_D^{-1} is comparable to ordinary transport rates for such systems. As a consequence, spin-momentum transferring effects are not negligible, and the generalized transport equations listed in table 4.2 are relevant improvements to the existing equations (section 3.2.1) derived by Valet and Fert.

When momentum is transferred between the two spin-current components, the resistivity and the spin-flip length is affected. Using the generalized transport equations we have found expressions for the drag enhanced resistivity and also for the drag diminished spin-flip length. The drag enhanced resistivity has a characteristic near T^2 behavior, well known from DQW drag experiments, and can hopefully be observed in future experiments.

Finally I would like to thank my supervisor, lector Karsten Flensberg, whose guidance has been invaluable, and ph. D. student Niels Asger Mortensen, for their patience and for many fruitful discussions.

Appendix A

The collision induced entropy production

In section 2.2.3 we claimed that the entropy production due to collisions

$$\left(\frac{\partial S}{\partial t}\right)_{coll} = 0, \tag{A.1}$$

in a Fermi-Dirac distributed electron gas. Here we will prove this statement, generalizing an approach used in [31] for a classical gas. In the following we suppress the spin index for notational conveniens.

Before showing (A.1), we prepare for it by making some general calculations. Let $\varphi(\mathbf{k}, f)$ be a an arbitrary function of $\mathbf{k}$ and the distribution function, f, and let os define the density, $\rho_\varphi(\mathbf{r}, t)$, as

$$\rho_\varphi(\mathbf{r}, t) = \int \frac{d\mathbf{k}}{(2\pi)^d} \varphi(\mathbf{k}, f) f(\mathbf{k}, \mathbf{r}, t). \tag{A.2}$$

We now ask how the influence of collisions effects this density. The rate of change is given by

$$\begin{aligned}\left(\frac{\partial \rho_\varphi}{\partial t}\right)_{coll} = \int \frac{d\mathbf{k}}{(2\pi)^d} \left(\frac{\partial(\varphi f)}{\partial t}\right)_{coll} = \int \frac{d\mathbf{k}}{(2\pi)^d} \frac{\partial(\varphi f)}{\partial f} \left(\frac{\partial f}{\partial t}\right)_{coll} = \\ \int \frac{d\mathbf{k}}{(2\pi)^d} \left[\varphi + f\frac{\partial \varphi}{\partial f}\right] \left(\frac{\partial f}{\partial t}\right)_{coll} = \int \frac{d\mathbf{k}}{(2\pi)^d} \bar{\varphi} \left(\frac{\partial f}{\partial t}\right)_{coll},\end{aligned} \tag{A.3}$$

where we have introduced

$$\bar{\varphi} = \varphi + f\frac{\partial \varphi}{\partial f}. \tag{A.4}$$

Let us consider an electron-electron scattering process, where two electrons with wave vectors $\mathbf{k}$ and $\mathbf{k}_1$ scatter on each other ending up with wave vectors $\mathbf{k}'$ and $\mathbf{k}'_1$, and assume that the process probability fulfils

$$w(\mathbf{k}, \mathbf{k}_1; \mathbf{k}', \mathbf{k}'_1) = w(\mathbf{k}_1, \mathbf{k}; \mathbf{k}'_1, \mathbf{k}') = w(\mathbf{k}', \mathbf{k}'_1; \mathbf{k}, \mathbf{k}_1) = w(\mathbf{k}'_1, \mathbf{k}', \mathbf{k}_1, \mathbf{k}). \tag{A.5}$$

When the Golden rule expression (2.55) can be used for $w(\mathbf{k}, \mathbf{k}_1; \mathbf{k}', \mathbf{k}'_1)$, (A.5) clearly applies.

Using an expression for the collision integral, $(\partial_t f)_{coll}$, that is equivalent to (2.59), we write (A.3) as

$$\left(\frac{\partial \rho_\varphi}{\partial t}\right)_{coll} = -\int \frac{d\mathbf{k}}{(2\pi)^d} \int \frac{d\mathbf{k}_1}{(2\pi)^d} \int \frac{d\mathbf{k}'}{(2\pi)^d} \int \frac{d\mathbf{k}'_1}{(2\pi)^d} w(\mathbf{k}, \mathbf{k}_1; \mathbf{k}', \mathbf{k}'_1) \bar{\varphi} [f f_1 (1-f')(1-f'_1) - f' f'_1 (1-f)(1-f_1)]. \tag{A.6}$$

For brevity the momentum and energy conservation is not written explicitly, but is included in $w(\mathbf{k},\mathbf{k}_1;\mathbf{k}',\mathbf{k}_1')$, and furthermore $f(\mathbf{k}_1',\mathbf{r},t)$ is denoted as f_1' etc. Using (A.5), we can write (A.6) in the following four equivalent ways

$$\left(\frac{\partial\rho_\varphi}{\partial t}\right)_{coll} = -\int\frac{d\mathbf{k}}{(2\pi)^d}\int\frac{d\mathbf{k}_1}{(2\pi)^d}\int\frac{d\mathbf{k}'}{(2\pi)^d}\int\frac{d\mathbf{k}_1'}{(2\pi)^d}w(\mathbf{k},\mathbf{k}_1;\mathbf{k}',\mathbf{k}_1') \times\begin{cases}\bar\varphi[ff_1(1-f')(1-f_1')-f'f_1'(1-f)(1-f_1)]\\ \bar\varphi_1[ff_1(1-f')(1-f_1')-f'f_1'(1-f)(1-f_1)]\\ -\bar\varphi'[ff_1(1-f')(1-f_1')-f'f_1'(1-f)(1-f_1)]\\ -\bar\varphi_1'[ff_1(1-f')(1-f_1')-f'f_1'(1-f)(1-f_1)]\end{cases}, \tag{A.7}$$

and see that

$$\left(\frac{\partial\rho_\varphi}{\partial t}\right)_{coll} = -\frac{1}{4}\int\frac{d\mathbf{k}}{(2\pi)^d}\int\frac{d\mathbf{k}_1}{(2\pi)^d}\int\frac{d\mathbf{k}'}{(2\pi)^d}\int\frac{d\mathbf{k}_1'}{(2\pi)^d}w(\mathbf{k},\mathbf{k}_1;\mathbf{k}',\mathbf{k}_1') \times(\bar\varphi+\bar\varphi_1-\bar\varphi'-\bar\varphi_1')[ff_1(1-f')(1-f_1')-f'f_1'(1-f)(1-f_1)]. \tag{A.8}$$

Now, we are armed to show (A.1). The key point is to consider the entropy density, $S(\mathbf{r},t)$, which we from statistical physics [22] known can be written as

$$S = -k_B\int\frac{d\mathbf{k}}{(2\pi)^2}(f\ln f+(1-f)\ln(1-f)) = -k_B\int\frac{d\mathbf{k}}{(2\pi)^2}\left(\ln f+\frac{(1-f)}{f}\ln(1-f)\right)f. \tag{A.9}$$

We want to find $(\partial S/\partial t)_{coll}$ and therefore define

$$\varphi_S(\mathbf{k},f) = -k_B\left(\ln f+\frac{(1-f)}{f}\ln(1-f)\right). \tag{A.10}$$

Since

$$\frac{\partial\varphi_S}{\partial f} = k_B\frac{\ln(1-f)}{f^2}, \tag{A.11}$$

we have that

$$\bar\varphi_S = \varphi_S+f\frac{\partial\varphi_S}{\partial f} = -k_B\ln\frac{f}{1-f}. \tag{A.12}$$

Inserting (A.12) into (A.8) gives that

$$\left(\frac{\partial S}{\partial t}\right)_{coll} = \frac{k_B}{4}\int\frac{d\mathbf{k}}{(2\pi)^d}\int\frac{d\mathbf{k}_1}{(2\pi)^d}\int\frac{d\mathbf{k}'}{(2\pi)^d}\int\frac{d\mathbf{k}_1'}{(2\pi)^d}w(\mathbf{k},\mathbf{k}_1;\mathbf{k}',\mathbf{k}_1')(1-f)(1-f_1)(1-f')(1-f_1') \times\left(\ln\frac{ff_1}{(1-f)(1-f_1)}-\ln\frac{f'f_1'}{(1-f')(1-f_1')}\right)\left(\frac{ff_1}{(1-f)(1-f_1)}-\frac{f'f_1'}{(1-f')(1-f_1')}\right). \tag{A.13}$$

It is obvious that $(\ln x-\ln y)$ and $(x-y)$ has the same sign, and since $(1-f)(1-f_1)(1-f')(1-f_1')>0$ we have

$$\left(\frac{\partial S}{\partial t}\right)_{coll}\geq 0. \tag{A.14}$$

Clearly (A.14) means that the entropy density never decreases due to electron-electron scattering processes.

If the system is in thermal equilibrium, we should have

$$\left(\frac{\partial S}{\partial t}\right)_{coll} = 0. \tag{A.15}$$

In section 2.2.3, it was shown that the Fermi-Dirac distribution satisfy

$$f^0(\mathbf{k})f^0(\mathbf{k}_1)[1-f^0(\mathbf{k}')][1-f^0(\mathbf{k}'_1)] = f^0(\mathbf{k}')f^0(\mathbf{k}'_1)[1-f^0(\mathbf{k})][1-f^0(\mathbf{k}_1)], \tag{A.16}$$

which can be written as

$$\frac{f^0(\mathbf{k})f^0(\mathbf{k}_1)}{(1-f^0(\mathbf{k}))(1-f^0(\mathbf{k}_1))} = \frac{f^0(\mathbf{k}')f^0(\mathbf{k}'_1)}{(1-f^0(\mathbf{k}'))(1-f^0(\mathbf{k}'_1))}. \tag{A.17}$$

Inserting (A.17) into (A.13) proves (A.15) for electron-electron collisions in a Fermi-Dirac distributed gas.

It is easy to realize that the entropy production due to the elastic impurity collision terms (2.57) and (2.58) is also zero, since

$$f^0_s(\mathbf{k}) = f^0_{s'}(\mathbf{k}'), \tag{A.18}$$

when $\varepsilon_{\mathbf{k}s} = \varepsilon_{\mathbf{k}'s'}$. Therefore (A.1) holds for a Fermi-Dirac distributed electron gas with elastic impurity and electron-electron scattering.

Bibliography

[1] Neil W. Ashcroft and N. David Mermin, *Solid State Physics*, W. B. Saunders Company, 1976.

[2] B. H. Bransden and C. J. Joachin, *Physics of atoms and molecules*, Addison Wesley Longman Limited, 1983.

[3] Henrik Bruus and Karsten Flensberg, *Introduction to quantum field theory in condensed matter physics*, Ørsted Laboratory, Niels Bohr Institute, 2001.

[4] John Crangle, *Solid state magnetism*, Edward Arnold, 1991.

[5] Irene D'Amico and Giovanni Vignale, *Theory of spin Coulomb drag in spin-polarized transport*, Phys. Rev. B **62** (2000), no. 8, 4853.

[6] John H. Davies, *The physics of low-dimensional semiconductors : an introduction*, Cambridge University Press, 1998.

[7] J. Wüstehube et. al., *Field effect transistors*, Mullard Limited, 1972.

[8] R. Fiederling, M. Kein, G. Reuscher, W. Ossau, G. Schmidt, A. Waag, and L. W. Molenkamp, *Injection and detection of a spin-polarized current in a light-emitting diode*, Nature **402** (1999), 787.

[9] K. Flensberg, B. Y. Hu, A-P. Jauho, and J. M. Kinaret, *Linear-response theory of Coulomb drag in coupled electron systems*, Phys. Rev. B **52** (1995), no. 20, 14761.

[10] K. Flensberg, T. Stibius Jensen, and N. A. Mortensen, *Diffusion equation and spin drag in spin-polarized transport*, Phys. Rev. B **64** (2001), 245308.

[11] Karsten Flensberg and Ben Yu-Kuang Hu, *Plasmon enhancement of Coulomb drag in double-quantum-well systems*, Phys. Rev. B **52** (1995), no. 20, 14796.

[12] T. J. Gramila, J. P. Eisenstein, A. H. MacDonald, L. N. Pfeiffer, and K. W. West, *Mutual Friction between Parallel Two-Dimensional Electron Systems*, Phys. Rev. B **66** (1991), no. 9, 1216.

[13] T. Gruber, M. Keim, R. Fiederling, G. Reuscher, W. Ossau, G. Schmidt, L. W. Molenkamp, and A. Waag, *Electron spin manipulation using semimagnetic resonant tunneling diodes*, Appl. Phys. Lett. **78** (2001), no. 8, 1101.

[14] N. P. R. Hill, J. T. Nicholls, E.H. Linfield, M. Pepper, D. A. Ritchie, G. A. C. Jones, B. Y. Hu, and K. Flensberg, *Correlation Effects on the Coupled Plasmon Modes of a Double Quantum Well*, Phys. Rev. B **78** (1997), no. 11, 2204.

[15] Ben Yu-Kuang Hu and Karsten Flensberg, *Electron-electron scattering in linear transport in two-dimensional systems*, Phys. Rev. B **53** (1996), no. 15, 10072.

[16] Antti-Pekka Jauho and Henrik Smith, *Coulomb drag between parallel two-dimensional electron systems*, Phys. Rev. B **47** (1993), no. 8, 4420.

[17] A. B. Stibius Jensen and T. B. Stibius Jensen, *RBS/TEM analyse af Cd & Pb implanteret i aluminium*, Bachelor Thesis, University of Copenhagen, 1998.

[18] Mark Johnson, *Spin Injection: A survey and Review*, Journal of Superconductivity: Incorporating Novel Magnetism **14** (2001), no. 2, 273.

[19] Bent Elbæk, *Elektromagnetisme*, Niels Bohr institutet, 1995.

[20] M. Kohda, Y. Ohno, K. Takamura, F. Matsukura, and H. Ohno, *A spin Esaki diode*, Not yet published (2001).

[21] J. König, J. Schliemann, T. Jungwirth, and A. H. MacDonald, *Ferromagnetism in (III,Mn)V Semiconductors*, cond-mat (2001).

[22] L. D. Landau and E. M. Lifshitz, *Statistical Physics*, Pergamon Press, 1959.

[23] Gerald G. Mahan, *Many-Particle Physics*, third ed., Kluwer Academic/Plenum Publishers, New York, 2000.

[24] M. C. Bønsager, K. Flensberg, B. Y. Hu, and A. H. MacDonald, *Frictional drag between quantum wells mediated by phonon exchange*, Phys. Rev. B **57** (1998), no. 12, 7085.

[25] M. Oestreich, J. Hübner, D. Hägele, P. J. Klar, W. Heimbrodt, W. W. Rühle, D. E. Ashenford, and B. Lunn, *Spin-Injection into semiconductors*, Appl. Phys. Lett. **74** (1999), no. 9, 1251.

[26] Y. Ohno, D. K. Young, B. Beschoten, F. Matsukura, H. Ohno, and D. D. Awschalom, *Electrical spin injection in a ferromagnetic semiconductor heterostructure*, Nature **402** (1999), 790.

[27] Michael Osofsky, *Spin-Injection*, Journal of Superconductivity: Incorporating Novel Magnetism **13** (2000), no. 2, 209.

[28] G. Schmidt, D. Ferrand, L. W. Molenkamp, A. T. Filip, and B. J. van Wees, *Fundamental obstacle for electrical spin injection from a ferromagnetic metal into a diffusive semiconductor*, Phys. Rev. Lett. **58** (1987), no. 21, 2271.

[29] Silvan S. Schweber, *Many-Particle Physics*, third ed., Harper & Row., 1961.

[30] Henrik Smith, *Introduction to Many-particle Physics*, H. C. Ørsted Institute, 1994.

[31] Henrik Smith and H. Højgaard Jensen, *Transport Phenomena*, Clarendon Press, Oxford, 1989.

[32] P. M. Solomon, P. J. Price, D. J. Frank, and D. C. La Tulipe, *New Phenomena in Coupled Transport between 2D and 3D Electron-Gas Layers*, Phys. Rev. B **63**, no. 22.

[33] T. Valet and A. Fert, *Theory of the perpendicular magnetoresistance in magnetic multilayers*, Phys. Rev. B **48** (1993), no. 10, 7099.

[34] P.C. van Son, H. van Kempen, and P. Wyder, *Boundary Resistance of the Ferromagnetic-Nonferromagnetic Metal Interface*, Phys. Rev. Lett. **58** (1987), no. 21, 2271.

[35] Kei Yosida, *Theory of magnetism*, Springer-Verlag Berlin, 1996.